 © 2000 Russian Academy of Sciences and Turpion Ltd

DOI 10.1070/RC2000v069n01ABEH000526

Chemical principles of preparation of metal-oxide superconductors

Yu D Tretyakov, E A Goodilin

Contents

I.	Introduction	1
II.	Characteristic features of high-temperature superconductors	2
III.	Phase diagrams of high-temperature superconductors	4
IV.	Development of advanced methods for the synthesis of high-temperature superconducting materials	18
V.	Practical applications of high-temperature superconducting materials	28

Abstract. The review deals with chemical aspects of the problem of preparation of a novel class of advanced materials, *viz*., **high-temperature superconducting cuprates of complex chemical composition and structure. Investigations into these types of superconductors not only made it possible to reveal the 'composition – treatment – structure – property' correlations, but also contributed significantly to the development of concepts of chemical interactions in complex oxide systems, high-temperature phase transformations, the nature of peritectic reactions, properties of cuprate melts and structural phase transitions. Particular attention is paid to the analysis of different experimental results obtained in the studies of features of physicochemical processes occurring in complex metal-oxide systems. The bibliography includes 292 references**.

I. Introduction

Complex cuprates with a high transition temperature to the superconducting state were discovered more than 12 years ago and called high-temperature superconductors (HTSC).[1–5] The discovery of HTSC has initiated fundamental investigations into their crystal structure and physicochemical properties as well as the search for possibilities of practical use of these phases.[6–24]

From the chemical viewpoint, the history of superconductivity is a chain of discoveries of materials with more and more complicated structures and can be considered as specific 'chemical evolution' of these materials from simple to complex ones (Fig. 1). This dates back to 1911 when the Dutch physicist H Kamerlingh-Onnes first obtained liquid helium. This breakthrough has made it possible to systematically investigate the properties of materials at temperatures close to absolute zero. Kamerlingh-Onnes had established[25] that mercury metal known as a 'bad metal' completely loses electrical resistance at 4.2 K. In 1933, Meissner and Oxenfeld showed[26] that superconductors (SC) are simultaneously ideal diamagnetics, which means that they completely exclude the magnetic field lines from their own bulk.

Yu D Tretyakov, E A Goodilin Department of Chemistry, M V Lomonosov Moscow State University, Leninskie Gory, 119899 Moscow, Fax (7-095) 939 09 98. Tel. (7-095) 939 20 74. E-mail: yudt@inorg.chem.msu.ru (Yu D Tretyakov), Tel. (7-095) 939 47 29. E-mail: goodilin@inorg.chem.msu.ru (E A Goodilin)

Received 27 April 1999
Uspekhi Khimii **69** (1) 3 – 40 (2000); translated by A M Raevsky

Following the discovery of superconductivity, the common belief was that superconductors would find extensive practical applications. However, this is limited mainly because of a very low transition temperature to the superconducting state (the so-called critical temperature, T_c). In the mid-1980s, it has been possible to raise this temperature[2, 12, 27, 28] to 23.2 K for Nb_3Ge intermetallide, despite the fact that commonly accepted theories of superconductivity (see, *e.g.*,[26]) casted scepticism concerning the possibility of attainment of this high-temperature barrier.

In 1986, Bednorz and Müller[29] discovered that ceramics based on copper, lanthanum and barium oxides ($La_{2-x}Ba_xCuO_4$) can

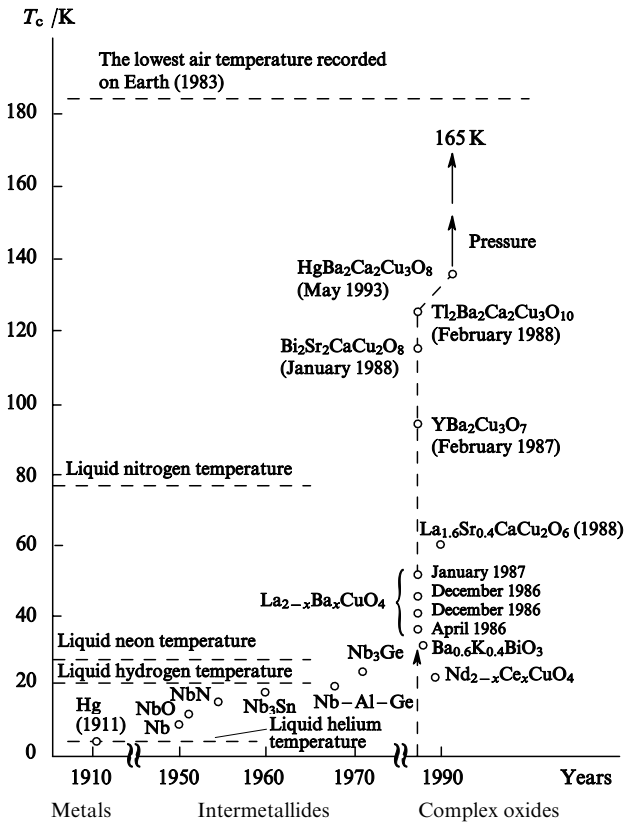


Figure 1. Chronology of discoveries in the field of high-temperature superconductors.

undergo a transition to the superconducting state at 30 K. Mention should be made of studies by Lazarev, Kahan and Shaplygin [30] who synthesised complex cuprates of analogous composition in 1978 and of those by a group of researchers from France,[31] carried out two years later. However, unfortunately, the electrical conductivity of these specimens was measured down to liquid nitrogen temperature (77 K) only, which precluded observation of the effect of superconductivity.

It should be emphasised that high-temperature superconductivity was first observed for an oxide ceramic, which usually possesses dielectric or semiconducting properties, rather than for conventional intermetallides, organic or polymeric structures.[26] This destroyed the psychological barrier to the synthesis of HTSC and allowed the synthesis of new generations of metal-oxide superconductors nearly simultaneously and over a short period. The brief history is as follows. In February 1987, using the idea of 'chemical compression' for structure modification, Wu *et al.*[32] prepared a superconducting ceramic based on barium, yttrium and copper oxides ($YBa_2Cu_3O_{7-x}$) with a critical temperature of 93 K, which is higher than the liquid nitrogen boiling temperature. In January 1988, Maeda *et al.*[33] synthesised a series of compounds with composition $Bi_2Sr_2Ca_{n-1}Cu_nO_{2n+4}$. Among them, the phase with $n = 3$ had a T_c of 108 K. A month later, Sheng and Hermann [34] prepared a superconductor $Tl_2Ba_2Ca_2Cu_3O_{10}$ with $T_c = 125$ K. Finally, in 1993, Antipov, Putilin *et al.*[35,36] discovered a series of mercury-containing superconductors with composition $HgBa_2Ca_{n-1}Cu_nO_{2n+2+\delta}$ ($n = 1-6$). Currently, the Hg1223-phase of this family has the highest T_c (135 K). It should be noted that at an external pressure of 350×10^3 atm the transition temperature increases to 164 K,[12,36] which is only 19 K lower than the lowest temperature ever reached under natural conditions on the Earth. These are the main stages of 'chemical evolution' of superconductors from mercury metal (4.2 K) to mercury-containing HTSC (164 K).

Currently, about 50 individual layered superconducting cuprates are known [14] (Table 1). Sometimes, sensational information on the preparation of novel 'copper-free' superconductors with T_c above room temperature is reported. 'Copper-free' superconductors have been known for some time; however, no high transition temperatures to the superconducting state have yet been observed for these compounds (the highest T_c values for copper-free superconductors were reported for $Ba_{1-x}K_xBiO_3$ and fullerene-based intercalation phase Cs_3C_{60} [37] (see Table 1).

A line of investigations associated with attempts to synthesise 'ecologically safe' HTSC free from heavy metals (Hg, Pb, Ba) deserves special mention. Oxycarbonate phases of Ca prepared under high pressure [38] can serve as an example of these HTSC.

Thus, most HTSC are oxide phases with very complicated chemical composition. These compounds are extremely sensitive to the conditions for synthesis, heat treatment and operating conditions; they are often called 'chemical' superconductors.[14] Numerous studies were devoted to structural,[12,17,18] physical,[19] synthetic [2–11,13,14,20–22] and technological aspects [15,16,23,24] of preparation of HTSC materials; however, only very few of them consider all these problems simultaneously. It should be noted that studies of the processes accompanying preparation of HTSC-materials by different methods not only allow the solution of a practically important problem of revealing the 'composition–treatment–structure–properties' correlations, but also favours the progress of general chemical ideas of the nature of complex oxide systems, *e.g.*, of the interaction between their components, the effect of mutual rare-earth (RE) element substitution, high-temperature phase relations, the nature of peritectic reactions, the structure and properties of the cuprate melts, oxygen and cation nonstoichiometry of solid phases and structural phase transitions. In this regard, the principles of the synthesis of metal-oxide superconductors are of considerable interest to chemical sciences. This review deals with a systematic consideration of fundamental physicochemical problems related to the preparation of HTSC-materials as well as with analysis of different experimental results obtained by researchers all over the world.

Table 1. Main types of high-temperature superconductors.

Type of high-temperature superconducting phase	T_c /K	Ref.
$La_{2-x}M_xCuO_4$ ('La201'-phase, M = Ca, Sr, K, Na, Rb)	35–45	29
$La_{1.6}Sr_{0.4}CaCu_2O_6$	58	18
$Nd_{2-x}Ce_xCuO_4$ (T-phase, electron superconductor)	23	18
$Nd_2CuO_{4-x}F_x$	27	18
$(Nd,Sr,Ce)_2CuO_4$ (T*-phase)	35	18
$(Y,R)Ba_2Cu_{3+n/2}O_{7+n/2}$	up to 95 ($n = 0$)	32
('R123'-phase, R is RE element)	60 ($n = 1$)	
	80 ($n = 2$)	
$YBa_2Cu_3O_6F_2$	94	18
$Bi_2(Ca,Sr)_{n+1}Cu_nO_{2n+4}$		33
'Bi2201'-phase	12 ($n = 1$)	
'Bi2212'-phase	85 ($n = 2$)	
'Bi2223'-phase	108 ($n = 3$)	
$TlBa_2Ca_{n-1}Cu_nO_{2n+3}$	125 ($n = 4$)	34
('Tl1212'—'Tl1234'-phases, $n = 1-4$)		
$Tl_2Ba_2Ca_{n-1}Cu_nO_{2n+3}$	95 ($n = 1$)	34
	105 ($n = 2$)	
	128 ($n = 3$)	
	115 ($n = 4$)	
$HgBa_2Ca_{n-1}Cu_nO_{2n+2+z}$	98 ($n = 1$)	35
	128 ($n = 2$)	
	135 ($n = 3$)	
	125 ($n = 4$)	
	113 ($n = 5$)	
$Hg_2Ba_2R_{1-x}Ca_xCu_2O_8$ (see [a])	70	35
$Pb_2Sr_2R_{n-1}Cu_{n+1}O_{2n+4+z}$	40–70	2
(R is RE element, RE element + Ca)		
$CuSr_2YCu_2O_7$	77	12, 14
$AuBa_2(Y_{1-x}Ca_x)Cu_2O_7$ (see [a])	82	
$Sr_{0.7}La_{0.3}CuO_2$ (see [a])	40	12, 14
$Sr_2CuO_2F_{2+z}$	47	12, 14
$Sr_{2-x}K_xCuO_2CO_3$ (see [a])	23	38
$Sr_2CaCuO_{4+z}Cl_{2-x}$ (see [a])	80	12, 14
$(BO)Sr_2Ca_{n-1}Cu_nO_{2n+2}$ (see [a])	100	12, 14
$(Sr,Ca)_{n+1}Cu_nO_{2n+2}$ (see [a])	100	12, 14
$(Cu_{0.5}C_{0.5})Ba_2Ca_{n-1}Cu_{3n}O_z$ (see [a])	124	12, 14
$Ba_2Ca_{n-1}Cu_nO_{2n-2+z}$ (see [a])	126 ($n = 3$)	12, 14
MC_{60} (fullerides, M = Na, K)	34	37
$Ba_{0.6}K_{0.4}BiO_3$	30	2
$Sr_{0.5}K_{0.5}BiO_3$ (see [a])	13	12, 14
RNi_2B_2C	23	12, 14

[a] Obtained under pressure.

II. Characteristic features of high-temperature superconductors

1. The crystal structure

An analysis of the available data on the structure and composition of HTSC allows some generalisations to be made.[14,36] First, almost all HTSC are complex layered copper-containing oxides whose structure contains oxygen-deficient perovskite-like blocks (Fig. 2). The $(Sr,Ca)CuO_2$ phase built of alternating blocks comprising alkaline-earth metal ions sandwiched with planar CuO_2 layers [38] is considered as a prototype of the oxide HTSC. It is the CuO_2 layers that are currently considered to be responsible for superconductivity in cuprates. In these layers, the copper atoms form a square network, whereas the oxygen atoms are placed on the lines connecting the copper sites. The electrons

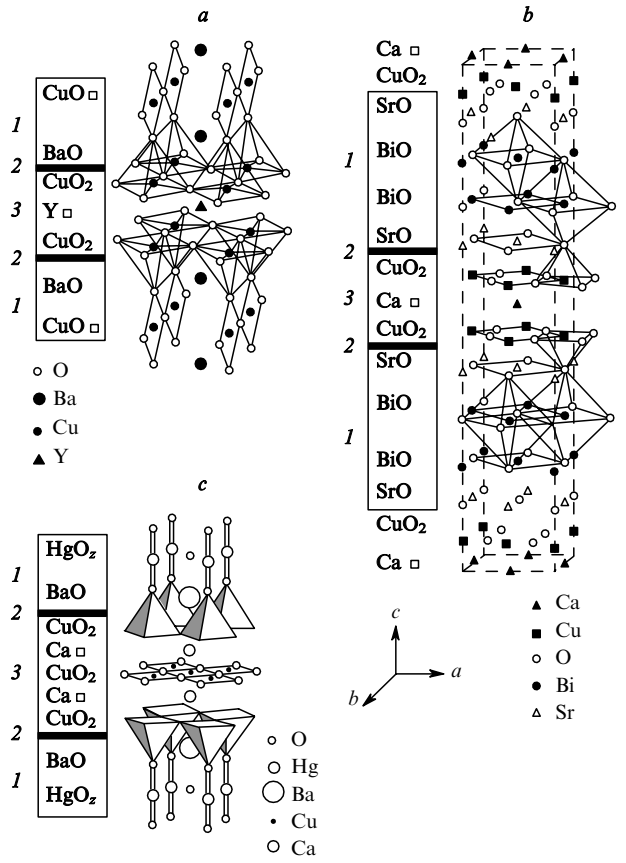


Figure 2. Crystal structures of HTSC $YBa_2Cu_3O_7$ (*a*), $Bi_2Sr_2CaCu_2O_8$ (*b*), $HgBa_2Ca_2Cu_3O_z$ (*c*).
Dielectric (*1*) and oxygen-deficient (*3*) perovskite-like blocks containing superconducting CuO_2 planes (*2*) are shown.

of copper and oxygen atoms that form Cu–O bonds in such a layer ($3d_{x^2-y^2}$ and $2p_{xy}$ electrons, respectively) are delocalised, which means that they belong not to one but to all of the atoms in the layer. Therefore compounds comprising CuO_2 layers in their structure can possess a metallic-type conductivity. At temperatures below the critical temperature, superconductivity arises upon doping of the CuO_2 layers with an optimum amount of charge carriers (Fig. 3); this occurs upon ordering of oxygen atoms and vacancies after the high-temperature superconducting phase has achieved a certain oxygen stoichiometry, upon heterovalent doping, upon applying an external pressure, *etc.*[12, 16, 19]

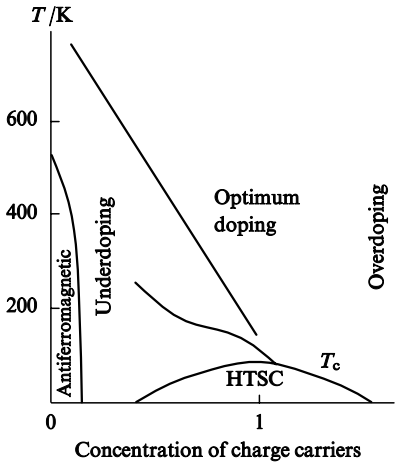


Figure 3. Generalised physical phase diagram of a high-temperature superconductor depending on the relative concentration of charge carriers in the superconducting planes.
Mark 1 on the abscissa axis corresponds to the state characterised by the maximum transition temperature to the superconducting state.

It was experimentally established that manifestation of superconductivity requires that the formal oxidation state of copper in the CuO_2 layers with collective electrons be somewhat different from +2 and lie within the range from +2.05 to +2.25 for hole superconductors (123-, Bi- and Tl-families) or from +1.8 to +1.9 for electron superconductors[2, 12] (phases of the Nd_2CuO_4 type). The Cu–O bond length in the layer is yet another important parameter determining the superconducting properties; this must be within the limits 0.190–0.197 nm provided that the distance between the nearest copper atoms lies in the range 0.380–0.394 nm. The copper atoms can also be bonded to the oxygen atoms in neighbouring layers; however, these bonds should be much longer and exceed 0.22 nm. In other words, the structure of superconducting cuprates contains inequivalent Cu–O bonds, *viz.*, strong in-plane bonds in each CuO_2 layer and much weaker bonds directed perpendicular to these layers. As a consequence, such superconductors have a layered structure, whereas the framework-type complex copper oxides (perovskites $CuBO_3$ with equivalent Cu–O bonds) possess no superconducting properties.

Electrical neutrality of crystals requires the presence of other charge-compensating layers or the presence of dielectric layers between superconducting CuO_2 planes. These interlayers consist of readily polarisable ions (*e.g.*, Ca^{2+}, Sr^{2+} and Ba^{2+} ions) which, along with the holes in the CuO_2 layer, can form the Cooper pairs upon transition to the superconducting state.[2] Most of the known superconductors are built of alternating CuO_2 and BaO, SrO, TlO^+, BiO^+, Ca^{2+}, Y^{3+}, *etc.* layers. Changes in the number of CuO_2 layers in the structure give rise to homologous series of compounds with a similar structure (see Fig. 2). In this case, the crystal structure will be stable if each constituent layer is commensurable with the layers lying above and below a given layer.

This analysis of the genesis of the structure of different HTSC families is not only useful for finding a general approach to the description of the phenomenon of high-temperature superconductivity, but also favours a targeted search for and chemical design of novel superconductors.

2. Physical properties

In most cases, the practical applications of superconductors are associated with their capability to resist in the superconducting state the destructive action of a current density of $\sim 10^5$ A cm^{-2} in magnetic fields from 2 to 10 T, while the first (ceramic) specimens of superconducting cuprates were characterised by more than modest critical current density[8, 10] of $\sim 1-100$ A cm^{-2} (Fig. 4).

Currently, synthesis of superconducting phases with the desired crystal structure and T_c above the liquid nitrogen temperature can be accomplished without difficulty. However, the attainment of high values for other important parameters, *e.g.*, the critical current density J_c and its stability in an external magnetic field, faces great difficulties for a number of reasons. For instance, evolution from metallic to ceramic superconductors results in an increase in T_c and, at the same time, in a dramatic decrease in the coherence lengths of oxide superconductors[19] compared to those of low-temperature intermetallide superconductors (0.2 nm and ~ 2 nm, respectively). The fundamental physical parameters of high-temperature superconducting $YBa_2Cu_3O_z$ phase are listed in Table 2 as examples. As a consequence, the grain boundary thickness in polycrystalline metallic superconductors is commensurable with the coherence length, which favours the appearance of efficient pinning centres and an increase in the critical current. On the contrary, the superconduction current in oxide superconductors is to a great extent limited by processes occurring at grain boundaries; this is

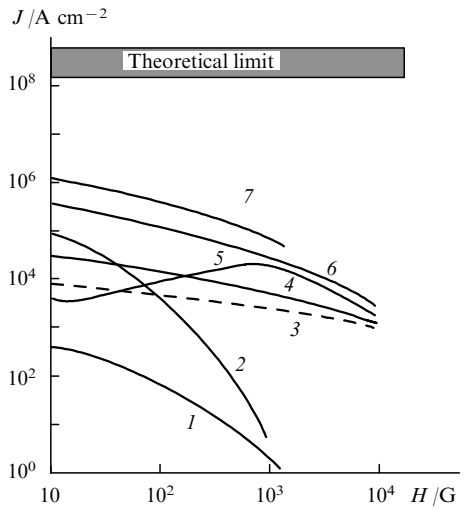


Figure 4. Dependence of the stability of the critical current density on the external magnetic field at 77 K for different classes of HTSC materials; (*1*) sintered ceramics; (*2*) Bi2212 tapes; (*3*) single crystals; bulk melt-solidified ceramics: (*4*) Y123; (*5*) Nd123; (*6*) Y123 doped with ^{235}U and irradiated with slow neutrons and (*7*) thin films.

the reason why the demands imposed on the state of the intercrystallite boundary are so severe.[9–11] The situation is complicated by the fact that, because of the specific layered structure, almost all high-temperature superconducting phases possess a very high crystallographic anisotropy of physical properties, which requires texturing of the polycrystalline material.[11]

Additionally, HTSC are type II superconductors. In an external magnetic field, they can exist in the mixed state where the magnetic flux partly penetrates the superconductor in the form of the so-called Abrikosov fluxoids.[19] As a rule, the vortex lattice thus formed becomes more stable if extra pinning centres are generated. It is assumed that each pinning centre is a distortion of the superconductor structure (a structural defect), the size of which is comparable with the coherence length.[11,19] Generation of efficient pinning centres in high-temperature superconducting materials is necessary since the practical use of HTSC in the heavy-current devices requires not only high critical current densities, but also enhanced current stability in external magnetic fields.

Table 2. The Ginsburg–Landau parameters of the HTSC $YBa_2Cu_3O_z$-phases (T_c = 92 K).[19]

Parameter	Calculation	Experiment	BCS [a]
Anisotropy			
$k_{\|\|ab}$	74	–	–
$k_{\perp ab}$	2750	–	–
k_{av}	245	–	150
Coherence length /nm			
$\zeta_{\|\|ab}$	1.2	–	–
$\zeta_{\perp ab}$	0.2	0.3	–
ζ_{av}	0.7	0.7	0.9
Landau's penetration depth /nm			
$\lambda_{\|\|ab}$	89	–	–
$\lambda_{\perp ab}$	550	–	–
λ_{av}	160	140	134
Critical magnetic field /mT			
$H_{c1}(\perp ab)$	90	95–110	–
$H_{c1}(\|\|ab)$	21	24	–
$H_{c1}(0)$	1.0	–	1.1
$-dH_{c1}/dT$ /mT K^{-1}	22	–	19
$-(dH_{c2}/dT)_{av}$ /T K^{-1}	8	–	4.6
$\Delta C/\gamma T_c$ (γ = 18.2 mJ mol^{-1} K^{-2})	2.21	–	2.23

[a] The Bardeen–Cooper–Schrieffer model.

3. Chemical behaviour

The preparation of modern high-temperature superconducting materials encounters considerable difficulties due to the complexity of their chemical composition and structure (and, as a consequence, to the thermal and chemical instability).[27] The fact that solid-phase (ceramic) synthesis of superconducting cuprates is simple and rapid, as well as giving a first preparation of defect-free (according to visual inspection) as-grown small single crystals only gave the deceptive impression that most problems had been left behind. However, conventional methods of solid-phase synthesis of HTSC appeared to be inefficient for the preparation of materials with the desired properties. Because of this, the development of melt solidification methods[6–11] has begun. These methods are based on melt crystallisation under controlled conditions, which allows a complex treatment of the real structure of the material. It should be noted that almost all HTSC are characterised by incongruent melting and their melts are multicomponent heterogeneous (containing both gaseous and solid phase along with the melt) open systems (participating in oxygen exchange with environmental gases), shifted apart from thermodynamic equilibria.

This can be exemplified in the family of high-temperature superconductors, *viz*., $RBa_2Cu_3O_z$ phases (R123-phases, R is a RE element) studied in most detail. These complex cuprates are composed of such chemically different components as stoichiometric (with respect to oxygen) high-melting oxides of alkaline-earth and RE elements (BaO and R_2O_3) and a low-melting 'acidic' oxide of a transition metal (copper) in different oxidation states. As a result, the problem arises of oxygen nonstoichiometry, which requires consideration of the phase diagrams for quaternary $R_2O_3-BaO-CuO_n-O_2$ systems with complicated 'pO_2–temperature–composition' relations (especially in the region where the solid and liquid phases coexist) instead of conventional isothermal $R_2O_3-BaO-CuO$ phase diagrams. In addition, RE-element-for-barium substitution solid solutions can be formed because of rather large ionic radii of 'light' RE elements (La, Pr, Nd, Sm, Eu, Gd); their equilibrium composition in the supersolidus region is determined by the composition of the melt equilibrated with the solid solution.[8] This complicates further the general pattern of phase relations and makes optimisation of the processes of preparation of high-temperature superconducting materials more difficult.

Thus, the main problems are (i) the formation of nonstoichiometric (with respect to both oxygen and cations) solid solutions with a preset composition, the degree of chemical homogeneity (*i.e*., with a particular macroscopic and microscopic distribution of the solution components) and (ii) targeted formation of a real structure of high-temperature superconducting material which provides the desired set of 'structurally sensitive' properties. Accompanying (and sometimes no less important) problems are the investigation of the stability of this type of solid solution including the study of metastable states of high-temperature superconducting phases and their low-temperature decomposition,[7,8] the study of equilibrium phase diagrams of high-temperature superconducting systems,[8–11] the effects of their prehistory and topochemical memory,[39,40] chemical degradation of HTSC,[2,22] procedures for the preparation of superconducting composites,[2,6,13,15,16,23,24] *etc*.

III. Phase diagrams of high-temperature superconductors

Phase diagrams reflect the phase states and phase relations depending on the temperature, pressure and the concentrations of the components in the systems. Therefore, it is reasonable to begin the analysis of efficient methods for the synthesis of metal-

oxide superconductors with the most comprehensively and reliably studied R – Ba – Cu – O systems in order to demonstrate general principles of the use of phase diagrams for the preparation of high-temperature superconducting materials. Investigations into the phase diagrams of a promising and technologically important Nd – Ba – Cu – O system,[7,8,16] which exhibits the salient features of the phase diagrams of cuprate superconductors in the supersolidus region seem to be the most interesting.

1. Subsolidus phase relations

a. Geometrical factors and phase stability

Most superconducting compounds are thermodynamically stable only in narrow ranges of temperature and partial pressure of oxygen; many of them are metastable under storage and operating conditions. Therefore, one can hardly find high-temperature superconductors (especially, among the last-generation materials) free from dopants stabilising their structure. As a rule, superconducting complex oxides are solid solutions with fairly wide homogeneity regions and comprise several elements with close crystallochemical characteristics. Internal structural strain is naturally relieved due to the difference in the ionic radii of the constituent elements.[2,17,18,36] 'Chemical' deformation of the crystal structure of superconductors due to doping, as well as that caused by external pressure, can lead to essential changes in the superconductivity parameters due to changes in the distances between the superconducting planes and dielectric blocks and/or to the charge redistribution between them.[41–45] Because of this, the consideration of geometrical factors seems to be of great importance. The following types of substitution affecting the properties of high-temperature superconducting phases and the phase relations in high-temperature superconducting systems can be distinguished, (i) variation of RE elements (R) in R – Ba – Cu – O systems; (ii) Bi/Pb substitution in bismuth-containing HTSC; (iii) Hg/Pb, Hg/Re and Ba/Sr substitutions in mercury-containing HTSC;[36,46,47] (iv) substitutions of alkaline-earth cations in binary and ternary cuprates; and (v) fluorination of $RBa_2Cu_3O_{z-y}F_y$ phases.[48]

The simplest method for assessing the stability of oxide superconductors is based on the well-known Goldschmidt criterion for tolerance, according to which a perovskite-like structure $ACuO_3$ is stable [2] if $0.8 < t < 1$, where

$$t = \frac{r_A + r_O}{\sqrt{2}(r_{Cu} + r_O)}$$

and r are the ionic radii of the elements constituting the crystal lattice. The use of different REE is the most prominent example and important method of chemical modification of HTSC, since the radii of R^{3+} cations with close chemical properties monotonically decrease due to the effect of lanthanide contraction. Along with the differences in the magnetic moments of R^{3+} ions, energies of their stabilisation by the ligand crystal field and possible oxidation states (+4, +3 or +2), the above-mentioned geometrical factor provides an additional degree of freedom in the synthesis of superconducting phases.

Currently, almost all RE analogues of $YBa_2Cu_3O_z$ have been synthesised by isomorphous substitution of yttrium.[7,12,18,22] As has been mentioned above, the unit cell of the $RBa_2Cu_3O_z$ phase can be represented as three perovskite-like blocks containing barium or yttrium ions at the centre (see Fig. 2). Phases of the $RBa_2Cu_3O_z$ type are characterised by two oppositely directed effects,[49] *viz*., by structure stabilisation towards simple oxides due to the coordination of barium ions and the formation of BaO_{10} polyhedra and by structure destabilisation owing to the formation of RO_8, CuO_4 and CuO_5 polyhedra. Small ionic radii (R^{3+}) of 'heavy' REE and yttrium result in the 'repulsion' of oxygen ions in a smaller polyhedron (RO_8) and generation of steric hindrances. Almost no structure destabilisation effect is observed for 'light' REE with the largest ionic radii (Nd – Gd) in the case of isomorphous isovalent replacement of the yttrium ion by its RE analogues.

The oxygen content, which affects both the concentration of the charge (hole) carriers in superconducting CuO_2 planes and the average Cu – O bond length, is the second factor influencing the stability of high-temperature superconducting phases with the $YBa_2Cu_3O_z$ structure. It is noteworthy that the estimates of both the lower and upper limits of thermal stability of the phases under consideration [50,51] suggest that tetragonal non-superconducting modifications ($RBa_2Cu_3O_6$) are more stable than the orthorhombic superconducting phases characterised by higher content of oxygen ($RBa_2Cu_3O_7$) and 'holes'. The decrease in the thermal stability of solid solutions with partial substitution of REE cations for barium cations in the structure, in which the average oxidation state of copper increases in parallel to the increase in the degree of heterovalent substitution, is an additional confirmation of this hypothesis.

The two above-mentioned structure destabilisation factors should also be taken into account when analysing the 'geometrical' stability of bismuth-containing superconducting cuprates (see Fig. 2*b*).[52] In these systems, almost all the most important phases are non-stoichiometric compounds with respect to all of the components. According to the data reported,[53–55] the superconducting phase of the $Bi_2Sr_2CaCu_2O_z$ type (2212-phase) is Bi-excessive and (Ca + Sr)-deficient and the 'ideal' 2 : 2 : 1 : 2 composition seems not to be a single phase. The reasons for the existence of such a wide homogeneity region can be [53] (i) isomorphous substitution of calcium ions for strontium ions [56] and, to a lesser extent, partial hetero-valent substitution of strontium and calcium ions for bismuth ions; (ii) the formation of intergrowth structures with higher and lower homologues containing different amounts of calcium and copper and (iii) exchange between the crystallographic positions of bismuth and copper atoms due to the packing faults of the layered structure. Compared to $RBa_2Cu_3O_z$ phases in which the dielectric 'barium' block exhibits a fairly high 'geometrical' stability, the dielectric Bi_2O_2 blocks can additionally contribute to the structure destabilisation.

A formula was proposed [52] for assessing the relative stabilisation of bismuth-containing HTSC with extra oxygen and with lead ions which replace bismuth ions in the structure

$$\frac{t}{t_0} = 1 + \left(\frac{\alpha}{y_0} + \frac{2\gamma}{nz_0}\right)\delta + \left(\frac{\beta}{y_0} + \frac{\gamma}{nz_0}\right)x\,.$$

Here t is the parameter of the criterion for 'geometrical' stability of a bismuth-containing high-temperature superconducting phase doped with lead and containing extra oxygen, t_0 is the analogous parameter for a 'pure' bismuth-containing high-temperature superconducting phase, α, β and γ are constants, n is the number of superconducting CuO_2 planes, δ is the amount of extra oxygen and x is the degree of lead-for-bismuth substitution.

It was assumed [52] that the length of the 'in-plane' Bi – O bond is determined by the relationship

$$y = y_0 + \alpha\delta + \beta x\,,$$

whereas the Cu – O(2) bond length is determined by the relationship

$$z = z_0 - \gamma h\,,$$

where h is the concentration of 'holes'. According to calculations, the highest stabilisation of superconducting structure (especially at large n, *i.e*., for higher members of the homologous series) can be achieved, as in the case of 123-phases, if the internal structural strain is relieved by doping the oxide matrix with cations with large ionic radii (in this case, by doping with lead ions in the Bi_2O_2 block).

The virtually planar structure of the CuO_2 layers [35,36] is a possible reason for the record transition temperatures to the

superconducting state for mercury-containing HTSC. Therefore the geometrical factors can directly affect fundamental superconducting characteristics of a system. Schematically, the structure of $HgBa_2Ca_{n-1}Cu_nO_{2n+2+\delta}$ phases can be represented as $(HgO_\delta)(BaO)(CuO_2)\cdot[(Ca)(CuO_2)]_{n-1}(BaO)(HgO_\delta)$ layers stacked along the c axis of the unit cell.[36] These compounds have primitive tetragonal unit cells in which the parameter c increases as the thickness n of the perovskite fragment c (Å) = 9.5 + 3.2(n−1) increases.

The coordination of the copper atoms in CuO_2 layers varies from octahedral in the Hg1201-structure to tetragonal-pyramidal in the Hg1212-phase and to the square and tetragonal-pyramidal in the Hg1223-phase as the thickness of the perovskite fragment increases. The octahedra and tetragonal pyramids are appreciably elongated along the c axis due to Jahn–Teller distortion. Long Cu−O bonds between the copper atom and the axial oxygen atom and, correspondingly, a very weak interaction between these atoms in the coordination polyhedra of copper are the salient features of the structure of mercury-containing HTSC. On the other hand, a successive increase in the thickness of perovskite fragments owing to the incorporation of additional $CaCuO_2$ blocks results in compression of interatomic planar Cu−O distances in the structures of higher homologues. This can be interpreted as anisotropic 'chemical' compression and results in the distortion of the CuO_2 layers with an increase in n and in corrugation of their planarity. As a consequence, the highest homologues are characterised by lower transition temperatures to the superconducting state. This effect of anisotropic chemical pressure is several times stronger than that caused by external isotropic pressure.[57] Therefore, it can be suggested that the use of non-traditional methods of chemical synthesis (*e.g.*, layer-by-layer epitaxial deposition of thin films on the substrates with specially chosen parameters) rather than conventional isovalent cation substitution resulting in isotropic compression of the structure will be the most promising way for structure modification to achieve higher T_c. The use of these substrates can result in anisotropic deformation of the crystal lattice of a high-temperature superconducting phase.[58]

A limited set of cations which constitute high-temperature superconducting phases along with copper and oxygen atoms is a factor that restricts the search for new superconducting materials. As has been mentioned above, this is associated with the necessity of meeting the conditions of commensurability of interatomic distances and electrical neutrality. The possibility of varying the composition of the anionic sublattice appreciably extends the area of search; this has been exemplified successfully with F^- anions, the crystallochemical characteristics of which are close to those of O^{2-} ions.[48] Incorporation of fluorine into the structure of the non-superconducting oxide $YBa_2Cu_3O_6$ results in its oxidation with the formation of the $YBa_2Cu_3O_6F_2$ phase with T_c = 94 K. In this case, several copper atoms in the structure have an octahedral environment consisting of four fluorine atoms and two axial oxygen atoms. In such a structure, the symmetry of the high-temperature superconducting phase remains tetragonal after oxidation because of the absence of ordering of the anions and oxygen vacancies in the CuO_z plane of the dielectric ('barium') perovskite-like block. An increase in the coordination number of copper atoms is accompanied by strong Jahn–Teller distortion of the $Cu(O,F)_6$ octahedra, which is responsible for the appreciably larger parameter c of the fluorinated phase compared with that of its oxide analogue (12.8–13.2 *vs.* 11.8 Å, respectively).

Geometrical factors also affect the stability of the most important non-superconducting phases in the systems under consideration, in particular, that of binary and ternary cuprates containing RE and alkaline-earth elements.[59–64] For instance, the formation of 'blue' phases of the $Y_2Cu_2O_5$ type (the 202-phase) is characteristic of REE of the yttrium group, whereas 'light' REE with large ionic radii form phases of the La_2CuO_4 type (the 201-phase).[59] 'Green' R_2BaCuO_5 phases with the framework structure, obtained for almost all REE, are stable in air up to 1250 °C.[8,17,59,61] 'Light' REE with large ionic radii form the '422-phases' with composition $R_{4-2x}Ba_{2+2x}Cu_{2-x}O_{10-2x}$ (R = La, Nd),[59,61] which is associated with the formation of brown solid solutions rather than green substances at $0.15 \leqslant x \leqslant 0.25$ for R = La and at $0 \leqslant x \leqslant 0.1$ for R = Nd, the latter being characteristic of the Y_2BaCuO_5 phase.

The changes in the ionic radii of alkaline-earth elements (Ba, Sr, Ca), whose binary cuprates play a special role in high-temperature superconducting systems, also result in essential changes in the phase diagrams.[60,61,63] It is suggested that two cuprates with Ba : Cu ratios of 2 : 3 and 3 : 5 exist in the Cu-rich region of the phase diagram of the BaO−CuO system (see **S.1**).† Like $BaCuO_2$, these cuprates can formally be considered as compounds belonging to the BaO−CuO−'Cu_2O_3' system since they have a rather wide oxygen homogeneity region (see **S.2**). An increase in the temperature and a decrease in the p_{O_2} results in decomposition of $Ba_2Cu_3O_5$ and $Ba_3Cu_5O_8$ with the liberation of CuO and the formation of $BaCuO_2$, which is stable in air up to ~ 1015 °C (at this temperature, the compound melts with the evolution of oxygen).

Barium cuprate Ba_2CuO_3, which is thermally stable at high p_{O_2}, is found in the Ba-rich region of the phase diagram of the BaO−CuO system. Cuprite $BaCu_2O_2$ containing monovalent copper is the only phase stable at reduced partial pressure of oxygen and(or) at high temperatures. The phase relations in the Ca−Cu−O system exhibit some specific features as compared with Sr−Cu−O and Ba−Cu−O systems, which is probably due to the impossibility of calcium ion, which has the smallest ionic radius among alkaline-earth metal cations, to stabilise Cu^{I} and Cu^{III}.[22,23,61] No stoichiometric quaternary compounds were found in the Sr−Ca−Cu−O system, whereas the stability of solid solutions of mixed strontium and calcium cuprates is determined by the temperature and partial pressure of oxygen, as in the case of the Ba−Cu−O system. At high p_{O_2} and moderate temperatures, the cuprate $Sr_{14-x}Ca_xCu_{24}O_{41+\delta}$ is stable. An increase in temperature and/or a decrease in p_{O_2} results in sequential formation of the cuprate phases $Sr_{1-x}Ca_xCuO_2$ (1 : 1) and $Sr_{2-x}Ca_xCuO_3$ (2 : 1) and the cuprite $Sr_{1-x}Ca_xCu_2O_{2+\delta}$ (1 : 2).

Perhaps the most spectacular example of changes in the phase relations caused by geometrical factors is represented by R−Ba−Cu−O systems. There are three main types of quasi-ternary isothermal cuts of the subsolidus phase diagrams of these systems.[62] The simplest type (Fig. 5*a*) is characterised by the presence of a 'point' $RBa_2Cu_3O_z$ phase formed by 'heavy' REE of the yttrium subgroup with the smallest ionic radii (Y, Dy, Ho, Er, Tm, Yb, and Lu), though the phase relations for Yb and Lu can have some peculiarities due to relative instability of the 123-phases.[63] Solid solutions of the $R_{1+x}Ba_{2-x}Cu_3O_z$ type (Fig. 5*b*) are formed in systems with 'light' REE with large ionic radii (La, Nd, Sm, Eu, and Gd). In these systems, the variation of the composition of non-superconducting (secondary) phases, which play a significant role in the processes of peritectic melting and crystallisation, and of the equilibrium tie-triangles depends on the ionic radii and nature of the REE. The third type of phase relations (Fig. 5*c*), which differs from the two preceding cases in the absence of the phase of the 211/422-type,[61–63] is characteristic of the Pr−Ba−Cu−O system. In the Pr- and Ba-rich region, the Pr123ss phase is in equilibrium with the Pr(IV)-containing phase of the $PrBaO_3$ type. No compounds with the 1 : 2 : 3 stoichiometric composition are formed in systems containing Ce and Tb for which the most characteristic oxidation state is +4.[61]

Systems Bi(Pb)–Sr–Ca–Cu–O, Tl–Ba(Sr)–Ca–Cu–O and Hg(Re,Pb)–Ba(Sr)–Ca–Cu–O are quinary or even septenary, therefore their phase diagrams are extremely com-

† The letter **S** denotes Supplement which contains notes added in proof (the results reported when preparation of the manuscript was completed as well as the results obtained in recent studies and accepted for publication elsewhere).

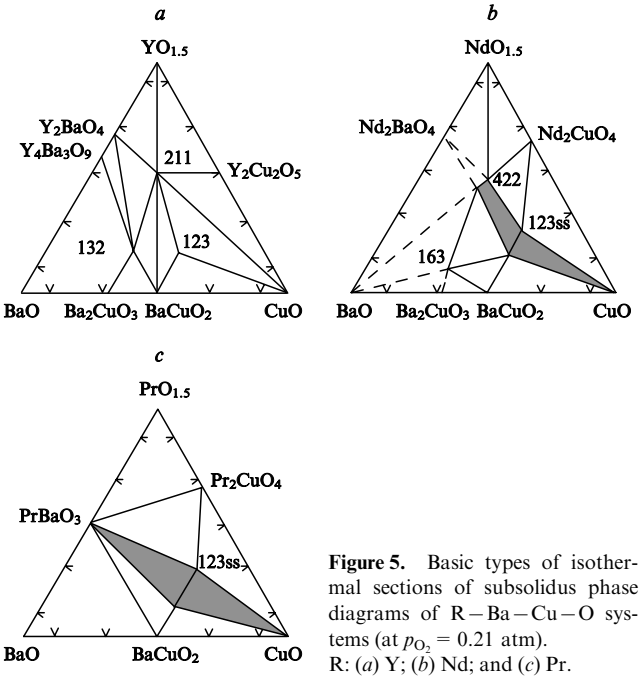


Figure 5. Basic types of isothermal sections of subsolidus phase diagrams of R–Ba–Cu–O systems (at p_{O_2} = 0.21 atm).
R: (*a*) Y; (*b*) Nd; and (*c*) Pr.

plex.[53, 61, 64–69] As a rule, the phase diagrams of these systems are only studied around the stability regions of the high-temperature superconducting phase or analysed using the corresponding software; the most important quasi-binary polythermal or quasi-ternary isothermal cuts (Fig. 6) are also considered.[64]

The phase diagrams of the Tl–Ba–Ca–Cu–O and Hg–Ba–Ca–Cu–O systems (Fig. 7) exhibit strong dependences not only on the partial pressure of oxygen, which is typical of all high-temperature superconducting systems, but also on the total pressure (p_{tot}) determining the partial pressure of the volatile metal component (mercury or thallium).[67, 68] For this reason, conventional methods of preparation of thallium-containing HTSC include 'as-filled' sintering, which provides the possibility of performing the reaction in an atmosphere of a gas enriched with thallium compounds. Moreover, mercury-containing SC are usually prepared in ampoules,[35, 36, 65] at elevated external pressure[36, 57] or in autoclaves at a high pressure of an inert gas atmosphere (argon, nitrogen).[68] However, it was reported[36] that even these methods also do not preclude the formation of mercury-deficient high-temperature superconducting phases with partly vacant mercury positions.[66]

The volatility of metal-containing components further complicates the problem of stabilisation of these structurally complex superconducting phases. If the doping of phases in the Bi–Sr–Ca–Cu–O system with lead oxides can be considered mostly as a convenient procedure for enhancing the formation dynamics of higher homologues of metal-oxide SC,[53, 69] the search for possibilities of stabilisation of the structure of mercury-containing HTSC (*e.g.*, by doping with rhenium,[36, 68] lead and/or strontium[46, 47, 65] compounds) is of prime importance.

b. The problem of low-temperature decomposition

In early studies, metastability of superconducting phases was often considered as the condition for the existence of high-temperature superconductivity;[1, 2] however, the results of modern investigations do not confirm this assumption. Nevertheless, the problem of chemical metastability of high-temperature superconducting phases still remains topical, since this can have both negative and positive consequences from the practical viewpoint. Generally, this is associated with the analysis of the evolution of states of a supersaturated (with respect to one or several components) solid solution under given conditions.

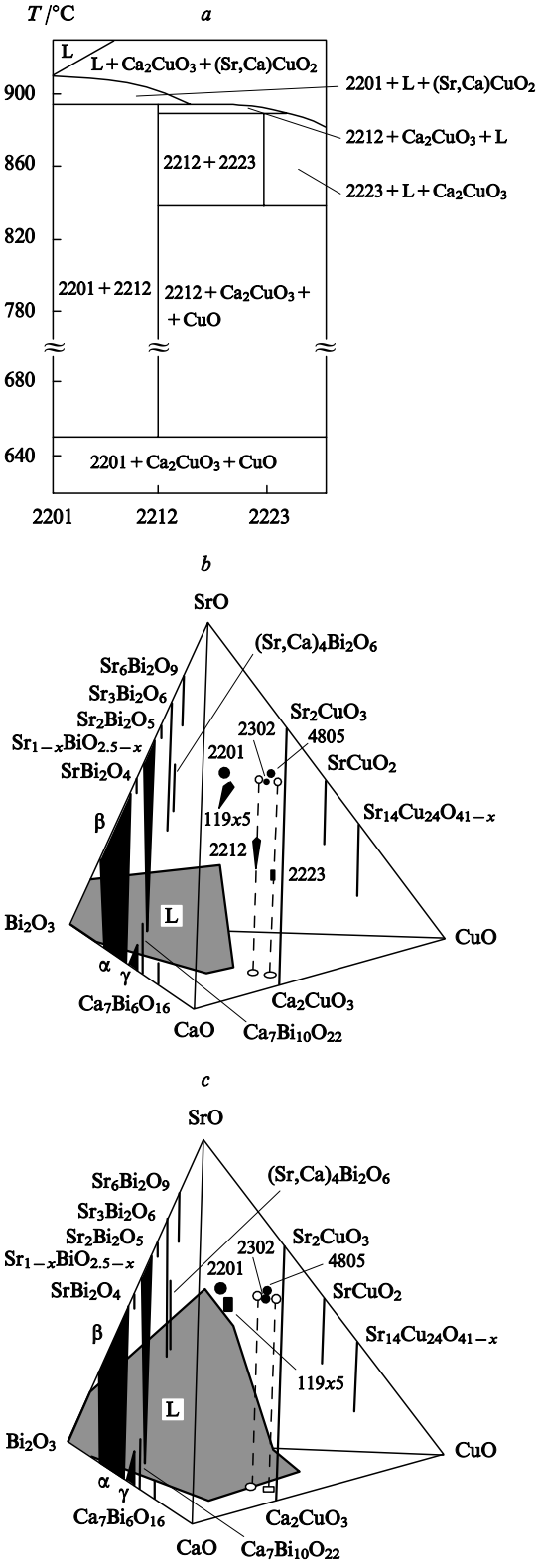


Figure 6. Types of phase diagrams of the Bi–Sr–Ca–Cu–O system (at p_{O_2} = 0.21 atm);
(*a*) polythermal section along $Bi_2Sr_2CuO_6$–$Bi_2Sr_2Ca_2Cu_3O_{10}$; phase relations in a quasi-quaternary system Bi_2O_3–CaO–SrO–CuO at 850 (*b*) and 910 °C (*c*).

Phase relations in systems containing 'light' REE (La, Pr, Nd, Sm, Eu and Gd) are very complicated because of the formation of solid solutions of the $LR_{1+x}Ba_{2-x}Cu_3O_z$ type; difficulties in synthesising several phases of the stoichiometric 123-composi-

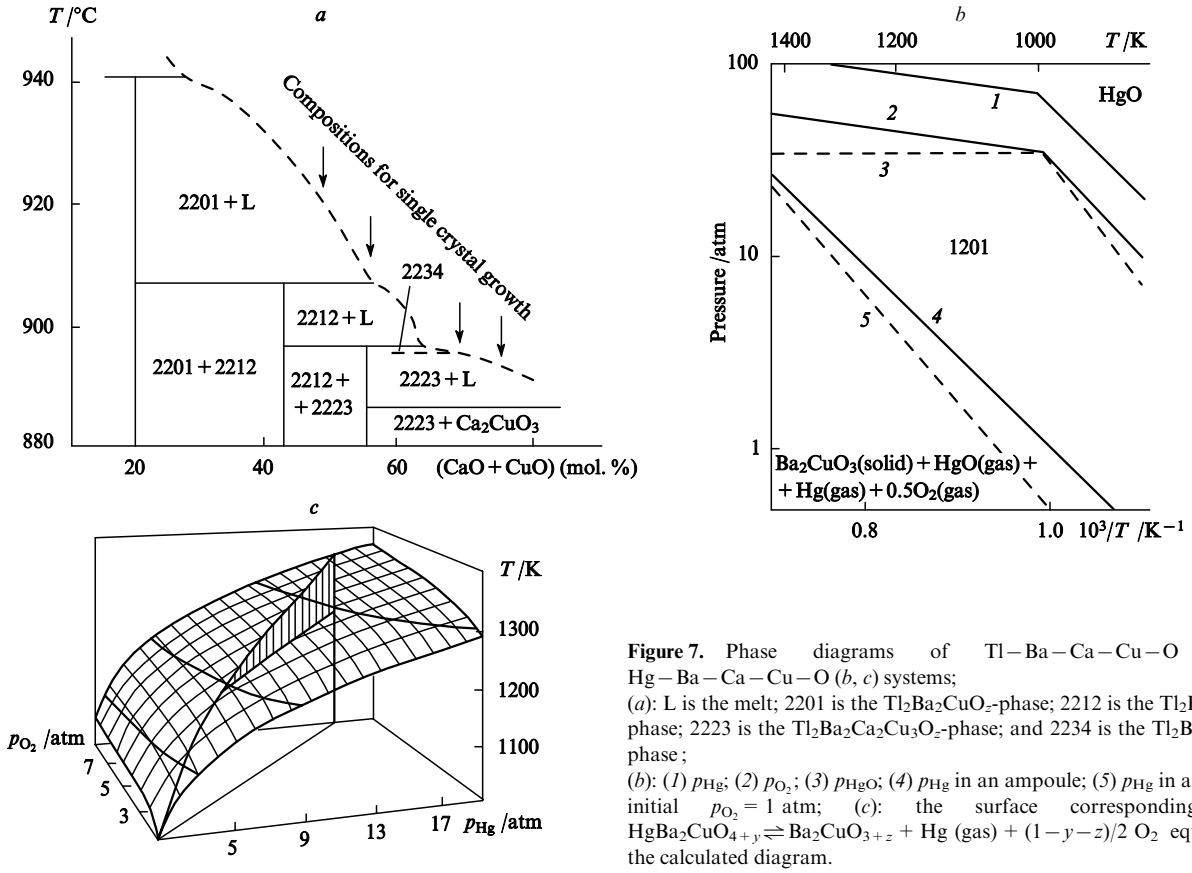


Figure 7. Phase diagrams of Tl – Ba – Ca – Cu – O (*a*) and Hg – Ba – Ca – Cu – O (*b*, *c*) systems;
(*a*): L is the melt; 2201 is the $Tl_2Ba_2CuO_z$-phase; 2212 is the $Tl_2Ba_2CaCu_2O_z$-phase; 2223 is the $Tl_2Ba_2Ca_2Cu_3O_z$-phase; and 2234 is the $Tl_2Ba_2Ca_3Cu_4O_z$-phase;
(*b*): (*1*) p_{Hg}; (*2*) p_{O_2}; (*3*) p_{HgO}; (*4*) p_{Hg} in an ampoule; (*5*) p_{Hg} in an ampoule at initial $p_{O_2} = 1$ atm; (*c*): the surface corresponding to the $HgBa_2CuO_{4+y} \rightleftharpoons Ba_2CuO_{3+z}$ + Hg (gas) + $(1-y-z)/2$ O_2 equilibrium on the calculated diagram.

tion containing REE (La, Nd and Sm) have also been reported.[7,8,70–79] It was shown that the homogeneity region of the $Nd_{1+x}Ba_{2-x}Cu_3O_z$ solid solution becomes narrower near the composition $NdBa_2Cu_3O_z$ as the temperature decreases[75] and near the composition $Nd_2BaCu_3O_z$.[63,76,78–81] In any case, the system becomes thermodynamically unstable as regards solid-phase decomposition in the region of subsolidus equilibria[82] (see **S.3**).

This problem is of interest first of all owing to pronounced variation of the superconductivity parameters of the metastable $R_{1+x}Ba_{2-x}Cu_3O_z$ solid solution depending on its state. Of great importance is also the degree of homogeneity of this solid solution, which depends on the preparation conditions and subsequent heat treatment. For instance, an increase in the parameter x of a solid solution homogeneous at the unit cell level can result in disordering of the oxygen sublattice in the basal plane due to the presence of additional amounts of REE[7,8,76,83–90] and in a reduction of the T_c value. If a solid solution decomposes with the formation of a heterogeneous mixture of particles of different compositions upon heat treatment, a mechanical mixture of phases with individual characteristics will be detected. A nanocomposite in which chemical inhomogeneity exists at a level comparable with the size of tens of unit cells can exhibit a fairly high T_c and nonlinear field dependence of superconducting properties (see Fig. 4).

It was reported that macroscopic phase segregation can occur in an atmosphere of elevated partial pressure of oxygen as a result of decomposition of supersaturated solid solution with the formation of barium cuprate.[76] The specific behaviour of single crystals on heat treatment[8] is most probably due to a fundamentally different mechanism, which manifests itself, in particular, in the formation of a quasi-periodic tweed structure and in quasi-periodic spatial modulations of the ratio of concentrations of the elements constituting the single crystal (the so-called 'compositional waves'). For instance, the Ba : Nd ratio in $NdBa_2Cu_3O_z$ varies from 2.0 to 0.7 (Fig. 8). Spinodal decomposition of the $Nd_{1+x}Ba_{2-x}Cu_3O_z$ solid solution, *i.e.*, its instability towards small fluctuations of x, resulting in phase demixing and eventually in the formation of coherent domains with appreciably different chemical composition, was suggested to be a possible reason for these changes.[8] Reduction of temperature enhances the driving force of decomposition; however, its rate can be low because of extremely slow diffusion of components (the maximum rate of the process was experimentally observed at ~ 500 °C, see also **S.3**). The possibility for spinodal decomposi-

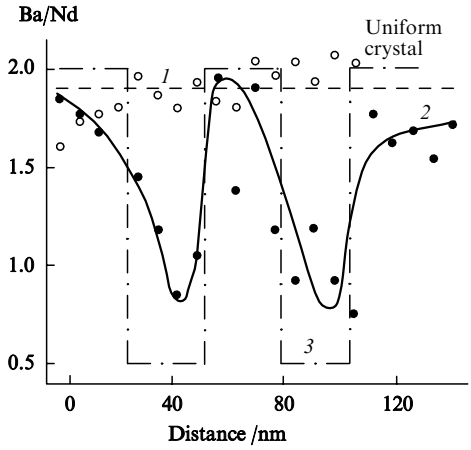


Figure 8. Quasi-periodic nanoscale fluctuations of the composition of $NdBa_2Cu_3O_z$ single crystals after low-temperature treatment at $p_{O_2} = 1$ atm.
The composition of crystal matrix without nanoscale fluctuations (*1*, open circles) and with nanoscale fluctuations (*2*, filled circles); (*3*) variations of composition that should be observed upon the formation of interphase boundaries between the particles of decomposition products and the crystal matrix into which they are incorporated.

tion to occur was inferred from the experimental results obtained for the specimens prepared by zone melting [91] and large-grain ceramics;[70,92] it was also postulated (based on the data on the equilibrium phase diagrams [80]) for a model of a regular-type solution with a high positive energy of interaction between the components (~ 40 kJ mol^{-1}).

Structurally, the segregation of a $Nd_{1+x}Ba_{2-x}Cu_3O_z$ solid solution can be represented as a local change in the occupation of the barium sites in the $NdBa_2Cu_3O_z$ structure, which results in the ordering of Nd^{3+} and Ba^{2+} ions in the BaO layer. The macroscopic picture of this phenomenon can be considered using the results of studies of the structure and properties of the $Nd_{1+x}Ba_{2-x}Cu_3O_z$ solid solution with a different degree of substitution (x).[76,78,89,90] This substitution has two salient features. First, it is hetero-valent ($Nd^{3+} \rightarrow Ba^{2+}$, the 'hole' redistribution in the structure); second, this leads to the substitution of a smaller neodymium ion for larger barium ion (the ionic radii are 1.11 and 1.35 Å, respectively; internal 'chemical pressure').

The entropy of mixing of an ideal solution based on the $NdBa_2Cu_3O_z$ phase and a hypothetical compound $NdNd_2Cu_3O_z$ should be maximum for the composition $NdBaNdCu_3O_z$ (the Nd213-phase) (Fig. 9). Therefore, from the viewpoint of the entropy factor, the formation of a continuous series of $Nd_{1+x}Ba_{2-x}Cu_3O_z$ solid solutions with statistical distribution of Nd^{3+} and Ba^{2+} ions at the barium positions is the most favourable up to $x = 1$. However, the thermal stability of such a solid solution decreases as the degree of substitution x increases, *i.e.*, compression of the structure can result in a decrease in the formation energy of the crystal lattice due to the internal steric strain.[76–81] The formation of the solutions with $x > 1$ is unfavourable both from the viewpoint of energy factors and because of the decrease in the contribution of the entropy of mixing.

Such an approach makes it possible to consider the solutions with $x = 1$ as a 'boundary' between real and hypothetical solid solutions. If the contributions of the entropy and energy factors are close, a distortion (puckering) of planar fragments of the structure can occur at $x \approx 1$, resulting in a new type of atomic ordering and in a reduction of the symmetry of the structure.[78,89,90] Despite the fact that such a structural transition results in a decrease in the entropy of the system, a gain in the free energy owing to the increased energy of the lattice formation can be obtained in the case of partial relief of internal strain caused by the 'chemical pressure'. Therefore, different types of cation ordering can be observed within the homogeneity region of the $Nd_{1+x}Ba_{2-x}Cu_3O_z$ solid solutions, which is also accompanied by changes in the oxygen sublattice.

The results of investigations of the $Nd_{1+x}Ba_{2-x}Cu_3O_z$ solid solution ($0 \leqslant x \leqslant 0.9$) by X-ray difraction (XRD) and Raman spectroscopy (RS) are shown in Fig. 10.[89,90] The range of variation of x may conventionally be divided into three intervals, *viz.*, $0 \leqslant x \leqslant 0.3$, $0.3 \leqslant x \leqslant 0.6$ and $0.6 \leqslant x \leqslant 0.9$.[76] The specimens for which the degree of substitution x varies within the first interval have tetragonal or orthorhombic crystal lattices; the unit cell parameters a and $c/3$ ($a < c/3$) regularly decrease due to replacement of the Nd^{3+} ions of a smaller radius for the Ba^{2+} ions. The unit cell of the tetragonal phase ($a = c/3$) of the solid solution with x values within the second interval is characterised by an 'isotropic' compression of the unit cell, which occurs as x increases. An orthorhombic distortion of the unit cell is observed for compositions within the third interval. This distortion is retained even in the high-temperature region.[81,89]

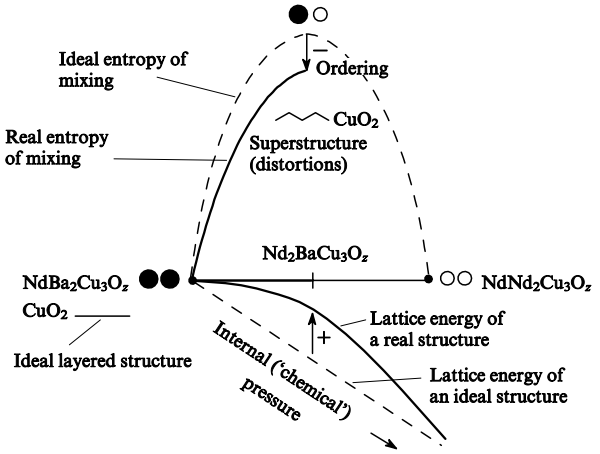


Figure 9. The effect of chemical pressure on the change in the structure of $Nd_{1+x}Ba_{2-x}Cu_3O_z$ solid solution.

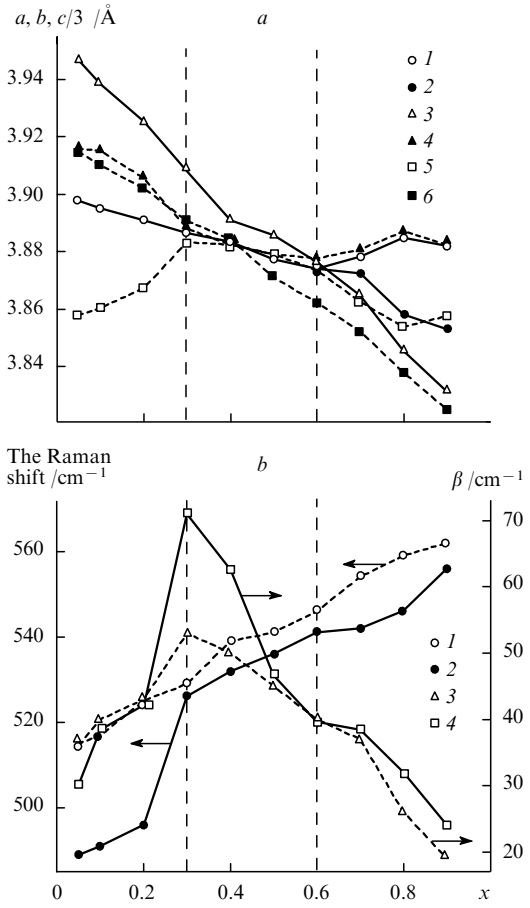


Figure 10. Results of investigations of $Nd_{1+x}Ba_{2-x}Cu_3O_z$ solid solutions by X-ray diffraction (*a*) and Raman spectroscopy (*b*);
(*a*): unit cell parameters: (*1* and *4*) *a*; (*2* and *5*) *b*; (*3* and *6*) *c*/3; (*1–3*) quenching; (*4–6*) oxidation; (*b*): (*1* and *2*) the Raman shift; (*3* and *4*) broadening of an apical oxygen vibration mode (β); (*1* and *3*) oxidation; (*2* and *4*) quenching.

It was established in structural studies [76,78,89,90] that the 123- and 213-phases ‡ are characterised by different types of ordering of the Nd^{3+} and Ba^{2+} cations, namely, 'vertical' ordering with the formation of uniform cation layers (Fig. 11) occurs in the former, whereas 'horizontal' superstructural ordering of barium ions and neodymium ions which replace the barium ions occurs in the latter. The appearance of a structure consisting of alternating chains of barium ions and those of neodymium ions that occupy the barium positions predetermines the ordering of oxygen ions. One of the oxygen positions along the shortest axis (*b*) in the high-temperature orthorhombic modification of the 213-phase is only partly occupied. Ordered rows of CuO_5 pyramids could be formed

‡ In the phase diagram, they are terminating points of the existence region of solid solutions.

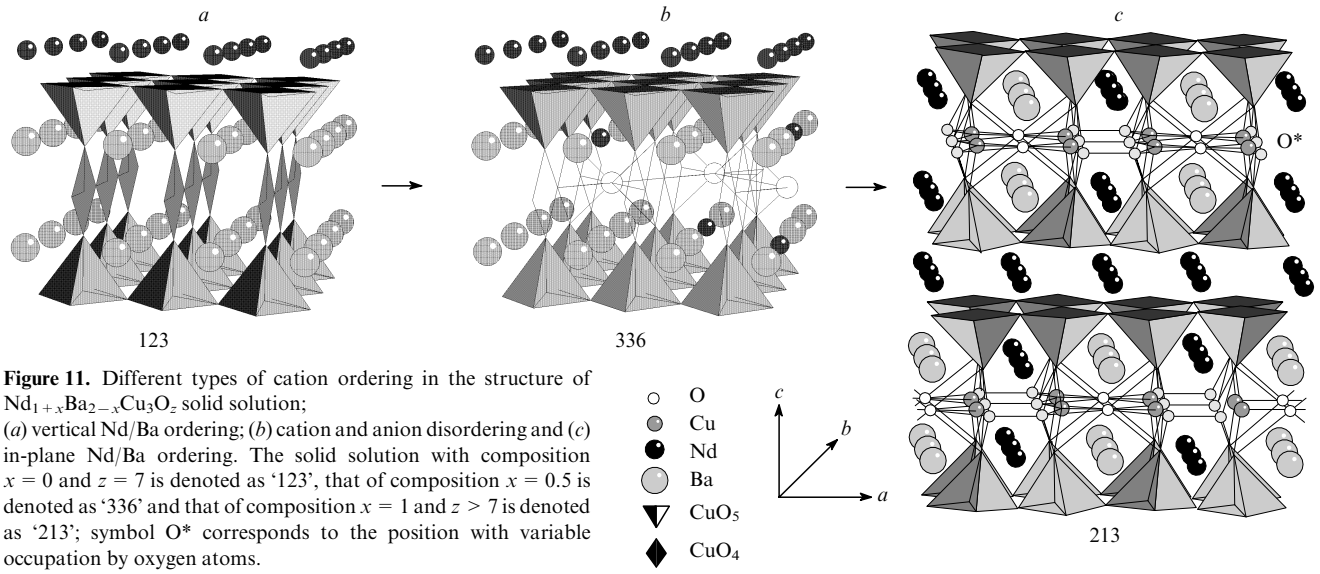


Figure 11. Different types of cation ordering in the structure of $Nd_{1+x}Ba_{2-x}Cu_3O_z$ solid solution;
(*a*) vertical Nd/Ba ordering; (*b*) cation and anion disordering and (*c*) in-plane Nd/Ba ordering. The solid solution with composition $x = 0$ and $z = 7$ is denoted as '123', that of composition $x = 0.5$ is denoted as '336' and that of composition $x = 1$ and $z > 7$ is denoted as '213'; symbol O* corresponds to the position with variable occupation by oxygen atoms.

in the 'former' [BaO] block in the ideal (most oxidised) structure; however, a more complicated superstructural ordering in the real low-temperature orthorhombic modification of the 213-phase is observed. The temperature dependence of the oxygen content has an apparent sigmoid shape, which probably reflects this structural transition (at 700 – 720 °C in air [89]) (see **S.4**).

The solid solution of intermediate compositions ($0.3 < x < 0.6$, the 336-phase) is tetragonal. Unlike the 123-phase, the 'vertical ordering' in this phase is distorted and a fraction of additional neodymium ions occupies the barium positions. At the same time, 'horizontal' ordering of cations in the barium positions does not occur yet in the 336-phase, which differentiates this phase from the 213-phase and results in disordering of the cationic sublattice.[84 – 90] A maximum on the curve of the dependence of apical oxygen mode broadening in the Raman spectra on the composition of solid solution (see Fig. 10) corresponds to disordering of the oxygen sublattice.[90] It should be noted that analogous structural transformations result in changes in the hole distribution,[84, 87] which also pertains in greater degree of substitution in solid solutions. In this case the hole concentration in the superconducting CuO_2 planes decreases (the average, 'collective' charge of the plane decreases), whereas the average oxidation state of the copper atoms in the CuO_y plane of the dielectric (Nd,Ba)O block increases (see **S.5**).

Phase 'separation' of HTSC is a common phenomenon, which should be taken into account when analysing the phase relations in all the systems in question. For instance, it was postulated [93] that nonuniformity of oxygen distribution in the Y123-phase at a microscopic level is due to the spinodal decomposition. Low-temperature annealing of a single-phase solid solution $(Bi,Pb)_2Sr_2CaCu_2O_z$ in the preparation of a bismuth-containing 2212-phase enriched with lead [94] resulted in its solid-phase decomposition with the formation of a lamellar nanostructure with alternating domains enriched with and depleted of lead. This decomposition should be extremely slow because of the low rate of cation diffusion, the necessity of overcoming the energy barriers associated with the formation of a solid-solid interface and elastic deformation of the matrix for phases with different molar volumes and crystal structure.[8, 75, 82] In accordance with the Ostwald rule, the degree of supersaturation of a solid solution can be partially reduced in several intermediate steps, where a coherent or semi-coherent interface is formed in the matrix of the initial phase rather than requiring that the energy barrier to hetero-phase nucleation of a new phase is to be overcome. Differences in the lattice parameters of solid solutions of different compositions give rise to local structural strain.[75]

Obviously, this problem requires studies of the initial stages of phase decomposition ('ageing' of the supersaturated solid solution) and construction of the so-called TTT (Time – Temperature – Transformation) diagrams for different initial states of solid solutions (ceramics, single crystals, films) as in the case of many alloys used in metallurgy.[82] Mention may be made that solid-phase decomposition of HTSC can significantly improve certain practically important characteristics; in particular, this can be used for targeted formation of microscopic structural defects capable of acting as efficient pinning centres.[7, 8, 94]

2. Phase relations in the supersolidus region

a. The use of the Gibbs phase rule

Experimental studies of phase relations in the supersolidus region and the development of realistic models of phase diagrams which fulfil the Gibbs phase rule are necessary for devising efficient methods for the preparation of high-temperature superconducting materials.[8, 9, 53, 61, 64, 74, 75, 95]

Experimental data on complex cuprate systems which would allow reliable calculation of the phase diagrams are extremely insufficient. Often, experimental phase diagrams (especially in the supersolidus region) are reported as being 'schematic' or 'tentative' ones, since they do not often fulfil the Gibbs phase rule. Nevertheless, several basic and doubtlessly reproducible characteristics (*e.g.*, melting temperatures and eutectic compositions) that are of great importance can be distinguished.[61, 95] The Y – Ba – Cu – O, Nd – Ba – Cu – O and Bi – Sr – Ca – Cu – O systems are a few examples of comprehensively studied high-temperature superconducting systems for which three-dimensional [78, 81, 96, 97] or multidimensional [64] models have been proposed for the description of phase relations.

Numerous experimental studies [96 – 108] and reviews [13, 21, 22, 63, 100 – 102] have been devoted to the investigation and description of the phase diagram of parent Y – Ba – Cu – O system containing the high-temperature superconducting Y123-phase characterised by a very narrow cation homogeneity region. In particular, ~ 11 invariant reactions involving the melt (L) were found in the phase diagram of this system in the supersolidus region,[96] *e.g.*,

$$YBa_2Cu_3O_z + BaCuO_2 + CuO \rightleftharpoons L$$

(a ternary eutectic at 890 °C with the liquid phase composition $Y : Ba : Cu \simeq 1.0 : 32.5 : 66.5$),

$$BaCuO_2 + CuO \rightleftharpoons L$$

(a binary eutectic at 910 – 920 °C, ~ 69 mol. % – 71 mol. % of CuO),

$$YBa_2Cu_3O_z + CuO \rightleftharpoons Y_2BaCuO_5 + L$$

(near 940 °C with the liquid phase composition Y : Ba : Cu ≃ 2.0 : 23.0 : 75.0),

$$BaCuO_2 \rightleftharpoons L$$

(at ~1015 °C) and the peritectic decomposition reaction at 1000 – 1015 °C

$$YBa_2Cu_3O_z \rightleftharpoons Y_2BaCuO_5 + L. \quad (1)$$

However, it should be noted that the peritectic decomposition temperature (T_p) of the Y123-phase appreciably decreases at low partial pressure of oxygen [8, 13, 100, 107] and increases at high pressure of oxygen (1 – 3000 atm), the phase relations in the system being changed in the latter case.[108] In both cases, the mechanism of decomposition of the 123-phase is also changed. Therefore, the simplified consideration of reaction (1) is incorrect. The peritectic decomposition reaction should be written as

$$HTSC \rightleftharpoons L + S + O_2, \quad (2)$$

where S and O_2 denote the melt, 'secondary' solid phases and the gaseous phase (oxygen), respectively.

Therefore, the $Y_2O_3-BaO-CuO-O_2$ system should be considered as a quaternary system for which four phases (two solid phases, one liquid and one gaseous phase) are in equilibrium at the peritectic decomposition point of $YBa_2Cu_3O_z$. Obviously, such an approach makes it possible to fix the partial pressure of oxygen in the gas phase (p_{O_2} = const). An assumption can be made which is useful in studying many high-temperature superconducting systems that the gas phase consists of the only component (oxygen) and, therefore, the total pressure $p_{tot} = p_{O_2}$. This is incorrect in the case of thallium- and mercury-containing HTSC (see above). Hence, the transformation (2) can be conditionally considered monovariant at $p_{tot} = p_{O_2}$ = const. In fact, a particular temperature of 'melting' (decomposition) of the 123-phase at fixed partial pressure of oxygen in the gas phase is observed, since it is necessary to introduce an additional condition (the cation stoichiometry), which imposes restrictions on the composition of the solid phase which undergoes decomposition.

This assumption is also valid if the decomposition of a solid solution follows the scheme [76 – 81]

$$Nd_{1+x}Ba_{2-x}Cu_3O_z \rightleftharpoons Nd_4Ba_2Cu_2O_{10} \text{ (or } Nd_2CuO_4) + L + O_2. \quad (3)$$

A substitution solid solution virtually degenerates into the stoichiometric 123-phase ($x \to 0$) at temperatures near peritectic melting. If both the cation composition (x) of the phase that undergoes decomposition and the partial pressure of oxygen are fixed, the experimentally determined peritectic decomposition temperature should have a unique value.

Interpretation of phase equilibria in R – Ba – Cu – O (R = Nd, Sm) systems would be incomplete without considering the recently reported data [81] which suggest the existence of a five-phase equilibrium in the Nd-rich corner of the phase diagram.

$$Nd_2Ba_1Cu_3O_z + CuO \rightleftharpoons Nd_2CuO_4 + L + O_2. \quad (4)$$

Obviously, this equilibrium is invariant at fixed p_{O_2} (see **S.6**).

Investigation of bismuth-containing high-temperature superconducting systems also confirms the necessity of considering all restrictions imposed on the system and thus reduce the number of degrees of freedom. As in the case of $Nd_{1+x}Ba_{2-x}Cu_3O_z$ system, the composition of phases that can be in equilibrium with the high-temperature superconducting phase at the point of peritectic decomposition, as well as the corresponding decomposition temperatures differ depending on the stoichiometric ratios of the cations constituting the high-temperature superconducting phase and on the p_{O_2} value in the gas phase. Consequently, the peritectic decomposition products of the Bi2212-phase ($Bi_{2+\delta}Sr_{2-x}$. $.Ca_{1+x}Cu_2O_z$) usually include different bismuthates [CF = $Bi_2(Sr,Ca)_{3+n}O_{6+n}$], alkaline-earth cuprates [AEC = $(Sr,Ca)_nCu_mO_z$] and a melt. Melting and crystallisation of bismuth-containing composites are strongly affected by silver metal used as the sheath of 'long-length' tapes; the solubility of silver metal in the melt can reach up to 4 at. % – 5 at. %.[23, 53, 54, 64] Therefore, the process of peritectic decomposition in this system can be represented as a six-phase equilibrium.

$$Bi2212 + Ag \rightleftharpoons AEC + CF + L + O_2. \quad (5)$$

Practically, it is important that the partial pressure of oxygen changes not only the composition, but also the composition-dependent morphology of particles of the AEC and CF phases which coexist with the melt [23, 54] and, hence, the resulting microstructure of high-temperature superconducting tapes. It is obvious that a simplified analysis of the process (5), *e.g.*, without considering the effect of gaseous atmosphere (O_2) or silver, can lead to failures in developing new procedures for the preparation of bismuth-containing HTSC.

b. The surface of the liquidus

A realistic model of a phase diagram of a system in the supersolidus region is constructed on the basis of determination of melt composition and using the results of an analysis of the composition of the equilibrium solid phases. The solubility of REE oxides in cuprate melts was studied by differential thermal analysis (DTA), the dissolution-extraction method, quenching experiments, the 'last droplet' method, high-temperature microscopy and liquid-phase epitaxy (LPE) and single-crystal growth experiments.[78 – 81, 109 – 116] Unfortunately, in some instances the complexity of peritectic reactions, slow dynamics of establishing a true equilibrium with the gas atmosphere, supercooling of the melt, corrosion of crucibles used and contamination of the melt with impurities can make the results of DTA studies incorrect. The use of a direct melt sampling procedure during the quasi-equilibrium heating and cooling of melt in a temperature-controlled chamber made it possible to appreciably increase statistical representativeness and reliability of the results.[109, 111, 113, 114]

Generally, the solubility of REE oxides in a melt increases with an increase in temperature and partial pressure of oxygen, as well as in the case of REE with large ionic radii and at high copper oxide content.[109, 114] Tendencies of changes in the slope of the liquidus near T_p observed on going to REE with large ionic radii and on increasing p_{O_2} are similar. Practically, of most interest are the solubility of REE oxides and changes in the slopes of the liquidus near T_p, which make possible the prediction of the features of crystallisation in the systems under consideration. For instance, the content of yttrium in the melt at the peritectic decomposition temperature of the Y123-phase increases from 0.4 at. % at p_{O_2} = 0.01 atm (at 985 °C) to 0.6 at. % at p_{O_2} = 0.21 atm (at 1005 °C) and to 0.7 at. % in pure oxygen (at 1030 °C), whereas the neodymium content at T_p = 1086 °C (at 0.21 atm O_2) is several times higher (3 at. %). The content of neodymium in melts with high concentration of copper oxide can differ from that of yttrium by an order of magnitude (~ 7 at. % Nd at 1065 °C in air for the melt with a Cu : Ba ratio of 6 : 1).[109]

Analysis of the solubility curves makes it possible to evaluate several important parameters, *viz*., the dissolution enthalpy of the solid phase (it is determined from the slope of the liquidus),[109, 113 – 115] the peritectic decomposition temperature of the solid phase (it is determined from the bending of the solubility curve, since the dissolution enthalpies of 123- and 211-phases are different),[113, 114] the Gibbs standard energy of a peritectic reaction (when determining the solubility limits at different p_{O_2}).[111]

The dependences of solubility of REE oxides on the 'geometrical' stability of R123-phases, which is determined by the ionic radius of REE, are shown in Fig. 12.[8, 63, 81, 113, 114] As can be seen, the thermal stability of phases, characterised by the peritectic decomposition temperature, and the thermodynamic stability associated with the dissolution enthalpy of the solid phase in a melt increase as the ionic radius of REE increases. The same reason is also responsible for an increase in the ability of the melt to exist in the supersaturated state, since the smaller the slope of

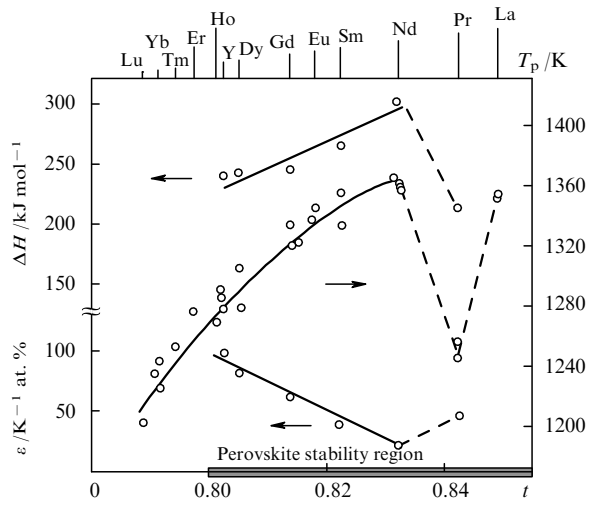


Figure 12. Dependences of thermal (T_p) and thermodynamic (ΔH) stability of $RBa_2Cu_3O_z$-phases on the 'geometrical' stability of their crystal lattices (t) (at $p_{O_2} = 0.21$ atm);
T_p is the peritectic temperature; ΔH is the dissolution enthalpy of R123 in the BaO : CuO = 3 : 5 melt; ε is the slope of the liquidus near T_p, which characterises the tendency to supersaturation; t is the Goldschmidt tolerance factor which reflects the 'geometrical' stability of the lattice.

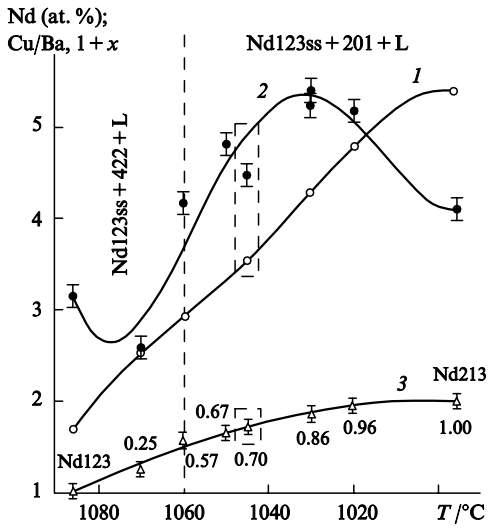


Figure 13. Temperature dependences of the Cu : Ba ratio (*1*), $NdO_{1.5}$ content (*2*) in melt L and the $(1 + x)$ parameter (*3*) of the solid phase of the $Nd_{1+x}Ba_{2-x}Cu_3O_z$ solution coexisting in two-phase '$Nd_{1+x}Ba_{2-x}Cu_3O_z$ + L' equilibrium (at $p_{O_2} = 0.21$ atm). Numbers on curve (*3*) are the values of the parameter x.

the liquidus near the peritectic decomposition temperature, the higher the supersaturation at a given supercooling of the melt and the larger the amount of the substance that can be solidified. As has been mentioned above, these changes are explained by stabilisation of a defect perovskite-like lattice of 123-phases upon introduction of REE ions with large ionic radii (except for praseodymium, which drops out of the common dependence).

Establishment of the composition of the solid phase that is in equilibrium with a given melt is the key problem in the analysis of the liquid phase composition. Obviously — and this is of prime importance — knowledge of the liquid phase composition permits control of the structure and properties of the solid solution that directly depend on its composition. Actually, according to the Gibbs phase rule, the number of degrees of freedom for the '$R_{1+x}Ba_{2-x}Cu_3O_z$ + L + O_2' equilibrium is $4-3+2=3$. Therefore, at a fixed temperature and partial pressure of oxygen, the solid phase composition is unambiguously determined by the melt composition. The dependences, which in combination with the equilibrium phase diagram can be used for predicting the composition of a solid solution with the maximum substitution degree, which can be crystallised from a melt of prescribed composition at a fixed temperature and partial pressure of oxygen, are shown in Fig. 13.[78–81]

Distribution of the neodymium oxide between the solid solution and the melt is the most sensitive parameter of the equilibrium under consideration.[80,81] The maximum on the curve of the content of neodymium oxide in the melt (see Fig. 13) is due to the influence of two oppositely directed factors, *viz.*, an increase in the neodymium content in the melt on an increase in the temperature and simultaneous decrease in the solubility limit of neodymium on the shift of the melt composition towards the BaO-rich region where a more thermally stable, less-substituted solid solution turns to equilibrium. In fact, the curve under consideration is a projection of the spatial trajectory of the point of ternary equilibrium 'Nd123ss – 201 – L' on the 'temperature – composition' plane. The equilibrium melt compositions of the solid solution depleted of and enriched with neodymium are strongly different and are shifted towards the region of Cu-rich compositions (Cu : Ba = 7 : 6 ≃ 5 : 3 for the 123-phase and Cu : Ba = 16 : 3 for the 213-phase). Quantitative analysis of the effects of the liquidus curvature near the '123-phase – melt' equilibrium showed that the substitution $x \simeq 0$ is achieved in the case of crystallisation from melts enriched with barium oxide and on lowering the crystallisation temperature.[79]

c. Characteristic features of polythermal sections

Technologically, the quasi-binary system '$Ba_3Cu_5O_8$' – $Nd_4Ba_2Cu_2O_{10}$ (Fig. 14 *a*) is the most important since the compo-

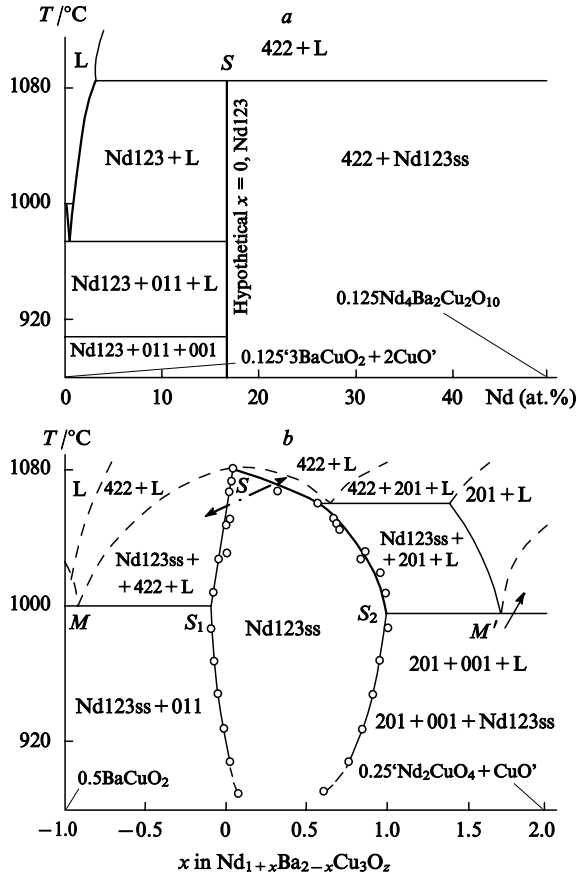


Figure 14. Most practically important quasi-binary polythermal sections of the Nd – Ba – Cu – O system (at $p_{O_2} = 0.21$ atm).

sitional point of the 123-phase belongs to this section. This can significantly simplify the consideration of transformations in this system. Investigations into phase relations in the vicinity of the 123-phase showed that the region of two-phase 'Nd123-phase–liquid' equilibrium in air lies in the temperature range 970–1090 °C (at $p_{O_2} = 0.21$ atm).[110–113]

The region of solid solutions based on the 123-phase belongs to another important $BaCuO_2$–'Nd_2CuO_4–CuO' quasi-binary section (Fig. 14*b*).[63, 76, 78] Invariant transformations involving the liquid phase ($MS_1 \sim 1000$ °C, $M'S_2$, 990 °C) characterise the highest probability of synthesising the solutions with the minimum (S_1) and maximum (S_2) substitution degrees. However, if the reaction with the 213-phase is fairly well studied,[78, 81] it is difficult to carry out quantitative studies of equilibria with the 123-phase because of the very large slope of the solidus in the vicinity of the (S_1) point.[75, 79] It should be noted that the appearance of a liquid in this section with the increase in the temperature near the 123-phase is explained by the melt field propagation towards the $BaCuO_2$ phase. According to the reported data,[78–81] the increase in temperature shifts the composition of the melt which is in equilibrium with 123- and 422-phases away from the point corresponding to barium cuprate because of the extension of the two-phase '422 + L' field. The maximum peritectic decomposition temperature of the 123-phase (S, $\sim$ 1085 °C) is achieved for those compositions that somewhat deviate from the ideal 123-phase (partial substitution of Nd for Ba). This fact is mistakenly ignored in some communications.

The composition of a solid solution with the maximum peritectic decomposition temperature T_p returns almost completely to the 123-composition only after appreciable reduction of the partial pressure of oxygen.[75] For instance, the composition of the solid solution with the maximum T_p is characterised by $x \simeq 0.1$ in oxygen, $x = 0.05$ in air and $x \simeq 0.0$ at $p_{O_2} = 10^{-3}$ atm. No solid solution based on the 123-phase is present in the system above the maximum temperature of peritectic decomposition (the '422 + L' field). Below this temperature, the solid solution region is 'gripped' from both sides by the '422 + Nd123ss + L' three-phase field. At 1060 °C, the '422–Nd123ss–L' tie-triangle becomes geometrically impossible for compositions with $x > 0.6$[81] and a decrease in temperature leads to establishment of equilibrium between the most neodymium-rich solid solution, neodymium cuprate and the melt. The slope of the solidus changes correspondingly.[80] As has been mentioned above, below 990 °C the solid solution is in equilibrium with other two solid phases (CuO and Nd_2CuO_4).

Thus, this type of systems is characterised by the following qualitative features.

1. The region of the solid solutions based on high-temperature superconducting phases can be rather extended. The problems of determining the composition of solutions with the lowest substitution degree and of the existence of solutions with Ba^{2+} substitution for R^{3+} in R–Ba–Cu–O systems (see Refs 7, 63, 76, 117) are poorly studied.

2. The decomposition temperature of a solid solution can vary over a wide range depending on its composition. This is probably associated with the complicated character of the cation ordering within the homogeneity region. The shape of the solidus near the maximum T_p (a sharp or flattened maximum) can provide information on the type of the solid solution, daltonide or berthollide that is formed.

3. As a rule, the reduction of p_{O_2} results in a change in the shape of the homogeneity region of the solid solution. In particular, the decomposition temperature of the solid solution and the slope of the solidus are changed and a narrowing or (more rarely) broadening of the homogeneity region is observed.

4. The compositions of equilibrium phases in the supersolidus region are different, which depends on the composition of the solid solution based on the high-temperature superconductor. Particular emphasis should be placed on quantitative determination of the equilibrium tie-lines in the 'solid solution–melt' two-phase region. Each tie-line is unique; therefore, the choice of a particular compositional point on the phase diagram (all other conditions being constant) determines not only the possible type and weight ratio of the coexisting phases, as in the case of the Y–Ba–Cu–O system, but also the chemical compositions of these phases and, hence, the physical properties of the crystallising solid solution. Determination of the actual chemical compositions of the coexisting phases is also necessary to avoid the errors when constructing the phase diagrams.

5. As a rule, polythermal quasi-binary sections of high-temperature superconducting systems are characterised by certain temperatures of invariant transformation (in this case, at about 1000 °C, see Fig. 14). Below this temperature, liquid phases disappear and the equilibrium between solid phases is established.

6. The narrowing of the homogeneity region can occur below the above-mentioned temperatures. In other words, solid solutions with the highest (lowest) substitution degrees appear to be less stable at both higher and lower temperatures. Analysis of this temperature region is closely related to studies on the decomposition dynamics of supersaturated solid solutions, the formation of a particular nanostructure and to changes in physical characteristics of the system.

3. Melt crystallisation mechanisms

a. Single-crystal growth

Peritectic decomposition is a salient feature of all oxide superconductors, which is due to their multicomponent composition and structural complexity. Crystallisation involves two different phases (the crystal and the mother liquid/melt) separated by a mesophase layer, which is a thin layer of the melt immediately adjacent to the solid phase.[8] The components are transferred from one phase (the 'mother' or nutrient phase) to the other phase (crystal) as this interface moves. In turn, the rate of the process can be limited by the kinetics of deposition of the substance on the crystal face, diffusion of the substance from the surrounding phase as well as by dissipation of the latent heat of crystallisation.

Crystallisation cannot proceed in the absence of the driving force (supersaturation, supercooling or metastability of homogeneous 'mother' phase). In the case of crystallisation from the solution or melt, the driving force is often represented as the relative supersaturation of the melt

$$\sigma = \frac{c_1 - c}{c_1},$$

where c_1 is the equilibrium (under given conditions) concentration in the melt of the component transferred to the solid phase and c is its running value. The region of supersaturated solution is divided into the region of metastability and the labile region. The interface between these regions corresponds to maximum supersaturation in the system that can be achieved until spontaneous crystallisation begins.[8] For the Y123-phase, this region is rather narrow (0.8 °C in air with respect to supercooling).[118]

Investigations of the primary crystallisation field (PCF) are important when considering single-crystal growth. Unfortunately, the PCF boundaries have not been reliably determined yet even for the Y123-phase, though it is obvious that the PCF does not include the melt of the 1:2:3 stoichiometric composition. In different studies, the ratios of barium and copper oxides (Ba:Cu) for PCF were estimated at 17:83–44:56, 24:76–46:54, 18:82–46:54 and 24:76–42:58, whereas the yttrium content (at. % Y) varied in the range 3.0–5.0, 1.0–2.0, 2.0–4.0 and 0.5–3.5, respectively.[13] Crystallisation of the $Nd_{1+x}Ba_{2-x}Cu_3O_z$ solid solution with $x > 0.7$ from the Ba:Cu = 3:12 melt has been reported.[109] The composition of the solid solution changed during isothermal annealing. Artifacts in the determination of the PCF (especially using thermal analysis) often arise because of the absence of local equilibrium with the gas phase; therefore, data on PCF should be interpreted carefully. In some instances, the results of determination of the position of the

liquidus surface should be used instead. The most important problem is the search for chemical additives that extend the PCF and allow the single-crystal growth over wider temperature and concentration ranges. Most often, BaF_2, Bi_2O_3, B_2O_3, Ag and $BaCl_2$ are used as such additives.[13, 119–121]

If a crystal face contacts the metastable 'mother' phase, it can grow. Several main growth mechanisms exist under conditions of fast diffusion of the components of the crystallising substance and the absence of problems with dissipation of the heat of crystallisation.[8] Depending on the driving force of crystallisation, continuous growth (face deposition), 'island' growth due to two-dimensional nucleation and spiral growth along the screw dislocations can be observed.

The last-named mechanism is the most probable for ordinary solution/melt supersaturations; the first two mechanisms are observed very rarely because of the high activation energy of the processes.[8] The 'Terrace-Ledge-Kink' (TLK) growth of the crystal due to the 'sliding' of the crystallising layers of the moving terraces over the surface is also characteristic of high-temperature superconducting materials,[8] whereas renucleation on the defects of the 'two-dimensional angle' type (the so-called 'Twin-Plane-Re-entrant-Edge' or TPRE growth) occurs much more rarely and was detected in high-temperature superconducting systems only recently (Fig. 15).[81] In real systems, the common events are (i) crystal face formation as a result of complex interaction of several crystallisation centres, (ii) combination of several growth mechanisms, (iii) growth due to the formation of macroscopic spirals and terraces, *etc*. Currently, the morphology of growth of the spirals of R123-phases and its dependence on the crystallographic indices of the crystal face,[122, 123] the degree of supersaturation, temperature and the nature of REE are well studied.[124–126]

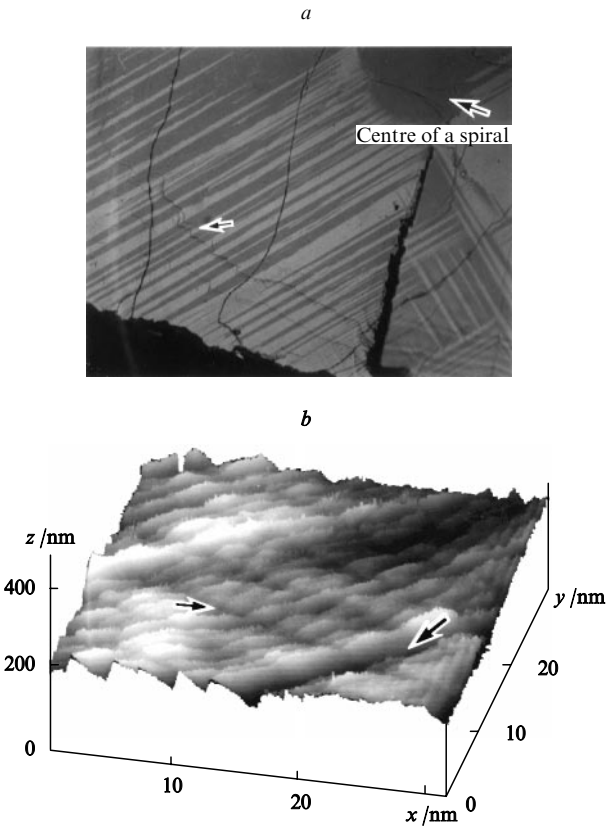


Figure 15. The mechanism of crystal growth in high-temperature superconducting systems (the $Nd_{1.85}Ba_{1.15}Cu_3O_z$-phase) by renucleation on defects of the 'dihedral angle' type (the so-called 'Twin-Plane-Re-entrant-Edge' or TPRE growth);[81]
(*a*) general view of the growing crystal face: twins are crossed by microscopic cracks arisen after thermal shock on detaching the crystal from the melt surface; the crystallisation front of the 'tail' of growth spirals that form a visually observed macroscopic spiral moving along the twinning direction at a higher velocity; (*b*) the structure of twins according to atomic force microscopy data; the twin boundaries are indicated by arrows.

b. Evolution of a polycrystalline system

The behaviour of the peritectic melt § obeys general regularities of crystallisation of an individual crystallite from the homogeneous melt. At the same time, analysis of this system is rather complicated and should be performed with consideration of the interactions between the melt and both the properitectic and gas phases that coexist at the peritectic decomposition point of HTSC. Additionally, the fact that crystallisation of a peritectic melt results usually in the formation of a polycrystalline product should be taken into account.

When polycrystalline HTSC are prepared using melt crystallisation techniques, their microstructure is formed under non-equilibrium dynamic conditions. Hence the problem arises of the search for methods of reproducible preparation of materials comprising well-shaped crystallites with an optimum size and optimum mutual orientation and sufficiently strong intercrystallite contacts. From this point of view, the most interesting is to analyse the regularities of the formation and evolution of an ensemble of crystallites at both small and large deviations of the system from the equilibrium state. Three types of crystallisation models of REE-containing cuprates are known, in which the interaction in the 211-phase–melt subsystem is considered. These are phenomenological models of the interaction between the particles of secondary phases and the melt, computer models of this interaction and mathematical models of propagation of the crystallisation front of the high-temperature superconducting phase and changes in its morphology. The models of REE-containing melt crystallisation with inclusion of interactions in the 'gas phase–melt' subsystem are much less developed.

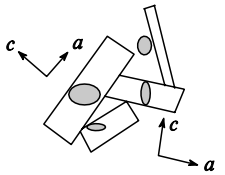
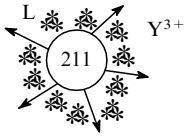
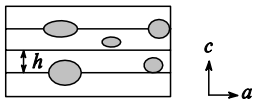
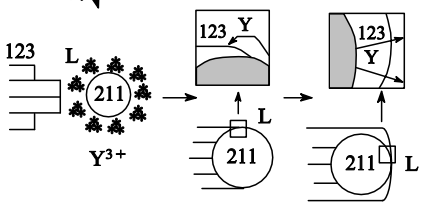
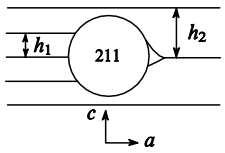
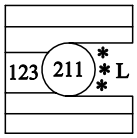
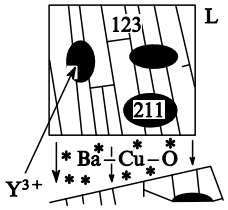
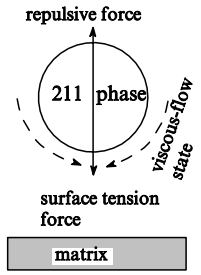
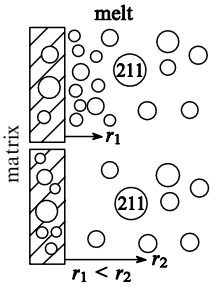
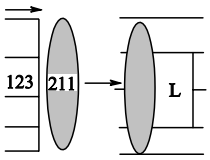
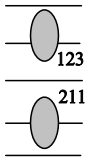
Superconducting phases are mainly formed owing to dissolution in the melt of 'secondary' phase particles, followed by homogeneous formation of the high-temperature superconducting phase in the melt.[8–11, 127–130] In the vicinity of the surface of the particles of the 211-phase, the melt is enriched with yttrium and the crystallites of the $YBa_2Cu_3O_z$ phase are formed near the surface of these particles rather than at the '211-phase–melt' interface. Crystallisation is accompanied not only by 'pushing' large particles of the 211-phase by the growing faces of crystallites of the 123-phase, but also by their trapping by the bulk of the growing crystallites. The formation of crystallites of the $YBa_2Cu_3O_z$-phase is preceded by an induction period, after which crystallisation proceeds in the bulk at an abnormally high rate. Different melt crystallisation models are presented in Table 3.

Mention should be made of considerable interest in the computer simulation of crystallisation processes. Different computer models and simulation concepts are used (*e.g*., 'cellular automata' and diffusion-in-melt models and the phase field concept for multiphase systems, see **S.7**). It can be assumed that solidification of a peritectic melt can proceed in different ways depending on the parameters of the initial state of the melt, which results in the appearance of three different crystallisation regions characterised by particular final microstructure of polycrystalline materials.[127, 128] The provision of stable crystallisation of the superconducting phase owing to stabilisation of the nucleation process is the most important condition for the preparation of high-temperature superconducting materials with high output characteristics.

The experimental proof of this statement was obtained in studies of the doping of melts with REE oxides.[128, 129] The melt

§ Hereafter a 'peritectic melt' is meant a system consisting of a liquid and a solid (high-temperature, properitectic) formed upon peritectic decomposition of the HTSC.

Table 3. Crystallisation mechanisms of peritectic melts.

Model	Morphology of particles of a 211-phase	Proposed scheme of the interaction	Result of interaction	Ref.
Heterogeneous nucleation	any			6
Dissolution in melt and homogeneous nucleation	isotropic (spheres)			6, 8
Edge effects, entrapment of particles of the 211-phase by the crystallisation front	highly disperse particles			9, 11
Formation of 'gaps' and displacement of the melt to grain boundaries on trapping the particles of the 211-phase	large particles			9, 11
'Pushing-and-trapping' of particles of the 211-phase by the crystallisation front [a]	–			8
Dispersion of particles of the 211-phase by the moving crystallisation front	anisotropic particles (needles)			9, 11

[a] The mechanism is determined by particle size, the energy of surface interaction and by the crystallisation rate.

analysed contained ~ 80% of Cu(I), which was confirmed by the results of quenching experiments and chemical analysis,[55, 129] by $BaCu_2O_2$ observation using X-ray phase analysis [13, 129, 131] and by *in situ* measurements of the EXAFS spectra of the melt.[132, 133] Cooling of the melt results in the recovery of the initial oxygen content, which occurs more easily with an increase in the partial pressure of oxygen in the gas phase.

In principle, the transformation Cu(I) → Cu(II) provides a possibility for crystallisation of a non-superconducting phase of barium cuprate $BaCuO_2$ to occur. This is favoured by the presence in the melt of the components necessary for the crystallisation of $BaCuO_2$ and by the fact that the temperature of its crystallisation in air [96] and the crystallisation temperature of the $YBa_2Cu_3O_z$-phase are close. In other words, a 'bifurcation'-like situation occurs in the 211-phase – melt system, which can be followed by crystallisation of either yttrium – barium cuprate $YBa_2Cu_3O_z$ or barium cuprate $BaCuO_2$.[127–129] It is this phenomenon that is observed experimentally. In these cases, the direction of crystallisation depends on many factors (which are often ignored) such as the oxidation rate of the melt during its cooling, the rate of dissolution of the Y_2BaCuO_5-phase in the melt, the partial pressure of oxygen in the system, the gradients of both the temperature and oxygen pressure at the gas phase – melt interface and, finally, the prehistory of the sample and its size. Because of this, small deviations from the empirically established conditions for the synthesis of the $YBa_2Cu_3O_z$ phase immediately result in undesirable formation of non-superconducting cuprate phases even in high-density specimens and in dramatic deterioration of properties of the high-temperature superconducting material prepared.

Crystallisation of the 123-phase can probably be the major process in the system if nucleation begins at a temperature which is higher than the crystallisation temperature of $BaCuO_2$. Superconducting layered yttrium – barium cuprate is the only phase

whose specific crystal structure can be selectively affected by the doping of the melt with REE ions. This makes it possible to experimentally distinguish between the melting temperatures of binary non-superconducting and ternary superconducting cuprates, thus performing targeted crystallisation of the high-temperature superconducting phase from a multicomponent melt.[128, 129, 134, 135]

The general pattern of the process can be changed dramatically upon a decrease in the partial pressure of oxygen in the gas phase. Oxidation becomes the limiting stage of crystallisation in an oxygen-deficient atmosphere.[129, 135] Copper (Cu^{2+}) ions formed upon melt oxidation are bound by the excess R^{3+} and Ba^{2+} ions to form the (R,Y)$Ba_2Cu_3O_z$-phase; however, no rapid crystallisation of the nonequilibrium product (binary barium cuprate) is observed. Thus it can be assumed [55] that the formation of the phase and microstructure of the material are strongly affected by three main factors. These are (i) the total flux of yttrium (REE) ions j_Y from the surface of the 'green-phase' particles to the melt, which is mainly determined by dispersity of the particles and by the surface energy of the interface; (ii) the oxygen flux j_O to the crystallising melt, which depends on both the partial pressure of oxygen in the gas phase and geometric characteristics of the specimen and (iii) the heat flux j_Q evolved from the specimen during its cooling, which is determined by the heat treatment regime.

Thus, the optimum procedure for preparation of high-quality high-temperature superconducting materials should take into account simultaneous and mutually dependent changes in these most important parameters of the process.

4. Oxygen nonstoichiometry of high-temperature superconducting phases

The oxidation stage is of particular importance when preparing, *e.g.*, the $RBa_2Cu_3O_z$ superconductors with a wide oxygen homogeneity region ($z = 0-1$).[1, 2, 8, 13, 17, 22, 50, 100, 108] For bismuth-, thallium- and mercury-containing high-temperature superconducting phases, the homogeneity region is much narrower.[17, 56, 67, 69, 101] On the contrary, several high-temperature superconducting materials [*e.g.*, the 'electron'-type (Nd, Ce)$_2CuO_{4+y}$ HTSC] require annealing in a reductive atmosphere.[2] In all cases, there are strong reasons for detailed investigation of the oxygen nonstoichiometry of HTSC. Here, it is well to bear in mind the following.

1. The oxygen content is correlated with the concentration of charge carriers, whose optimum value provides the maximum T_c value (a T_c 'dome'). 'Underdoped' ('underoxidised') or 'overdoped' ('overoxidised') phases can have a much lower T_c (Fig. 16). In the general case, it is the concentration of the charge carriers localised on particular elements of the structure that determines the physical phase diagram of HTSC (see Fig. 3).[16]

2. Changes in the oxygen content can result in significant changes in the phase stability and in structural phase transitions. For instance, ferroelastic $RBa_2Cu_3O_z$-phases undergo an 'order–disorder' second order phase transition which is accompanied by a tetragonal-to-orthorhombic distortion of the crystal lattice and simultaneous formation of extended twins.[8, 22, 93, 126] The changes in thermodynamic characteristics of high-temperature superconducting phases with different oxygen content can result in the appearance of the low-temperature stability threshold,[50, 51, 75, 106] phase separation in such solid solutions and in nonuniform oxygen distribution over the superconducting matrix.[8, 93]

3. Investigations of oxygen diffusion in high-temperature superconducting phases is not only of practical, but also of theoretical importance since the diffusion coefficient is a 'structurally sensitive' quantity, which depends on the concentration of oxygen vacancies (and, hence, on specific features of the equilibrium $p_{O_2}-T-z$-diagram), their ordering (the crystal lattice symmetry of the high-temperature superconducting phase and second order phase transitions, effects of various types of

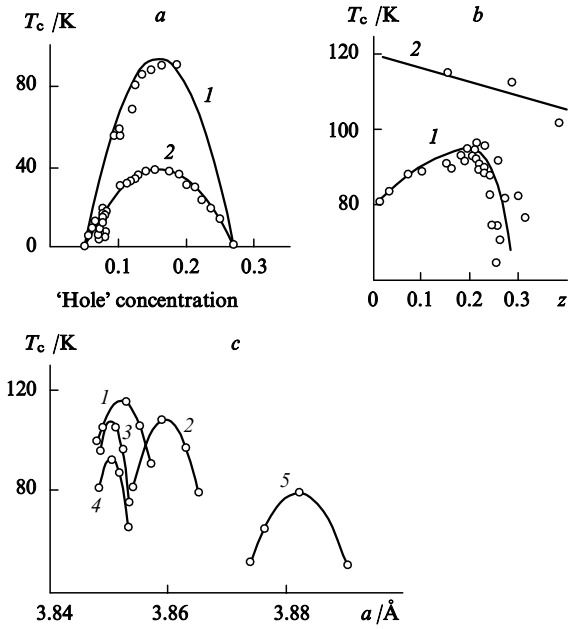


Figure 16. Dependence of the transition temperature to the superconducting state on the 'hole' concentration (*a*), oxygen nonstoichiometry (*b*) and unit cell parameters which are determined by the oxygen content (*c*) for the most abundant types of HTSC ;
(*a*): $YBa_2Cu_3O_z$-phases (*1*) and $(La,Sr)_2CuO_{4+y}$ (*2*); (*b*): $Bi_2Sr_2CaCu_2O_{8+z}$ (*1*) and $Bi_2Sr_2Ca_2Cu_3O_{10+z}$ (*2*); (*c*): the $HgBa_2Ca_{n-1}Cu_nO_{2n+2+z}$ homologous phases, Hg1223 (*1*), Hg1212 (*2*), Hg1234 (*3*), Hg1245 (*4*) and Hg1201 (*5*).

substitution in the structure), the energy parameters of different oxygen sites (the activation energy and the probability of exchange between the oxygen positions, *etc.*). A rather high anisotropy of the diffusion coefficients along the main crystallographic directions can indicate a layered structure of the HTSC (two-dimensional diffusion in CuO_y planes in which the vacancies are concentrated, *etc.*). Relatively large absolute values of the diffusion coefficients of high-temperature superconducting phases compared to those of other systems [136–139] indicate that they are highly defective. Studies of the diffusion mechanism give useful information on the different types of the oxygen bonding in the structure.[140] Finally, parameters of the oxygen diffusion can essentially depend on the size of grains of the high-temperature superconducting phase, the quality of their surfaces, specific features of the interface between the superconducting and gas phases, the presence of internal microscopic strain, *etc*. Thus, analysis of these dependences makes it possible to obtain information on the real structure of high-temperature superconducting materials. The results of the diffusion studies can be used for determination of thermodynamic properties of high-temperature superconducting phases.

a. Phase diagrams of $RBa_2Cu_3O_z-O_2$ systems and the oxygen ordering processes

The problem of oxygen nonstoichiometry in $RBa_2Cu_3O_z-O_2$ systems and related phenomena are extremely complicated.[13, 100, 141–148] Different types of diagrams used to represent the oxygen nonstoichiometry in high-temperature superconducting phases of the Y–Ba–Cu–O system are shown in Fig. 17.

The $p_{O_2}-T-x-z$-diagram presented in Fig. 18 illustrates the effect of cation ordering on the 'behaviour' of the oxygen sublattice in the $Nd_{1+x}Ba_{2-x}Cu_3O_z$ solid solution.[89]

Obviously, the temperature, total pressure and partial pressure of oxygen in the system affect significantly the oxygen content in the HTSC-phase, peculiarities of oxygen ordering and symmetry of the crystal lattice of this phase, the stability of various homologues of the high-temperature superconductors (123-, 247-

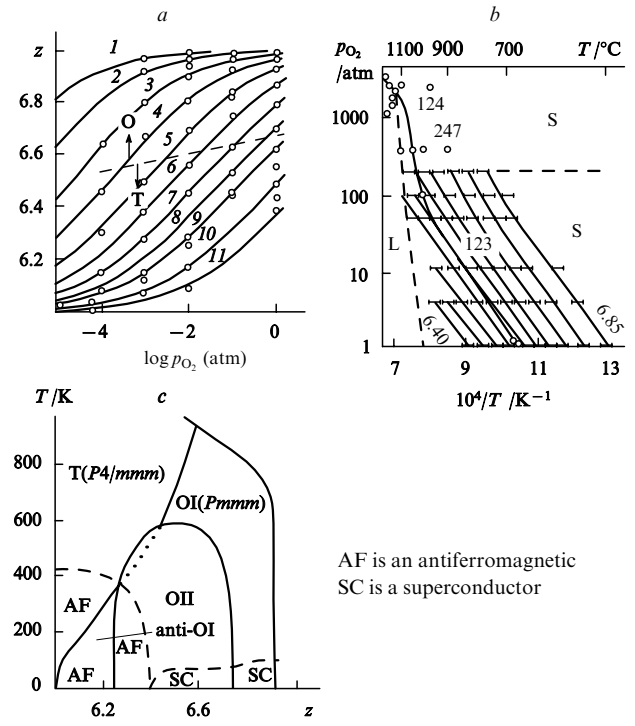


Figure 17. Types of representation of the diagrams of equilibrium oxygen content in $YBa_2Cu_3O_z-O_2$ systems;
(*a*): $p_{O_2}-T-z$-diagram; *T*/ K: (*1*) 573; (*2*) 623; (*3*) 673; (*4*) 723; (*5*) 773; (*6*) 823; (*7*) 873; (*8*) 923; (*9*) 973; (*10*) 1073; and (*11*) 1173; (*b*) phase relations at a high pressure of oxygen, the *z* value varies from 6.40 to 6.85; (*c*) calculated low-temperature diagram of oxygen content in the Y123-phase and different types of ordering of the oxygen sublattice.

or 124-phases) and that of the high-temperature superconducting phase against peritectic and/or solid-phase decomposition.

The highest T_c values are achieved at the optimum oxygen content in the high-temperature superconducting phase.[148] The $(T_c)_{max}$ values for $YBa_2Cu_3O_z$ are 93.5 K at $z = 6.94$ and 87 K at

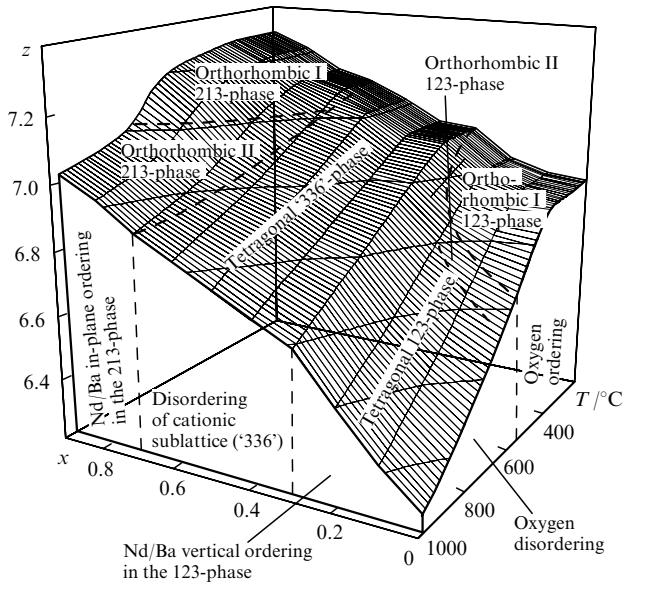


Figure 18. Section of the $p_{O_2}-T-x-z$-diagram of the $Nd_{1+x}Ba_{2-x}$. $Cu_3O_z-O_2$ system at $p_{O_2} = 0.21$ atm, which illustrates the effect of the character of cation ordering on the equilibrium oxygen content in this solid solution.

$z = 7.0$ and 6.85. 'Heavy' REE of the yttrium subgroup with smaller ionic radii form 123-phases for which $(T_c)_{max} < 90$ K, which means that the maximum value is shifted towards lower oxygen content. For instance, $(T_c)_{max} = 87$ K at $z = 6.90$ for $YbBa_2Cu_3O_z$. On the contrary, HTSC containing 'light' REE are characterised by higher $(T_c)_{max}$ values at higher oxygen content. Probably, the $(T_c)_{max}$ values of $NdBa_2Cu_3O_z$ with $z = 7$ and its analogue $LaBa_2Cu_3O_z$ with $z > 7.0$ reach 96 K[7,8,43,86] and 98–100 K,[86] respectively. High oxidation degrees of these phases are achieved by heat treatment at low temperatures (350 °C) and high pressure of oxygen (100–900 atm).[7,8,92] The effect of ionic radii of REE on T_c of the 123-phases is explained [17,42,43] using the model of charge redistribution between the superconducting CuO_2 planes and dielectric CuO_y blocks in the structure under conditions of internal chemical pressure (followed by compression or expansion of the structure) which results from changes in the geometrical size of cations occupying the sites of REE ions. Analogous dependences are also known for other cuprate superconductors and the optimum oxygen content is different for different HTSC homologues (see Fig. 16 *c*).

The formation of twins owing to relaxation of internal strain which appears upon orthorhombic distortion of a tetragonal unit cell in the course of oxygen diffusion into the grains of superconductor is clear evidence of the ordering of oxygen atoms in the unsubstituted 123-phases. The distance $\Delta\lambda$ between the twin boundaries in the twin ensemble varies in accordance with the formula:[149]

$$\Delta\lambda = \left(\frac{128\pi\gamma G}{ES}\right)^{0.5},$$

where γ is the specific energy of the twin boundary, G is the size of twinned grain, E is the elastic modulus of the material and S is the coefficient of orthorhombicity.

Thus, one can expect that the largest twins will be formed in single crystals and that the size of these defects will to a great extent depend on the elasticity and 'degree of orthorhombicity' of the material used. Twinning results in microscopic cracking of melt-solidified ceramics. Perfect specimens can be obtained using both the single-crystal detwinning and twin-free crystal growth methods.[150,151]

b. Diffusion of cations and anions

Oxygen diffusion in high-temperature superconducting phases has been studied using different methods such as dynamic [152] and isothermal [153] thermogravimetry, electrochemical potentiometry,[143] O^{18}/O^{17} tracer diffusion method,[154–156] determination of internal friction coefficients,[155] *in situ* measurements of electrical resistivity,[157] direct observations of the twinning front propagation in single crystals,[158,159] method of isotope exchange with the gas phase [160,161] and computer simulation using the cellular automata method.[147] The diversity of methods used and factors affecting the oxygen diffusion explains a great scatter (several orders of magnitude) of results obtained by different groups of researchers. Nevertheless, mention may be made of several important regularities.

1. One must discriminate between the coefficients of self-diffusion D_{self} and the coefficients of chemical diffusion of oxygen D_{chem} in high-temperature superconducting phases related by a simple formula [157]

$$D_{chem} = D_{self}\,\Phi,$$

where Φ is the so-called thermodynamic factor. Usually, the Φ value is nearly constant if the oxygen content z in the R123-phases lies in the range from 6 to 6.8; however, it increases rapidly as z approaches the value corresponding to the most oxidised state ($z = 7$). As a rule, the D_{chem} value is 4–5 orders of magnitude higher than that of D_{self}.

2. For polycrystalline materials based on the Y123-phase, the D_{chem} and D_{self} values vary in the ranges $10^{-5}-10^{-11}$ and $10^{-9}-10^{-13}$ cm^2 s^{-1}, respectively. The activation energies of

self-diffusion in the R123-phases decrease as the ionic radii of REE increase.[143]

3. For single crystals, the coefficient of self-diffusion of oxygen along the *c* axis at 400 °C ($D_c = 10^{-16} - 10^{-17}$ cm^2 s^{-1}) is six orders of magnitude lower than for polycrystalline samples (D_{poly}), whereas the rate of diffusion along the *b* axis at 300 °C in detwinned crystals ($D_b = 2 \times 10^{-12}$ cm^2 s^{-1}) is at least two orders of magnitude higher than that of diffusion along the *a* axis ($D_a = 5 \times 10^{-14}$ cm^2 s^{-1}).[154] Thus, self-diffusion in single crystals is highly anisotropic and proceeds almost completely in the *ab* plane [$D_{ab} = D_{poly} = (10^4 - 10^6)D_c$, $D_b = 100D_a$, $D_b = 10D_{ab}$]. At the same time, the coefficient of chemical diffusion for these types of single crystals lies in the range $10^{-8} - 10^{-7}$ cm^2 s^{-1}.

4. Second order phase transitions, occurring on ordering or disordering of the oxygen sublattice, must result in jumpwise changes in the diffusion coefficients. This is confirmed by the results obtained in the studies of diffusion coefficients of $RBa_2Cu_3O_z$ (R = Y and Nd) phases over a wide range of temperature and partial pressure of oxygen.[143] According to the reported data, the rate of oxygen diffusion in the orthorhombic phase is higher than that in the tetragonal phase despite the fact that the number of available oxygen vacancies in the latter is larger than in the former. Probably, this indicates changes in the elementary mechanism of the process.

The role of mobility of the cationic sublattice is at least as important as, and in some instances even more important than, that of oxygen diffusion; however, it has been much less studied.[136–140] Migration of cations in single crystals of oxide superconductors follows ordinary diffusion mechanisms (vacancy-type, interstitial, dissociative, along dislocations and point defects); in polycrystalline HTSC, diffusion along the grain and pore surface, twin boundaries, *etc*., is additionally observed.[140]

Self-diffusion of Cu^{2+} in the $YBa_2Cu_3O_z$ phase was studied by the tracer diffusion method.[137–139] The activation energy of this highly anisotropic process lies in the range 165–255 kJ mol^{-1} and the diffusion coefficient at 780–900 °C lies within the limits $\sim 5 \times 10^{-12} - 10^{-13}$ cm^2 s^{-1}. The value of the diffusion coefficient of copper at 600 °C found by extrapolation is estimated at $\sim 6 - 9 \times 10^{-14}$ cm^2 s^{-1}. The bulkier Ba^{2+} ion has a lower coefficient of self-diffusion in the same temperature range ($\sim 10^{-14} - 5 \times 10^{-15}$ cm^2 s^{-1}).[137–139] The coefficient of self-diffusion of Y^{3+} ion in the Y123-phase varies from 10^{-14} to 10^{-16} cm^2 s^{-1} in the temperature interval 780–980 °C (the activation energy is 280 kJ mol^{-1}).[137–139]

Therefore, self-diffusion of oxygen in high-temperature superconducting phases proceeds at a rate which is 1–3 orders of magnitude higher than that of self-diffusion of cations, especially in those regions where low-temperature oxidation of superconductors occurs. This is first of all due to the differences in the atomic weights of the elements, the charge of their ions and structural features of high-temperature superconducting phases containing oxygen-deficient perovskite-like blocks. Taking into account different values of diffusion coefficients, the cationic framework can be considered virtually immobile when studying various low-temperature processes with participation of high-temperature superconducting phases (see also Section III.1.b and **S.3**).

The final stage of preparation of HTSC can be optimised using the data on the equilibrium oxygen content and the parameters of its diffusion in high-temperature superconducting phases (see above). In combination with specific features of phase relations described above, this opens additional opportunities of targeted design of high-temperature superconducting materials.

IV. Development of advanced methods for the synthesis of high-temperature superconducting materials

Preparation of high-temperature superconducting materials with desired characteristics is the most important problem that became topical immediately after the discovery of this class of complex cuprates. However, only a few types of high-temperature superconducting materials such as highly homogeneous powders (used as intermediate products for the preparation of ceramics, coatings, silver-sheathed tapes), thin films and hetero-structures, large-grain ceramics and long-length composites can be used in such areas as power engineering, electronics and medicine. A general view of the main classes of materials based on HTSC-phases is shown in Figs 19–21 (see **S.8**–**S.10**)

1. Chemical homogenisation and preparation of high-quality powders

Early studies of high-temperature superconducting materials were carried out using the so-called ceramic method, which includes thorough mechanical mixing of oxides (in some instances,

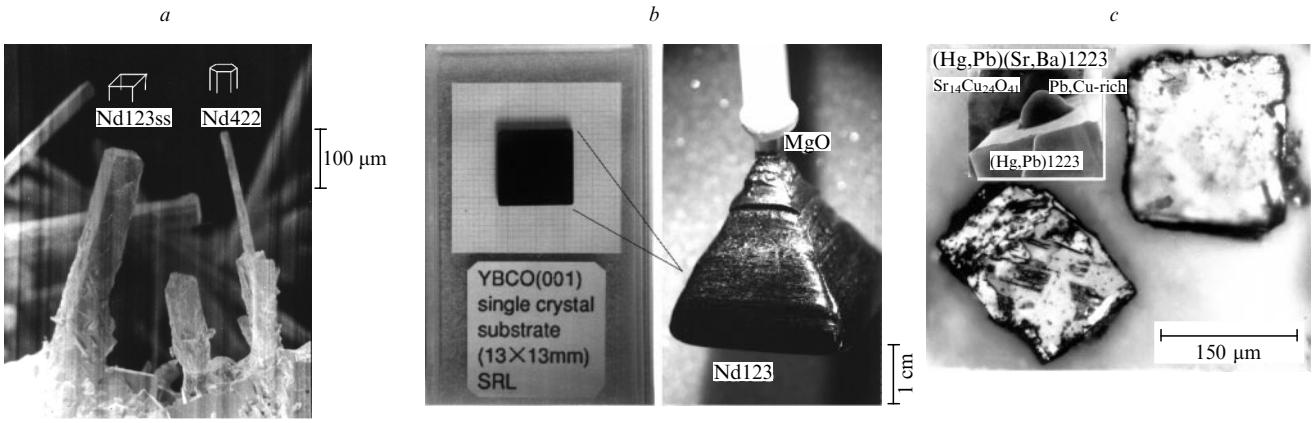


Figure 19. Single crystals of HTSC;
(*a*), general view of needle-shaped $Nd_{1+x}Ba_{2-x}Cu_3O_z$ 'stalactitic' crystals grown under isothermal conditions by the 'pellet-in-pellet' method with addition of a small amount of BaF_2 (see **S.8**); (*b*) the largest (by the date of publication of this review) 'pyramidal' $NdBa_2Cu_3O_z$ HTSC-crystal grown by the modified Czochralski method and a polished experimental substrate for thin film deposition, obtained by sawing a 'bulk' $YBa_2Cu_3O_z$ crystal grown by using this method (published by courtesy of Professor Y Shiohara, SRL, ISTEC, Japan);[114] (*c*) general view of plate-like mercury-containing HTSC-crystals obtained by ampoule synthesis using the contact pair method (the only Hg-based crystals with peak effect known to date, see **S.9**); a pronounced peak effect observed on the 'critical current *vs*. external magnetic field' dependence is assumed to be due to double (Hg/Pb and Ba/Sr) substitution (published by courtesy of S R Lee, M V Lomonosov Moscow State University, Russian Federation).

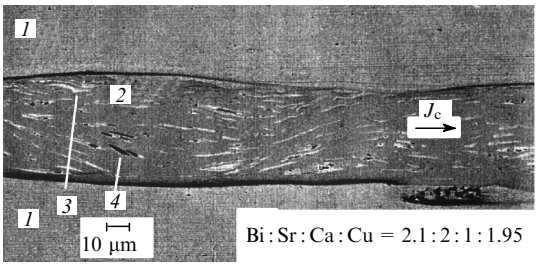


Figure 20. A SEM graph of a cross section of a long-length HTSC-composite (a silver-sheathed tape fabricated by the 'powder-in-tube' method) with optimised composition of the superconducting core; (*1*) silver sheath; (*2*) phase of the $Bi_2Sr_2CaCu_2O_8$ type; (*3*) inclusions of particles of Ca–Sr bismuthates; (*4*) inclusions of particles of Ca–Sr cuprates; J_c denotes the direction of current in the superconducting wire (published by courtesy of Professor E Hellstrom, ASC, UWM, USA).[54]

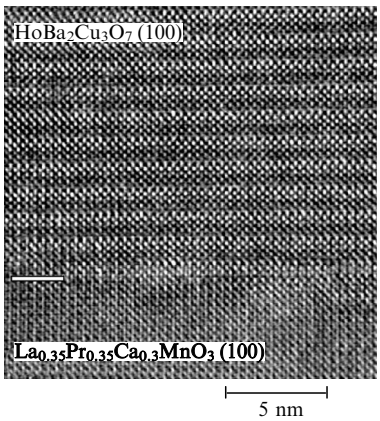


Figure 21. A cross section of $HoBa_2Cu_3O_z$/(La, Pr, Ca)MnO_3 epitaxial film grown on the $LaAlO_3$ substrate (the 001 orientation) in the region of the HTSC–manganite interface according to high-resolution transmission electron microscopy data (see **S.10**). The smooth atomic layers at the interface indicate chemical compatibility of HTSC cuprate and manganite with giant magnetoresistance effect (published by courtesy of Professor A R Kaul, M V Lomonosov Moscow State University, Russian Federation).

alkaline-earth metal oxides and carbonates) and repeated 'calcination–grinding' (beat-and-heat) cycles needed for the solid-phase reaction between the reagents to proceed.[2–5, 14]

This conventional method for the preparation of many types of structural and functional ceramics has essential drawbacks, the most important of which consists in long-term heat treatment because of rather large grain size and mixing inhomogeneity of the reagents (see **S.11**). Often, the growth of crystallites is uncontrollable, which results in both chemical and granulometric inhomogeneity. In combination with anisotropy of crystallites constituting the HTSC, this results in irreproducibility of their electrical and magnetic properties. Almost all oxide superconductors known to date are complex multicomponent chemical compounds. Distinctions in properties of the elements constituting high-temperature superconducting phases due to their different positions in the Periodic Table preclude development of a unified procedure for the preparation of HTSC by the ceramic method.

Publications concerning the development and application of the so-called chemical methods for the preparation of HTSC powder have been known since 1987.[162–172] These methods allow improvement of the product homogeneity owing to the achievement of a nearly molecular level of component mixing in solution and its retention to a greater or lesser extent in subsequent stages of the synthesis. As a rule, the oxide powders thus obtained are characterised by a rather large specific surface and, as a consequence, readily enter into solid-phase reactions and are active in sintering. Additionally, the efficiency of chemical methods of synthesis is also manifested in increased chemical homogeneity of ceramics.[14]

It is also appropriate to use chemical methods along with the most widely used melt solidification methods for the preparation of ceramics despite marked levelling of distinctions in the morphology of powders with different prehistory, because of complete or partial melting. The establishment of the nature of pinning centres requires materials with strictly specified content and distribution of impurities. The easiest way of doing this is to use chemical methods. Mention has been made[9, 129, 173] of the possibility of controlling the size of crystallites of the secondary phases through the so-called effect of topochemical memory observed when varying the chemical prehistory of specimens.[39, 40] Of particular importance is preparation of high-quality, highly disperse 'soft' powders for fabrication of long-length HTSC–metal composites (*e.g.*, silver-sheathed tapes) by the 'powder-in-tube' method.[16, 23, 54, 55] The size of internal cross sections of such composites varies from several to several tens micrometres. Therefore, 'coarse' and inhomogeneous powders (with broad distribution of the particle size) prepared by conventional ceramic method are unusable in this case.

The coprecipitation methods are widely used for the preparation of various types of ceramics. Therefore, it is not surprising that they were among the first chemical methods for the synthesis of HTSC powder.[2, 29, 162] In some instances (in correctly designed experiments) it has been possible to prepare homogeneous disperse mixtures of salts with the predetermined cation ratio and to reproduce the results obtained. In an ideal case, the conditions under which precipitation of cations from a solution occurs simultaneously and at equal rates are optimum. Most of the methods used include precipitation of carbon-containing salts (oxalates and carbonates) the thermolysis of which is completed at 900–950 °C. Unfortunately, the presence of carbon-containing salts should be considered as a drawback of this type of method because of the possibility of the formation of oxycarbonate phases.[36, 100, 136]

The citrate method [2, 171] is the most widely used of the different versions of the sol-gel methods. Closely related to this method is the method of polymerised complexes, which has been successfully developed in a number of research laboratories worldwide.[163] In this case, the ability of α-hydroxy acids (*e.g.*, citric acid) to form chelate complexes with metal ions is used. When heated to 100–140 °C, such complexes react with polyfunctional alcohols (*e.g.*, ethylene glycol) to give low-molecular-weight oligomers (esterification). Subsequent heating to 180–200 °C results in their polymerisation and the formation of a viscous resin (gel) with uniformly distributed metal atoms. The gel can be decomposed to give the oxide powder. The sol-gel method is rather simple and inexpensive since almost no complex equipment is needed (the method requires no centrifuging, filtering, washing, drying, *etc.*) and readily available nitrates are most often used as initial substances. The viscosity of the gel obtained can be controlled by varying the component ratio and the duration and temperature of polymerisation. Therefore, the sol-gel method is used for the preparation of not only powders, but also thick films, fibres and planar ceramics.

Currently, the spray drying and spray pyrolysis techniques have received the widest acceptance among chemical methods for preparation of HTSC powders.[162, 172] The latter method includes sonication of a mixture of salt solutions to obtain a mist with a droplet size of 0.5–0.8 μm, the transfer by a carrier gas into a hot chamber where instantaneous (complete or partial) decomposition of the droplets occurs. The oxide-salt product that is formed is collected on a filter at the outlet of the gas flow from the decomposition zone.

The molecular level of mixing of components (most often, nitrate solutions) and nearly instantaneous dehydration and

decomposition of microscopic spray droplets make it possible to prepare a homogeneous product. Repeated grinding and calcination characteristic of the ceramic technology and responsible for contamination of the product and uncontrollable grain growth are excluded in this case. However, the powders obtained can be contaminated with the material of the drying chamber (at high temperatures, in the presence of free acid). Additionally, the spray pyrolysis technique requires careful purification of large volumes of the carrier gas (oxygen) from CO_2 to avoid the formation of barium carbonate.

The method of rapid expansion of supercritical solutions (RESS)[169, 170] at elevated temperature and pressure is based on the phenomenon of an anomalous increase in the solubility of inorganic compounds in water (or in other solvents such as ammonia, carbon dioxide, xenon, *etc*.) above its critical temperature (in autoclave). When such solutions are expanded in a chamber at a reduced pressure and temperature, the solubilities of the solutes decrease substantially and these are isolated as ultradisperse particles (often, as an X-ray amorphous phase or metastable crystalline modifications). Oxide materials can be best prepared using aqueous supercritical solutions.[169]

The drawbacks of most chemical methods used for the synthesis of HTSC powders can be to a great extent compensated using cryochemical technology.[162, 165–168] This method consists in the preparation of highly disperse and highly homogeneous salt (and the oxide) precursors by fast freezing of finely disperse salt solutions (preparation of cryogranulates) followed by removal of water by sublimation. Experimental conditions should exclude physicochemical processes resulting in deterioration of chemical and granulometric homogeneity of the product, *e.g*., separation of sprayed microscopic drops into solvent-rich and solvent-depleted regions due to insufficiently high cooling rate, partial melting of cryogranulates and, hence, segregation of the components during the freeze-drying or on subsequent heat treatment of the freeze-dried product, *etc*.

Therefore, the highest homogeneity of the product is often achieved by (i) spraying the solution over a massive metal plate cooled by liquid nitrogen,[168] (ii) replacing (if possible) nitrate solutions by acetate[168, 174] or nitrate–nitrite solutions and (iii) drying in a thin layer with slow heating to 125 °C in an argon stream[14, 168] and decomposing the dried salt product in a furnace preheated to the desired temperature.

The use of highly disperse (tens of nanometres) and highly homogeneous precursors prepared by the cryochemical method makes it possible to accelerate substantially the phase formation and to prepare high-temperature superconducting phases that can hardly be synthesised by other methods. For instance, the Bi2223-phase was obtained[168] after annealing for 12–16 h only (*cf*. 200–300 h required when using the ceramic technology) at 750 °C and the Y124-phase was synthesised[168] after annealing in air at 815 °C (120 h). In the latter case, high-pressure stages (p_{O_2} up to 100 atm) usually required to synthesise this phase were excluded. Considerable achievements have been made in the preparation of different homologues of mercury-containing HTSC by the ampoule method using cryochemical technology and other methods of chemical homogenisation.[175]

2. Thin film preparation

The known technologies of thin film preparation can formally be divided into physical and chemical ones.[2, 24, 176] The former comprise the most widely used methods of pulse laser deposition and magnetron sputtering of films including the transfer of the material of the dense and chemically homogeneous target in the form of microscopic clusters knocked out by a high-energy beam from the target onto a substrate. These methods make it possible to prepare high-quality thin films with record physical characteristics and to carry out a layer-by-layer synthesis of novel types of structures (structural design) by 'assembling' the film literally at the atomic plane level.

However, expensive physical methods are almost inapplicable for the preparation of large specimens. This is achieved by using such chemical methods as liquid phase epitaxy (LPE)[8, 112, 120] and chemical vapour deposition (CVD).[24] However, despite the advantages of precipitation from a solution in a melt by LPE, this has not acquired wide acceptance to date and has been developed by only a few research groups.[120] Among accepted methods for the preparation of thin high-temperature superconducting films, deposition on single-crystal substrates of thermally decomposed products of highly volatile organometallic precursors (Metal-Organic Chemical Vapor Deposition or MOCVD) is the most interesting.

Currently, the efforts of researchers from about 40 laboratories[14] including those of the biggest electronic companies are focused on the development and improvement of CVD technology for the preparation of HTSC. This fact, as well as information on large-scale applications of the CVD method for the preparation of diverse epitaxial semiconducting films and oxide coatings suggest that this method can become one of the main methods for the preparation of high-temperature superconducting films in the future.

The MOCVD method[2, 24] includes transfer of the metal constituents of films to the reactor as vapours of volatile organometallic compounds, mixing of the vapours with a gaseous oxidant and decomposition of the vapours in a hot-wall reactor or on a heated substrate followed by the formation of a HTSC film. Metal β-diketonates are most often used as volatile compounds (precursors). Novel volatile organometallic compounds[2, 24, 177–179] made it possible to improve substantially film characteristics and to extend the potentialities of the MOCVD method.

The MOCVD method makes it possible to prepare thin HTSC films with characteristics that are at least as good as those of films prepared by physical methods. The obvious advantages of this method include first of all its versatility as regards the composition of the materials obtained, the possibility of single- and double-sided deposition of films with homogeneous composition and the same thickness on substrates with complex shapes and large surface areas (including continuous film deposition on a long-length metallic substrate, *e.g*., a tape).[176] Unlike physical methods of sputtering, in which high performance of equipment is achieved due to the high energy of the particle beam of the sputtered substance and is connected with the risk of disturbing the morphology and stoichiometry of the film thus formed, the performance of the MOCVD method is achieved by increasing the vapour pressure of the volatile component and/or by increasing the flow rate of the carrier gas. Other advantages of the MOCVD method are the possibility of achieving higher deposition rates (up to several millimetres per hour) with retention of high quality of the film, the use of a flow-through setup operating at pressures of 10^{-3}–1 atm instead of high-vacuum equipment, its simplicity and low cost compared to those required when using physical methods and, finally, 'flexibility' of the process in the adjustment stage (primarily due to the smooth change in the vapour phase composition).

A common problem of all methods of thin film preparation including the MOCVD method is 'symbiotic' choice of substrates. The substrates should be highly chemically inert (to prevent contamination of high-temperature superconducting phase with alien components), cheap and readily available. Additionally, the substrate material must possess specific physical properties such as (i) rather small (< 2%) mismatch between the crystal lattice parameters and those of the deposited film to provide conditions for the epitaxial growth, (ii) close values of the thermal expansion coefficients (TEC) of the substrate and HTSC phase to avoid the formation of microscopic cracks in the film due to compression and, especially, tension caused by temperature variations; (iii) the absence of twinning-type phase transitions that can appreciably deteriorate the film morphology and (iv) low dielectric constant and dielectric loss tangent to provide the possibility of using the films in microelectronics and in microwave devices.

Unfortunately, almost none of the known substrates meets all the above-mentioned requirements (Fig. 22). Usually, $SrTiO_3$, $NdGaO_3$ and $LaAlO_3$ are used as substrates.[179] Recently, large Y123 and Nd123 single crystals were used for homoepitaxy of the R123-phases of high-temperature superconducting films.[180] However, these single-crystal substrates are superconductors rather than dielectrics. Intrinsic in these substrates is the tetragonal-to-orthorhombic phase transition (*tetra–ortho*-transition) accompanied by the formation of a twin structure. Non-superconducting tetragonal solid solutions of the $Pr_{1+x}Ba_{2-x}Cu_3O_z$ type, in which no twinning occurs, seem to be more promising.[8] Dielectric $Nd_{1.85}Ba_{1.15}Cu_3O_z$ single crystals are characterised by a high degree of orthorhombicity, the absence of *tetra–ortho*-transition, close TEC values, high lattice parameter matching with high-temperature superconducting films of the R123-phases and a narrow range of oxygen nonstoichiometry. For these reasons, they are also promising for use as substrates.[80, 81, 181]

The second, chemical problem arising when using the MOCVO method is the control of the cation and anion stoichiometry of the films. The chemical vapour deposition is an incongruent process and depends on several factors such as the temperature, total pressure, partial pressures of oxygen, carbon dioxide and water (the oxidation products of the organic component of compounds used), their flow rates and distribution of the flows in the reactor and above the substrate, total composition and homogeneity of mixing of volatile components in the gas phase, *etc*. The most promising way of controlling the vapour composition is to carry out instantaneous evaporation of the mixture of volatile components from one source. This is achieved by using an aerosol obtained from the solution of organometallic compounds in organic solvent (*e.g*., diglyme) or by pulse evaporation of microscopic portions of a mixture of organometallic compounds fed using a belt-conveyer feeder.[24]

In the first case, the solvent vapour has a strong effect on the film deposition, namely, the thermal effect of solvent oxidation: a decrease in the partial pressure of oxygen and an increase in the partial pressure of carbon dioxide and water are observed. Using the results of thermodynamic analysis, it is possible to minimise the influence of these effects and to optimise the conditions for film deposition in the reactor with cold walls and induction heating of the substrate.[2, 24, 179] At $p_{CO_2} < 10^{-5}$ atm and $T < 800$ °C, no barriers to the formation of the $YBa_2Cu_3O_z$-phase are observed. Using an aerosol source, it is possible to attain high deposition rates and reproducibility of the composition and morphology of the R123- and Bi2212-films.[177]

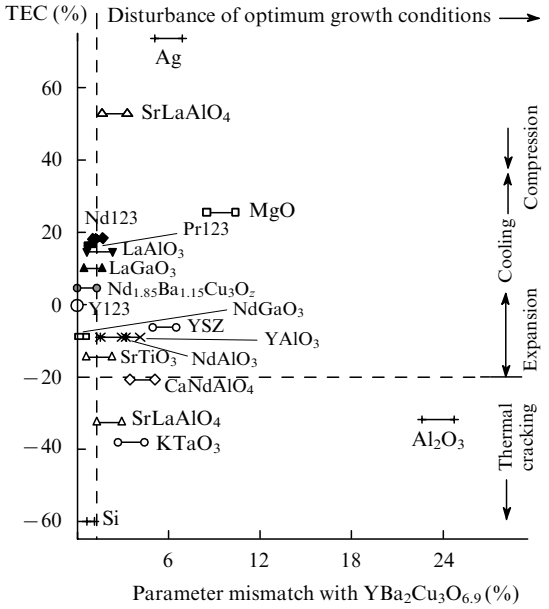


Figure 22. Properties of materials used as substrates for the deposition of high-temperature superconducting thin films.

The second method consists in placing small droplets of an organic solution containing volatile metal complexes in a predetermined ratio on a fibre glass transport tape. The vapour formed on pulse heating of the tape in a vacuum chamber moves to the substrate. The amount of substances evaporated per pulse as well as the vapour composition can easily be varied from pulse to pulse. This method appeared to be very useful in the preparation of multilayered film structures of complex chemical composition.[182, 183]

The third problem that arises only when using the MOCVD method consists in the necessity of a targeted search for highly volatile substances with reproducible volatility. The most serious problems are associated with barium transfer through the vapour phase. Because of coordinative unsaturation of Ba^{2+} ions and high ionicity of the barium–oxygen bond, barium complexes are oligomerised in both the solid and vapour phases. Stabilisation of barium dipivaloylmethanate is achieved by using the adduct of dipivaloylmethanate with phenanthroline, which saturates the coordination sphere of barium, thus resulting in nearly quantitative transition of this complex to the vapour phase.[2, 24]

The fourth (technological) problem is associated with the necessity of designing the optimum film morphology. It was shown in the studies of the effect of various factors on the orientation of films that the introduction of an excess of bismuth and copper compounds in the course of growth of high-temperature superconducting Bi2212-films favours the formation of *c*-oriented films, whereas the introduction of an excess of an alkaline-earth metal results in *a*-oriented films.[177] This is associated with the fact that the presence of the excess of bismuth and copper results in the formation of an equilibrium liquid phase or, at least, in a shift of the compositional point towards the regions where a melt should be present. This increases the mobility of the film components and facilitates the formation of thermodynamically more favourable *c*-oriented films, whereas *a*-oriented films are formed under kinetically controlled conditions. This is confirmed by the LPE experiments.[120] Generally, the morphology (polycrystallinity, planarity, film orientation, the presence of microscopic inclusions of non-superconducting phases, microscopic cracks, *etc*.) depends on numerous process factors that should be optimised thoroughly.

The most topical problems associated with the development of the MOCVD technology and requiring practical solution are connected with deposition of $RBa_2Cu_3O_z$-films on bicrystalline substrates ($SrTiO_3$, sapphire) and fabrication of devices based on the Josephson effect (logistors, SQUID magnetometers, *etc*.), preparation of high-temperature superconducting films using substrates with a large surface area (up to 70 mm in diameter), *in situ* double-sided deposition of films and attainment of high superconduction characteristics of thin high-temperature superconducting films using conventional substrates (R-sapphire, Si) and high-quality CeO_2 buffer layer.[184]

Recently, R123-films (R is the 'light' RE element), the effects of stabilisation of metastable phases (see **S.11**) and an increase in the critical currents in solid solutions have attracted the attention of researchers. Yet another topical problem is the preparation of thick films with high current-carrying ability deposited on flexible tapes made of nickel metal and its alloys (the so-called 'Rolling-Assistant Biaxially Textured Substrates' or RABiTS) preliminarily coated with a buffer layer.[176] The CVD method is certain to play a key role in solving this problem.

3. Large-grain ceramics and single crystals

a. Characteristic features of materials based on large-grain ceramics

Real structure. As a rule, the idea of designing any material is based on a concept of a real structure with several hierarchical levels.[185, 186] The basic crystal structure determines the fundamen-

tal properties of HTSC and is responsible for their structural organisation at the microscopic level. Individual crystallites, which are always imperfect and consist usually of smaller subcrystallites (mosaic blocks, coherent scattering domains) separated by extended defects, form an intermediate (mesoscopic) level. Ensembles of crystallites (grains, granules) and pores form the macroscopic level of structural organisation of HTSC. The current concepts on complicated structure of melt-processed specimens of superconducting ceramics are illustrated in Fig. 23.[9, 11, 55, 187–191]

Ensembles of large pseudo-single-crystal domains (their size reachs 0.5–5 cm depending on the precipitation conditions) separated by large-angle boundaries are the main microstructural motifs of large-grain ceramics. Each domain is a stack of thin (5–50 μm) $RBa_2Cu_3O_z$-plates or lamellae rather than a true single crystal. The lamellae are characterised by the aspect ratio of ~ 1000. The plates are oriented parallel to one another and separated by low-angle boundaries, which makes them 'transparent' to the critical current. It should be noted that the real structure of melt-processed HTSC is characterised by the presence of various extended defects such as twin boundaries, ultradisperse inclusions of non-superconducting phases, different types of microscopic and macroscopic cracks, appeared due to low plasticity of the $RBa_2Cu_3O_z$-phase, and increased concentration of dislocations. In principle, all levels of structural organisation of HTSC should be taken into account. However, only the composition, structure of boundaries and nature of various defects have been studied in detail,[187–191] though such parameters as porosity and density of ceramics as well as the size of crystallites and pores should also be considered.

The real structure of melt-processed HTSC can be considered as a large-domain system with pronounced 'collective' superconducting properties resulting in very high integral superconductivity characteristics due to the specific crystallisation mechanism of the peritectic melt.[9, 11] For instance, an increase in the total density of specimens as a result of melt solidification eliminates the percolation problems characteristic of the current flow in the specimens obtained by solid-phase synthesis. 'Pseudo-single-crystalline domains' are united to form macroscopic aggregates that (potentially) can carry heavy critical currents. Finally, a large number of structural defects (inclusions, dislocations, low-angle boundaries) favours the appearance of new pinning centres.[6] Unfortunately, only the 'lamellar' level of the structure of melt-processed materials is formed spontaneously and is characterised by high superconducting parameters. The remaining hierarchical levels of the structure can be formed only by using special techniques.

Methods of generation of new pinning centres. Generation of efficient pinning centres of the magnetic flux, which make it possible to increase substantially the critical current density J_c inside the grains, is the most important stage of the preparation of materials with a high repulsion force. The methods of solving this problem can arbitrarily be divided into physical and chemical ones.

Currently, the highest J_c values have been obtained using samples of superconducting ceramics irradiated with high-energy particles. Irradiation of samples with neutrons or heavy ions to produce cluster-type radiation defects (tracks) of size 20–100 nm was found to be the most efficient.[192, 193] In this case, the J_c value increases in proportion to the irradiation dose. However, this type of treatment encounters considerable technological difficulties. Additionally, it has such drawbacks as residual activity of materials and the possibility of radiation-induced degradation of samples if the radiation doses exceed an optimum.

More promising are chemical methods which make it possible to introduce non-superconducting highly disperse inclusions in the matrix of the 123-phase.[194–203] Particles of the Y_2BaCuO_5-phase, an intermediate crystallisation product, are most often used as inclusions.[194–197] The results obtained in the studies of pinning [6, 9, 11] suggest that changes in J_c depend on the content and

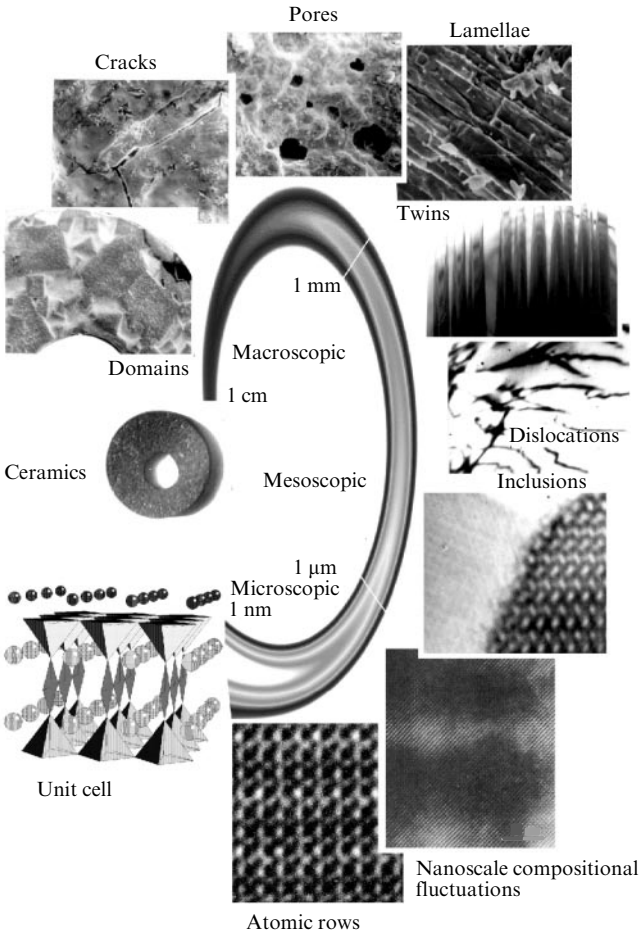


Figure 23. Macroscopic (10^{-3}–10^{-2} m), mesoscopic (10^{-6}–10^{-3} m) and microscopic (10^{-10}–10^{-6} m) levels of real structure of large-grain ceramics.

dispersity of the Y_2BaCuO_5-phase. It is noteworthy that particles of this phase are not the pinning centres themselves and that the major contribution is made by the 123-phase–211-phase interface and the interfacial defects. Introduction of zirconates, titanates, stannates, nickel metal, uranium-235 oxide (its radioactive decay leads to 'internal' irradiation of the superconducting matrix) also results in generation of new pinning centres (see Fig. 4).

Types of intercrystallite boundaries. Generation of efficient pinning centres plays an important role in the preparation of high-temperature superconducting materials characterised by high values of the transport critical currents. However, in this case the perfection of intercrystallite boundaries and their 'transparency' to the critical current are the most important points. As has been mentioned above, the oxide superconductors are characterised by abnormally low coherence lengths (ξ). Because of this, two types of links are formed between the crystallites, *viz*., strong links (ordinary intergrain phase contacts similar to intercrystallite 'necks') and weak links which, in the general case, are the breaks of the phase continuity. The extension of weak links is comparable with ξ values. The reasons for the phase discontinuity can be the formation of both the domains with local changes in stoichiometry and amorphous domains on intercrystallite boundaries, or the appearance of microscopic cracks, as well as high crystallographic anisotropy of HTSC and spatial disordering of crystallites.[204–206]

In accordance with the formation mechanism of the 123-phase, the ensemble of growing crystallites formed in the early stages of melt crystallisation consists of *c*-oriented nuclei with disordered orentations in the *ab* plane. Growth of particles of such

an ensemble and their coalescence result in the formation of large-angle boundaries that are parallel to the *c* axis and the tilt boundaries that are perpendicular to the *c* axis. The best transport characteristics will be obtained if the current will flow through both types of boundaries without a considerable loss. Based on these grounds, a 'brick wall' model of the transport current flow through high-temperature superconducting materials was proposed.[207] According to this model, the tilt boundaries enabling the maximum surface area of intercrystallite contacts play an important role in the formation of high transport current.

However, the 'brick wall' model does not consider the current flow through large-angle boundaries along the *ab* plane. According to the 'railway switch' model,[208] there are both large-angle intergrain boundaries and a rather large relative amount of intercrystallite links 'transparent' to the current flow, which favours low current loss. These links responsible for the current flow through intercrystallite boundaries and the current flow through the tilt boundaries necessary for obtaining the maximum surface area of intercrystallite contacts form a three-dimensional superconducting network. Such a mechanism is most characteristic of bismuth-containing HTSC. Probably, it can also be postulated for yttrium-containing polycrystalline superconductors.

Thus, the density of the critical current that flows through intercrystallite boundaries is mainly determined by mutual spatial orientation of their constituent crystallites. Nevertheless, it was assumed[209] that in the general case the J_c values are only dependent on the surface area of the 'strongly linked' areas of intercrystallite boundary. Obviously, the probability for two oriented (textured) crystallites to be 'strongly linked' is much higher than for disordered grains. However, it was reported[209] that high J_c values can also be retained in the latter (unfavourable) case. The results of recent studies[176, 210] indicate the presence of high-angle-but-low-energy (HABLE) boundaries, thus confirming this conclusion. This means that probability factors come into play when considering the problem of a critical transport current in bulk specimens.[9, 55, 128, 129]

b. Methods of preparation

Large-grain ceramics cannot be a chemically and structurally homogeneous material. It is a composite whose practically important superconducting properties are superior to those of highly homogeneous specimens and single crystals. Therefore, the development of melt solidification processes revolutionised the production technology of high-temperature superconducting ceramics since it opened a new way to the practical use of superconducting ceramic materials.

Minimisation of the inclusion size of secondary phases. The modern classification of melt solidification procedures for preparation of HTSC and the most important details including the chemical type of the starting precursor, mechanical prehistory and the heat treatment regime are presented in Fig. 24. Some trends in the development of melt solidification methods can be traced, which made possible the preparation of materials with high superconducting characteristics. These are:[7–11]

(1) a step-by-step change in the regime of high-temperature treatment in order to increase the degree of nonequilibrium in all stages of the process;

(2) the use of methods of synthesis resulting in more homogeneous and disperse starting oxide powders;

(3) the use of precursors in different initial states and the introduction of various additives.

The first trend is associated mainly with attempts to shorten the duration of treatment of samples at maximum temperatures. This made it possible to prevent the rapid growth of particles of secondary phases at temperatures above the peritectic temperature, which was probably a reason for passing from the classical 'Melt-Textured-Growth' (MTG) method to its modified version, *viz*., 'Liquid Phase Processing' (LPP).

The 'Quenched-Melt-Growth' (QMG) method involves a chemically induced increase in the degree of nonequilibrium of the system. In this case, the 211-phase is formed in the region of thermodynamic stability as a result of a fast 'downward' interaction of Y_2O_3 with the melt rather than due to relatively slow 'upward' decomposition of $YBa_2Cu_3O_z$. Experiments on superfast cooling of droplets of a high-temperature Y_2O_3 + L melt in an evacuated vertical metallic tube[211] are probably one of the most successful implementations of this method.

The QMG method has an important alternative, the doping of melts with, *e.g*., platinum[212] (the 'Platinum-Doped-Melt-Growth' or PDMG technique) and cerium dioxide.[213] In this case, the formation and decomposition of not-too-stable Pt-containing complex oxides ($Ba_4CuPt_2O_9$, $R_2Ba_2CuPt_2O_8$, $R_2Ba_3Cu_2PtO_{10}$, *etc*.) not only affects the nucleation processes,

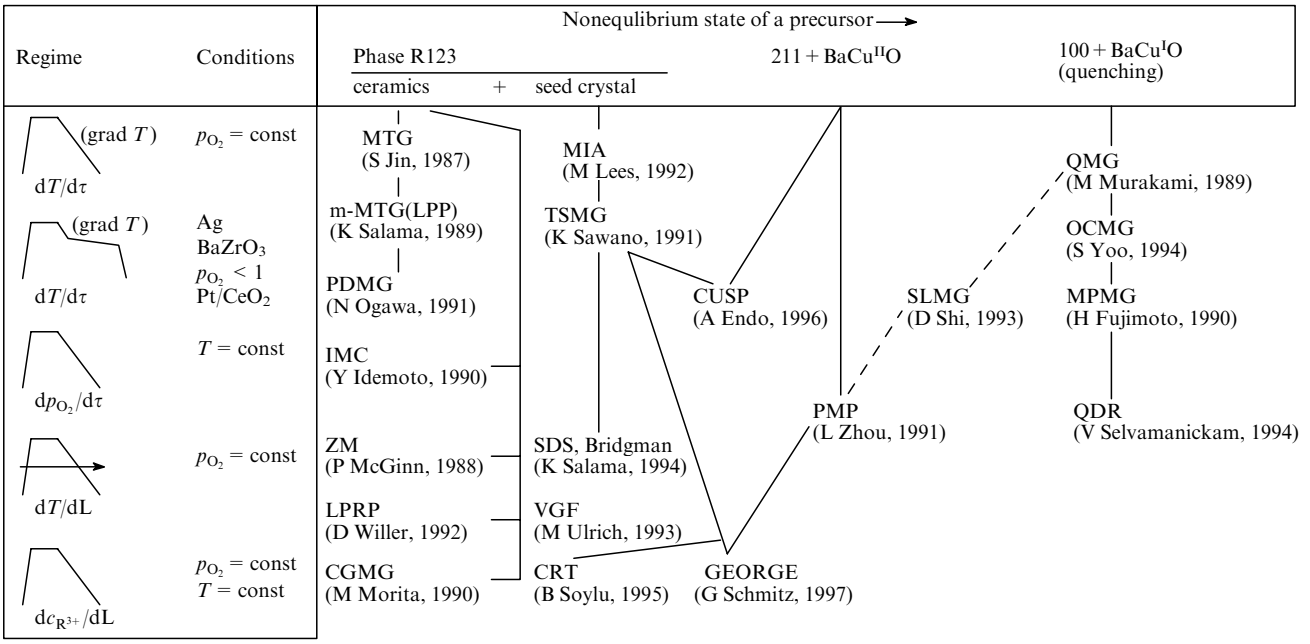


Figure 24. Melt solidification methods of preparation of large-grain ceramics.

but also retards the growth of individual faces of crystallites of the 211-phase. This results in a change in their shapes and sizes and prevents coalescence of the crystallites into larger aggregates.[213]

Several methods such as the 'Melt-Powder-Melt-Growth' (MPMG) and 'Powder-Melt-Process' (PMP) involve additional grinding of both the starting reagents and intermediate products in order to increase their dispersity and homogeneity of mixing.[6,214] A successful attempt has been performed at using a highly homogeneous mixture of barium cuprate and copper oxide with yttrium oxide, which simulates the phase composition of the specimens prepared by the QMG method (the so-called 'Solid-Liquid-Melt-Growth', or SLMG method).[197] Yet another, basically new modification of this method is the directional recrystallisation of amorphised quenched melt at temperatures ~ 100 °C below the peritectic decomposition temperature of the 123-phase (the so-called 'Quench-and-Directional-Recrystallisation' or QDR method). This allows a rather fast (over 3–5 min) formation of the 123-phase and ultradisperse 'green' phase and preparation of highly textured superconducting ceramics using conventional zone melting technique with reduced hot zone temperature.[215]

A positive effect of the above-mentioned innovations becomes more understandable when considering numerous experimental data indicating that the particle size of the 211-phase depends on prehistory of the system, despite the extreme conditions for the synthesis.[9,173,216,217] This is probably due to the possibility of intermediate formation of a superheated metastable (congruent) melt of the 123-phase. Numerous structural defects (grain boundaries mostly) accumulated mainly in the fine crystalline material facilitate strongly the decomposition of the congruent melt into a melt and the 211-phase. However, the excess 'green' phase can inhibit the growth of faces of the 123-phase on sintering, thus resulting in a more fine-grained structure.[217] The addition of Pt or CeO_2 changes the surface energy at the 211-phase–melt interface and results in the formation of the 211-phase with another morphology (needle-shaped particles). In accordance with the mechanism considered above, this facilitates dispersion of anisotropic particles of the 211-phase by the moving crystallisation front and, finally, the formation of more finely disperse inclusions of the 211-phase in the 123-phase matrix (see Table 3). The possibility of controlling the composition of composites by extracting the excess of $BaCuO_2$ from stoichiometric specimens of the $YBa_2Cu_3O_z$-phase using porous Y_2BaCuO_5-substrates (the so-called 'Liquid-Phase-Removal-Process' or LPRP method) was also reported.[200]

Thus, the analysis of the published data[9,11,55] shows that an increase in the dispersity and uniformity of distribution of the particles of secondary phases is simultaneously one of the major lines of modification of the 'melt solidification processes' and a criterion for evolution of these methods. The 211-phase has a complex effect on the microstructural and functional characteristics of specimens. This phase is responsible for completeness of crystallisation, strength of materials, morphology of the superconductor grains and the appearance of new pinning centres. Eventually, controllable modification and variation of the above-mentioned processes and parameters results in an essential improvement of functional characteristics of the materials obtained.

The role of gas atmosphere. As has been mentioned above, gas exchange with the environment plays an essential role in the preparation of high-temperature superconducting materials. By varying the partial pressure of oxygen it is possible to solve several important problems. First is the problem of reduction of the crystallisation temperature and provision of compatibility of the melt with low-melting substrates. The second problem is associated with modification of procedures for creation of supersaturation by smooth variation of the partial pressure of oxygen, which can favour both controllability of the process and a decrease in the amount of impurities in the final product. Third, prevention of bubbling and deformation of melt-processed material. Finally, the fourth problem is the control of both the width of the homogeneity region and the cation ordering in the solid solutions based on the 123-phase.

The effect of partial pressure of oxygen on the processes of preparation of high-temperature superconducting materials has been little studied.[13,218–222] A decrease in the temperature of peritectic melting of the 123-phase at reduced oxygen content and the formation of low-melting eutectics[220] containing Cu(I) (at 770–800 °C) was observed.[218,219] This made it possible to lower the growth temperature of single crystals of the 123-phase (down to ~ 910 °C at $p_{O_2} = 5 \times 10^2 - 2 \times 10^4$ Pa)[220] and to prepare thick films on a silver substrate [T_m(Ag) ≈ 960 °C] as well as rather dense bulky polycrystalline specimens.[13,221,222] An original synthetic method consisting of isothermal crystallisation accompanied by a slow increase in the partial pressure of oxygen has been reported.[218,220] In this case, the process begins at a low partial pressure of oxygen and is completed in pure oxygen (the so-called 'Isothermal Melt Crystallisation' of IMC method).

Obviously, the density of superconducting materials should be maximum. However, the specimens prepared by melt solidification processes change their linear dimensions and shapes during oxygen exchange,[9,11,55,129] which results in an increase in their volumes and in the formation of a well-developed pore system which can hardly be removed. This problem is usually considered as applied to bismuth-containing high-temperature superconducting silver-sheathed tapes.[23] Unfortunately, almost no studies on this effect in high-temperature superconducting R–Ba–Cu–O materials have been reported, though it also plays a negative role, especially in the fabrication of materials with high critical transport currents. Experiments have shown that the main factors affecting the oxygen exchange between a sample and a gas phase are the phase composition, chemical homogeneity, relative content of Cu(I) in the solid phase, partial pressure of oxygen and the procedure used for compacting the sample.[9,129]

Currently, the 123-phases containing 'light' RE metals (La, Nd, Sm and Eu) are often synthesised using the single-crystal growth and preparation of melt-processed ceramics in an inert atmosphere. This is first of all due to the necessity of decreasing the degree of REE substitution for Ba in solid solutions in order to increase the transition temperature to the superconducting state.[7,8]

Formation of single-domain structure. Taking into account the grain boundary models considered above, it can be assumed that the most favourable way of fabricating the HTSC capable of carrying strong critical transport currents is to prepare textured materials.[223–231] Attempts at preparing superconducting ceramics with oriented (plate- or rod-like) structure were based on conventional texturing procedures such as slow cooling in a uniform temperature field (grad $T = 0$), slow cooling in a temperature gradient field (grad $T > 0$) without moving a specimen (versions of the Bridgman method: 'Vertical Gradient Freezing' or VGF, 'Seeded Directional Solidification' or SDS), a gradient crystallisation with a moving hot zone (the 'Zone Melting' or ZM method) and the use of seed crystals (the 'Top-Seeded-Melt-Growth' or TSMG method). Non-traditional methods, *e.g.*, crystallisation along the concentration gradient (the so-called 'Constitutional-Gradient-Melt-Growth' (CGMG) and 'Geometrically-Organised-Growth-Evaluation' (GEORGE) processes) are also used.

Introduction of artificial nucleation centres of the 123-phase is an efficient method for controlling the nucleation. Such centres are formed by introducing relatively large seed crystals of REE-containing analogues of the 123-phase with higher peritectic decomposition temperature.[223] Usually, Sm123 ($T_p \approx 1050$ °C) and Nd123 ($T_p \approx 1085$ °C) phases are used as seed crystals. As a rule, the seed crystals are placed on top of a dense substrate (a pellet or a rod). Then the melt–crystallisation cycle is performed using the temperature gradient or movement of the hot zone along the sample. The seed crystal with higher melting temperature initiates the growth of the desired phase along the direction of

propagation of the crystallisation front, which results in the formation of giant pseudo-single-crystal domains whose dimensions are comparable with those of the sample.[7, 8, 224–226]

It is noteworthy that the orientation of pseudo-single crystals thus formed virtually coincides with that of the seed crystal, therefore the growth direction of the 123-phase is readily controllable. This is probably due to the epitaxial character of the process on the faces of the seed crystal, the unit cell parameters of which are close to those of the desired 123-phase. Often, the observed formation of differently oriented domains indicates complexity of the actual growth mechanism.[8] It was proposed to coat the 'non-working' surface of the seed-crystallising specimens with compounds that form the Yb123-phase with a lower peritectic decomposition temperature, thus preventing crystallisation on the lateral surface of the pellet.[225] Single crystals of magnesium oxide and strontium titanate were also proposed as seed crystals; however, no epitaxy was observed because of the chemical reaction between the melt and seed crystals and the formation of a buffer layer of the reaction products, so the efficiency of using such seed crystals decreases drastically.[6, 7]

If the seed crystals are introduced at the beginning of melt crystallisation in the course of its cooling, it is possible to obtain large-grain specimens of high quality. The 'Constant-Undercooling-Solidification-Processing' (CUSP) method,[8, 226] consisting in isothermal crystallisation of the 123-phase after introduction of a seed crystal into the hot zone, is a modification of the above-mentioned approach. Unfortunately, it is difficult to introduce a large number of oriented seed crystals anisotropically distributed in the bulk of the sample, which is necessary for the corresponding texturing of a high-temperature superconducting material (the 'Composite Reaction Texturing' or CRT method).[227] Only a few studies concerning the introduction of multiple seed crystals either into the bulk or on the surface of specimens have been reported so far.[228]

Magnetically induced alignment (MIA)[229, 230] is performed using REE atoms with large magnetic moments (Gd, Dy and Ho). The degree of magnetically induced texturing of the specimens prepared even by ordinary sintering increases in proportion to the applied magnetic field. Combination of this approach with crystallisation from the melt increases its efficiency, which reaches an optimum value in magnetic fields higher than 1 T.[230]

Mention should be made of the original CGMG method in which crystallisation is driven by the gradient of the REE concentration in the melt, resulting from varying the concentration of REE (*e.g.*, Yb and Y) with different peritectic decomposition temperatures.[231] It is believed that this method can serve as a basis for the development of a process of preparation of long-length textured materials including tapes sheathed with highly oriented 123-phase.[228]

Chemical modification and generation of efficient pinning centres. The 'Oxygen-Controlled-Melt-Growth' (OCMG) method is a new method for the preparation of high-temperature superconducting materials at reduced partial pressure of oxygen (0.1 mol. % – 1 mol. % O_2).[7, 232] It is based on the ability of REE with the largest ionic radii (in particular, Nd, Sm, Eu and Gd) to form solid solutions of the $R_{1+x}Ba_{2-x}Cu_3O_z$ type. Crystallisation from the melt at reduced partial pressure of oxygen results in a considerable decrease in the degree of barium substitution and in appreciable increase in the transition temperature to the superconducting state (up to 95 – 96 K).[7, 8, 76, 86, 88] This is also connected[88] with possible cation ordering in the crystal lattice, *e.g.*, with the formation of pairs of neodymium ions in the barium positions, which results in the ordering of the oxygen sublattice. At the same time, domains with fluctuations of chemical composition can appear in such a superconducting matrix. These domains are efficient pinning centres because of the strong suppression of superconductivity therein in nonzero magnetic fields, which results in the peak effect (see Fig. 4).[7, 8]

The advantage of the pinning centres thus generated over point defects consists in higher efficiency of modulations of chemical composition of the structure at relatively high temperatures (the liquid nitrogen temperature) corresponding to the operating mode of high-temperature superconducting materials. The formation of these types of pinning centres that were not observed for the Y123-phases is the major advantage of the OCMG method, which allows the preparation of superconducting materials with record characteristics.[7]

Several reasons for the appearance of pinning centres are discussed in different models.[7, 8, 76, 232–234] The first of them is connected with random fluctuations of the Nd : Ba ratio in the superconducting matrix due to local fluctuations of temperature, p_{O_2} and the melt composition during the growth of the pseudo-single-crystal domains (for the OCMG method). The next reason is the formation of a quasi-ordered nanostructure as a result of spinodal decomposition of the solid solution caused by post-crystallisation annealing. Third, it is the formation of clusters, oxygen vacancies and twin boundaries in the case of nonuniform oxygen distribution in the superconducting matrix. Next, the pinning centres can appear due to the formation of highly disperse inclusions of the R422-phases and redistribution of cations between the matrix and these non-superconducting inclusions. Finally, antistructural defects produced in the course of (probable) mutual exchange of Nd^{3+} and Ba^{2+} ions between the corresponding crystallographic positions can also result in the appearance of pinning centres (see **S.12**).

The peak effect observed in all R123-phases including R = Y is associated with the presence of local oxygen-deficient regions characterised by lower T_c as compared to that of the entire matrix.[233, 234] It is assumed[233] that this effect increases due to the presence of impurities (*e.g.*, the components of the crucible) which reduce the oxygen mobility and favour its nonuniform distribution. It was hypothesised[93] that nonuniformity of the oxygen distribution in the materials based on the Y123-phases can be due to the spinodal decomposition of the solution formed by the $YBa_2Cu_3O_6$ and $YBa_2Cu_3O_7$ phases.

An alternative model[7, 8, 91, 92] relating the peak effect in the materials based on the R123-phases (R = Nd, Sm, Eu, Gd) to the fluctuations of the cation composition does not contradict the preceding model since it considers variations of the cation composition as a primary phenomenon responsible for a side effect, *viz.*, nonuniform distribution of oxygen. The possibility was reported[7, 8, 92] of controlling the peak effect by different parameters of the process, such as the post-crystallisation annealing temperature, oxidation degree of the specimens and introduction of a 'cocktail' of REE dopants.

c. Methods of single-crystal growth

Unlike the production technology of polycrystalline materials, single-crystal growth is focused on growth of chemically and structurally homogeneous crystals of a specified size, shape, composition and controllable low level of defects and impurities. Meeting these requirements allows the crystals to be used in basic or applied investigations, *e.g.*, in structural analysis,[17, 235, 236] spectroscopy,[237, 238] studies of oxygen diffusion,[154, 157] atomic force microscopy,[7, 8, 12] measurements of fundamental physical constants,[19] *etc.*[8, 239]

Anisotropy of the rate of crystal growth along crystallographic directions depends in a complex manner on the nature of REE and conditions of crystallisation.[8] This can be due to the crystallographic anisotropy, different face energies and different mechanisms of the face growth. In turn, the growth anisotropy causes changes in the morphology and shape of the entire crystal. For instance, the crystals grown by spontaneous crystallisation are usually thin plates oriented perpendicular to the ⟨001⟩ direction,[126, 240, 241] since the growth rate of the {100} faces is approximately five times higher than that of the {001} faces at high cooling rates (kinetic control). If the rate of melt cooling decreases down to 0.5 – 1.0 K h^{-1}, thick prisms-parallelepipeds or even isometric crystals are formed.[241] The {101}, {011} and {111} faces grow under these conditions along with the {100},

{010} and {001} faces, which indicates a quasi-equilibrium crystal growth (thermodynamic control).[126]

The method of top-seeded crystal pulling from supercooled melt is characterised by a rather low supersaturation.[8, 114, 239, 242] Such factors as the melt hydrodynamics and the distribution of temperature and concentration near the growing single crystal begin playing a significant role in this case (see **S.13**). By controlling the pulling rate and taking into account the growth anisotropy it is possible to obtain various 'bulk' single crystals, *e.g.*, pyramidal crystals with expanded bases, large isometric crystals with a small angle of inclination of edges, pyramidal crystals with 'concaved' bottom face and cylindrical crystals.[8, 114, 239, 243] Other crystallisation methods allow the obtaining of needle-shaped and plate-like single crystals and crystals in the form of parallelepipeds as well.[244–249] Thus, modern crystallisation methods make it possible to grow the HTSC crystals of any desired shape.

Crystallisation from melts is strongly affected by the nature of RE elements. In particular, introduction of 'light' REE can cause a chain of interrelated 'domino'-like changes in the characteristics of the R123-phases. The chain is as follows: an increase in the 'geometrical' stability → an increase in the thermal and thermodynamic stability → an increase in both the peritectic decomposition temperature and dissolution enthalpy of the R123-phases in melts → an increase in the solubility of REE and a decrease in the slope of the liquidus near the peritectic decomposition temperature, a decrease in the viscosity and acceleration of diffusion of the components in the melt. As a result, the crystallisation rate of the R123-phases containing 'light' REE (especially, Nd and Sm) should be higher than that of the same phases containing 'heavy' REE (Y, Yb, *etc.*) at a given supercooling degree of the melt, which favours the preparation of larger Nd123, Sm123, *etc.*, crystals.[114] The predicted regularities of the growth rate of 123-phases with different REE are observed experimentally, which can be seen from comparison of the growth rates along the direction of pulling the crystals grown by the modified Czochralski method:[8, 114]

Phase	Y123	Y123	Pr123	Nd123
Atmosphere	air	oxygen	air	air
Growth rate /mm h^{-1}	0.075–0.108	0.16	0.1	0.24

The growth rate of the crystals of a mixed (Y,R)123-phase was increased by doping the melt with samarium and neodymium.[114]

Unfortunately, the advantages of using 'light' REE to assist single-crystal growth and preparation of 'melt-processed' ceramics are combined with problems in controlling the chemical composition of products due to cation nonstoichiometry of the 123-phases containing 'light' RE elements. A simplified consideration of crystallisation in the frame of the Y_2BaCuO_5–$Ba_3Cu_5O_8$ quasibinary system is possible only for the 'point' Y123-phase (Fig. 25). In the case of systems whose phase diagrams contain regions where solid solutions can exist,[8] the C° compositional point moves from the melt region L or a 422–L ($PrBaO_3$–L) two-phase region of the peritectic melt (at $T = T_b$), which contains particles of 'secondary phases' at elevated temperatures, to the R123ss–L two-phase region where the compositions of equilibrium solid [$c(ss)$] and liquid [c(L)] phases are determined at $T_s < T_b$ ($T_b > T_p$) by tie-lines.

The ratio of the coefficients of cation diffusion in the melt plays a particularly important role in the establishment of an interrelation between the true compositions of the liquid and solid phases in the case of steady-state crystal growth. Obviously, the close values of these coefficients favour the choice of a tie-line that is the closest to the equilibrium tie-line. If the diffusion coefficient of a given cation is lower than those of other cations, the true tie-line is shifted with respect to the equilibrium tie-line.[8] As a rule, the differences between the diffusion coefficients are not too large and the use of equilibrium phase diagrams makes it possible to correctly (quantitatively) predict the compositions of phases that crystallise under given conditions.

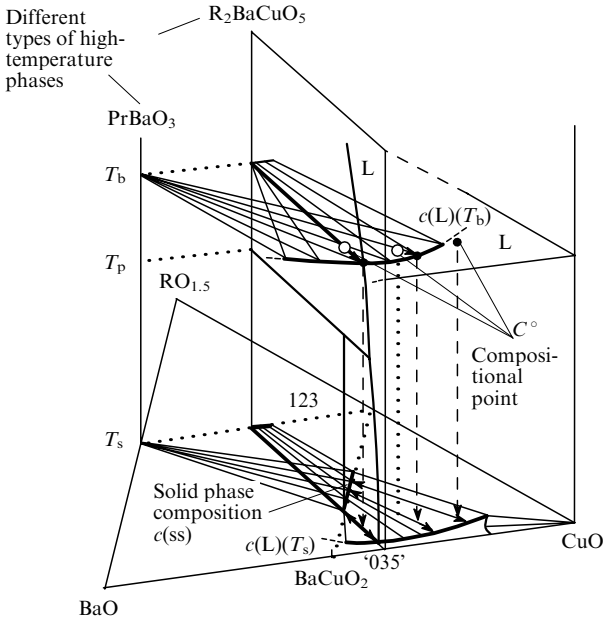


Figure 25. Supersolidus phase diagrams and single-crystal growth of HTSC.

Analysis of the data presented in Table 4 indicates that the volume of single crystals of the R123-phases can be appreciably increased and their perfection can be essentially improved[250] using two modifications of the Czochralski method [the 'Solute-Rich-Liquid-Crystal-Pulling' (SRL-CP) and 'Top-Seeded-Solution-Growth' (TSSG) procedures].[8] This is a universal method since it allows one to grow large single crystals of almost all R123-phases (R = Y, Nd, Sm, Pr) and $(R_1R_2)Ba_2Cu_3O_z$ (R_1 = Y, R_2 = Sm, Nd) solid solutions[8, 80, 81, 114, 251] as well as $Nd_{1+x}Ba_{2-x}Cu_3O_z$, $Pr_{1+x}Ba_{2-x}Cu_3O_z$, $Nd_{1+x}Ba_{2-x}Cu_{3-y}$. .Ga_yO_z, $YBa_2Cu_{3-y}Zn_yO_z$ phases, *etc.* According to the reported data,[252] superconducting crystals of the Pr123-phase can be obtained by the 'Top-Seeded-Floating-Zone' (TSFZ) procedure[8] at reduced partial pressure of oxygen (see **S.14**).

Considerable attention has been paid recently on the development of growth methods of single-crystal high-temperature superconducting whiskers.[76, 244, 253–256] The growth of whiskers in the systems with regions of solid solutions of the Bi–Sr–Ca–Cu–O[254–256] and R–Ba–Cu–O (R = Sm,[244] Nd[76]) types was reported. It is known that this type of crystals possesses unique electrophysical[253] and mechanical[257] properties.

4. Preparation of long-length composites

Almost all the HTSC materials considered above (except for single crystals) are composites comprising the superconducting matrix and non-superconducting phases that determine specific properties and areas of application of a particular composite. For instance, highly diperse powders prepared by the chemical homogenisation methods are usually a mixture of different phases and dopants. The components of a film–substrate pair affect strongly each other. Large-grain ceramics are also a composite containing 'secondary phases' as inclusions in the superconducting matrix.

High-temperature superconducting silver-sheathed tapes are a typical example of industrial superconducting composites.[16, 23, 54] To prevent thermoresistive instability of such tapes, they are fabricated as multifilament wires in which disappearance of superconductivity due to a local overheating above T_c will cause the current to flow round the resistive area through adjacent superconducting cores. Usually, superconducting wires are made of bismuth- or (more rarely) thallium-containing HTSC which possess higher plasticity and can be textured much easier than the

Table 4. The progress in the preparation of single crystals of the $RBa_2Cu_3O_z$-phases.[8, 114, 126, 239–256]

R	Single-crystal growth regime					Crystal size [a] mm × mm × mm	T_c /K	Note	Ref.
	flux	crucible	p_{O_2} /atm	cooling /°C	v_{cool} /°C h^{-1}				
Spontaneous crystallisation (flux growth)									
Y	'$YBa_4Cu_{10}O_x$'	–	0.21	–	4–15	4 × 4 × 0.5	–	–	249
	~4 at.% Y, 30 at.% Ba, 66 at.% Cu	Al_2O_3	0.21	1010–960	0.5	5 × 5 × 2	88	–	126
	Y : Ba : Cu = 1 : 6 : 18	Al_2O_3 with polished walls	0.21	1000–970	0.1–0.4	5 × 4 × 1.5	90	temperature oscillations	251
	Y : Ba : Cu = 1 : 18 : 45	ZrO_2/Y_2O_3	0.21	990–950	0.3–0.8	5 × 3 × 0.7	93.2	–	246
	64% Y123–36%(7$BaCuO_2$ + 11CuO)	Y_2O_3	0.21	1050–970	0.5	4.3 × 4.3 × 3.6	91	temperature gradient	241
	0.13(1/6)$YBa_2Cu_3O_y$–0.87(0.28BaO + + 0.72CuO) + 1 mass % BaF_2	Al_2O_3	0.21	1000–900	2	20 × 10 × 0.5 12 × 10 × 1	93	–	119
	KCl : NaCl (1 : 1) + 5 mass % $AgNO_3$	Al_2O_3	0.21	1030–850	1	8 × 6 × 2	90	–	245
	1.5 mol.% Y123, 2CuO · $BaCuO_2$	ZrO_2/Y_2O_3	$5 \cdot 10^{-3} \rightarrow 0.2$	910	for 50 h	5 × 5 × 0.1	92	T = 910°C = const	220
Y, Pr	10 mol.% R123, flux of an eutectic composition	$BaZrO_3$, density 98.5%	0.21	1005–950	0.7	2 × 2 × 0.5	91	–	248
Nd	flux of an eutectic composition	ZrO_2/Y_2O_3	0.05	1030–950	–	4 × 4 × 4	94.8	–	126
Floating zone melting									
La, Nd, Sm	Nd : Ba : Cu = 1 : 4 : 6–1 : 29 : 66	–	10^{-2}–10^{-4}	–	–	3 × 1.5 × 1.5 (single-crystal grains)	90 91 94	hot zone movement at 0.4–1 mm h^{-1}	8
Nd	Nd : Ba : Cu = 1 : 7.6 : 21.5	–	0.001	–	–	∅ 3 × 32	94	hot zone movement at 0.46–0.50 mm h^{-1}	110
Top-seeded solution growth by crystal pulling (a modified Czochralski method)									
Y	0.15(1/6)$YBa_2Cu_3O_y$–0.85(0.3$BaCuO_2$– –0.7CuO)	Al_2O_3	0.21	930	for 17 days	8 × 6 × 5	90	crucible rotation at 2–8 rpm	118
Y, Sm, Nd	211 + 0 : 3 : 5, 5 : 36 : 59	Y_2O_3	0.21	1000	–	8 × 8 (5)	89	pulling rate 0.2 mm h^{-1}, seed crystal rotation at 120 rpm	8
Y	211 + 0 : 3 : 5	Y_2O_3, ∅ 100 mm	0.21	1002–997	–	14 × 14 × 14 (angle of inclination of faces < 25°)	92	pulling rate 0–0.14 mm h^{-1}, seed rotation at 120 rpm	8
	211 + 0 : 3 : 5, 5 : 36 : 59	Y_2O_3	1.0	1015	–	19.8 × 19.5 (16.5)	92.7	pulling rate 0.05 mm h^{-1}, seed rotation at 70–120 rpm, cooling in N_2	114
Nd	(~0.84–1.98) at.% Nd, (28.49–28.16) at.% Ba, (70.67–69.86) at.% Cu	SnO_2	0.21	1030–960	0.5	22 × 15 × 3	92	crucible rotation at 15 rpm, doping by Ga	251
	Nd : Ba : Cu = 0 : 0.78 : 1	Nd_2O_3	0.21	1058–1070	for 67 h	24 × 24 (21)	95	pulling rate 0.1–0.25 mm h^{-1}, seed rotation at 70–120 rpm	114

[a] Values in parentheses refer to the height of the pyramidal crystal.

Table 5. Chemical compatibility of phases and the superconduction characteristics of the composites based on $Bi_2Sr_2CaCu_2O_8$-phase doped with non-superconducting oxides.[264–270]

Element (A)	Solubility/mol A/mol 2212			Phase in the 2212-matrix containing A			T_c/K (2212)	Pinning [a]
	in 2212	in a melt	T/°C	composition	size /μm	state		
Zr	< 0.05	< 0.05	1300	$SrZrO_3$	0.2	in 2212, agglomerated	93	0.092
Hf	< 0.05	< 0.05	1300	$SrHfO_3$	–	–	93	–
Sn	< 0.03	< 0.05	1300	$Sr_{1-x}Ca_xSnO_3$ ($x \approx 0.1$)	0.2	in 2212, agglomerated	90	0.074
Mg	< 0.05	< 0.1	1300	$Mg_{1-x}Cu_xO$ ($x \approx 0.1$)	1.0	in 2212	92	0.021
Al	< 0.03	0.05	900	$Sr_{1.7}Ca_{1.3}Al_2O_6$	2–5	in 2212, agglomerated	90	0.026
				$BiSr_{1.5}Ca_{0.5}Al_2O_z$	2–5	–	–	0.016
Ga	0.15	0.8	900	$Sr_{1.3}Ca_{1.7}Ga_2O_6$	20	between 2212-grains	80	–
				$Bi_{0.2}SrCa_{0.8}Ga_2O_z$	10	–	–	–
				$Bi_{1.7}Sr_{2.3}Ca_{0.6}Cu_{1.6}Ga_{0.4}O_z$	–	–	–	–
In	< 0.05	< 0.1	900	$Sr_{1-x}Ca_xIn_2O_4$ ($x \approx 0.55$)	0.5 × 5	in 2212, agglomerated	82	–

[a] ΔM(60 K, 10 mT)/ΔM(5 K, 1 T), where ΔM is the width of a hysteresis loop; this value for the undoped phase equals 0.01.

materials based on the R123-phases.[258–263] Additionally, rather low melting temperatures of bismuth-containing HTSC provide a wider choice of metals and alloys for fabricating the sheath.

Silver is one of the most widely used materials for the outer sheath. It is plastic and relatively available, has high electrical and heat conductivity, causes no decrease in the transition temperature to the superconducting state of HTSC and serves as a specific membrane for oxygen exchange between the superconducting cores inside the tape and the gas atmosphere outside the tape. This system is closed as regards the mass transfer of bismuth, calcium, strontium and copper oxides. In addition, the walls of silver-sheathed tapes can favour nucleation and oriented grain growth near the surface areas of HTSC adjacent to the sheath,[23, 54, 263] especially in the case of tapes with planar (ribbons) or pseudo-1D (multifilamentary wires) geometry. Often, the strength characteristics of the sheath are improved using the effect of dispersion hardening, *e.g.*, due to the formation of the MgO microcrystals in the silver matrix upon oxidation of silver–magnesium alloys by atmospheric oxygen.

The essential feature required of superconducting silver-sheathed tapes is that they be capable of carrying heavy currents. This first of all requires the attainment of perfect mutual orientation of highly anisotropic superconducting crystallites and exclusion of weak links between them. The negative effect of 'secondary phases' and gas evolution on peritectic melting or high-temperature annealing, which can cause a nonuniform current flow through the cross section of the tape, local violation of the optimum orientation of the HTSC grains and even shut off the orifice of the wire of size 1–30 μm, should also be prevented.

The optimum microstructure is usually formed by varying the composition, external gas atmosphere and thermal annealing regime. This requires a detailed knowledge of the phase diagrams.[53, 54, 69, 263] To attain high transport characteristics of high-temperature superconducting tapes, it is also appropriate to use the methods of chemical homogenisation for preparation of highly disperse chemically and granulometrically homogeneous carbon-free powders for filling the silver sheathes that should undergo a plastic deformation. The methods used in the fabrication of superconducting silver-sheathed tapes should include (i) modern processes for the preparation of composites ('powder-in-tube', 'tube-in-tube', 'rod-in-tube' methods, *etc.*), (ii) thermomechanical treatment (repeated drawing and rolling) resulting in elongation of the silver sheath filled with powder by a factor of several tens, in an appreciable increase in the density of the superconducting cores inside the tape and in forced orientation of the HTSC grains along the deformation axis and (iii) low-temperature vacuum annealing to optimise the oxygen content inside the tape and to prevent bubbling.

Thus, it is now possible to fabricate tapes with a microstructure close to the desired one using modern processes and production methods. However, the fundamental problem associated with a dramatic decrease in the critical currents of bismuth-containing HTSC (compared to other types of HTSC and first of all, to R123-phases) on raising the temperature or an increase in external magnetic field (see Fig. 4) remains unsolved. Therefore, the operating temperatures of bismuth-containing tapes are lowered to the liquid hydrogen temperature (20 K), despite the fact that their T_c values (90–110 K) are higher than the boiling point of a cheap coolant, liquid nitrogen (77 K), which is effectively used with other types of HTSC.

The most promising way of increasing the critical current density for bismuth-containing high-temperature superconducting materials is associated with the preparation of composites with uniformly distributed microscopic inclusions of non-superconducting phases formed by the constituents of the system or by introducing 'alien' phases compatible with the HTSC.[264–270] The main characteristics of the composites thus prepared (homologues of the 2212- and 2223-bismuth-containing HTSC) are presented in Table 5. As can be seen, the most pronounced positive effect is observed with zirconates and stannates, although there are many phases compatible with the high-temperature superconducting matrix which do not result in appreciable decrease in its T_c and do not suppress the HTSC formation dynamics. At the same time, measurements of physical properties indicate an increased stability of superconducting characteristics of the composites.[270] Obviously, this promising investigation line will be developed in the future.

V. Practical applications of high-temperature superconducting materials

The possibility of practical applications of high-temperature superconducting materials has opened fresh opportunities for microelectronics, medicine, production of efficient energy storage and power transmission systems and industry as a whole.[7, 8, 15, 16]

The use of high-temperature superconducting films allowed production of small-scale systems belonging to a new generation of communication devices including electromagnetic screens, modulators, antennas, commutators, filters of microwave and pulse signals, multilayered film hetero-structures including dielectric, ferroelectric and normal metal layers in addition to the HTSC layers. Such films made it possible to develop bolometers operating in the millimetre, submillimetre and infrared bands, basic circuit arrangements of superfast computers, ultrasensitive tomographs and diagnostic devices capable of responding even to changes in the mental condition of a man (measuring devices based on the Josephson effect).

High-temperature superconducting tapes with high superconducting characteristics can actually be used in practice for

production of super-power magnets and lines for nondissipative transmission of electrical power. Currently, silver-sheathed tapes can be manufactured commercially. Large-scale production and wide use of these tapes are still limited by high cost. Nevertheless, many small-scale systems and test lines are already at work.

The prospects of using HTSC based on the 123-phase are associated with the possibility of production of bulky items of a rather simple shape using the most suitable and operationally convenient methods. Such items can be divided into two classes. The first of them comprises the specimens characterised by a high ability to shield the external magnetic field or to be repelled by the field. This ability can be characterised by the so-called levitation force, which is dependent on the intracrystallite critical current density. The other class comprises the specimens of high-temperature superconducting materials with high transport (intercrystallite) current. In the future, such ceramic devices can find practical use in the production of permanent magnets with 'frozen-in' magnetic flux, magnetic repulsion trains (the MAGLEV project), flying wheels, bearings rotating virtually without friction, efficient and economical motors, super-power generators and transformers, magnetic separators, superconducting relays, fast current limiters, powerful nondissipative electrical current leads, medical tomographs, powerful magnetic systems for thermonuclear fusion and accelerators of elementary particles (new-generation Tocamac) and, finally, magnetohydrodynamic generators.

Preparation of substrates in thin film technology and microelectronics seems to be the most realistic practical use of large single crystals of HTSC. Such substrates should be characterised by small mismatch between the unit cell parameters and those of materials of the films, have close TEC values and favour epitaxial growth of films. Additionally, all crystallochemical and thermomechanical parameters of high-temperature superconducting single-crystal substrates can be precisely adjusted by using solid solutions with different types of substitution of the yttrium and barium positions.

Supplement

S.1. The presence of a metastable orthorhombic $BaCu_3O_4$ phase [$a = 10.986(3)$, $b = 5.503(1)$, $c = 3.923(1)$ Å] was found in thin films of the R123-phase.[271] Stabilisation of this phase requires the formation of a coherent interface between the phase and surrounding high-temperature superconducting matrix. The $BaCu_3O_4$ phase decomposes if the film thickness exceeds ~ 0.3 μm.

S.2. Discrepancies in determination of the limits of oxygen nonstoichiometry in $BaCuO_{2+z}$ can be due to the formation of oxycarbonates [*e.g.*, $Ba_{44}Cu_{48}(CO_3)_6O_{87.9}$, see Aranda and Attfeld [272]] or to an ambiguous assignment of the specimens with other cation compositions to this phase.[273, 274] A reliable thermodynamic assessment of the Ba–Cu–O system was reported.[273] The oxygen nonstoichiometry in the Ba_2CuO_3-, $BaCuO_2$- and $Ba_2Cu_3O_5$-phases was also discussed.[274–276]

S.3. The low-temperature decomposition of $NdBa_2Cu_3O_z$ was considered.[277] It was established that degradation of superconducting properties of high-quality polycrystalline specimens ($T_c = 94$ K) in the temperature range 450–750 °C occurs nonlinearly depending on the 'ageing' temperature and duration of low-temperature isothermal annealing. Prolonged annealing at 400–600 °C for 450 h in air can result only in a slight decrease in T_c after complete oxidation of the sample ($T_c = 89$ K), whereas the annealing at 700 °C for 165 h brings about a decrease in T_c by 11 K.

S.4. The first reliable determination of the structure of a low-temperature (oxidised) modification of the $Nd_{1.9}Ba_{1.1}Cu_3O_z$-phase using the data of X-ray, electron and neutron diffraction experiments and IR and Raman spectroscopy was reported recently.[278]

Studies carried out by neutron diffraction, differential scanning calorimetry, Raman and Mössbauer spectroscopy and EXAFS have confirmed that, unlike the $NdBa_2Cu_3O_z$-phase, oxidation of the $Nd_{1.9}Ba_{1.1}Cu_3O_z$-phase can occur owing to 'one-dimensional' oxygen diffusion along the b axis of the structure. This is accompanied by a second order phase transition resulting in the appearance of an inversion centre (the high-temperature modification has the *Amm*2 space group *vs.* the *Ammm* group for the low-temperature modification [278]), ordering of the oxygen sublattice and coupled zigzag-shaped displacements of copper atoms from the 'ideal' positions at the centres of perovskite-like structural blocks, which is most likely due to 'compression' of the structure along the long axis c caused by introduction of extra oxygen atoms.[279]

S.5. Discussion of the charge transfer between the superconducting planes and dielectric block using the results obtained by X-ray structural analysis and Raman spectroscopy can also be found elsewhere.[278, 280]

S.6. At a given partial pressure of oxygen, the compositions with the minimum $x(S_1)$ and maximum $x(S_2)$ substitution degrees in the $Nd_{1+x}Ba_{2-x}Cu_3O_z$ solid solution are fixed, because they correspond to the invariant quinary equilibria (the number of degrees of freedom is $4-5+2-1=0$)

$$Nd_{1+x(S_1)}Ba_{2-x(S_1)}Cu_3O_z + BaCuO_2 \rightleftharpoons \rightleftharpoons Nd_4Ba_2Cu_2O_{10} + L + O_2,$$

$$Nd_{1+x(S_2)}Ba_{2-x(S_2)}Cu_3O_z + CuO \rightleftharpoons Nd_2CuO_4 + L + O_2.$$

The corresponding phase transformation temperatures are also fixed, which provides the optimum conditions for achieving the above-mentioned substitution degrees. For instance, it was experimentally established that a temperature range between 985 and 1030 °C is optimum for preparation of the $NdBa_2Cu_3O_z$ phase with $T_c \simeq 94$ K (at $p_{O_2} = 0.21$ atm).[281]

S.7. One of the most promising and intensively developing universal approaches to computer simulation of crystallisation of HTSC systems is the phase field concept for multiphase systems (PFCMS).[282] In the classical nucleation models, the liquid–solid interface is assumed to be infinitely thin. The PFCMS model considers a liquid–solid interface of finite thickness. Obviously, this is a great stride toward deriving a fundamental generalisation of crystallisation mechanisms. An additional continuous function (the phase field) is also introduced in this model, which plays the role of the order parameter used for identification of the regions of the liquid and solid states. In the simplest case (one solid phase in melt), the phase field can be described using a function $p(x,t)$ whose values vary between 0 and 1. If $p(x,t) = 1$, then at a point x and at instant t the system is in the solid state, whereas $p(x,t) = 0$ corresponds to the liquid. The liquid–solid interface is described by all $p(x,t)$ values between 0 and 1. The following equation for the phase field function was derived [282] by minimising the density of the free energy of the system

$$\tau\left[\left(\dot{\mathrm{p}}\right)(x,t)\right] = \varepsilon \nabla^2 \mathrm{p}(x,t) - \mathrm{f}'(p) + \mathrm{m}(\mathrm{p},T,c).$$

This equation includes most of the physically important melt solidification parameters such as the (free) energy gradient ε; the crystallisation front propagation velocity (by means of the orientation-dependent function τ, which describes an anisotropic or facet growth); the derivative $\mathrm{f}'(p)$ of the potential determining the phase boundary stability under equilibrium conditions, as well as the driving force $\mathrm{m}(\mathrm{p},T,c)$ of the process, which is proportional to the degree of deviation from thermodynamic equilibrium and should include the temperature dependence $T(x,t)$ and the concentration profile of the distribution of constituents (c). The necessity of inclusion of the function c is explained by considering the diffusion processes occurring in the system (*e.g.*, the dissolution rate of the solid phases in the melt).

S.8. The mechanism of the needle-shaped crystal growth under isothermal conditions remains unclear as yet. At the same time, this phenomenon is not observed for those REE of the yttrium subgroup whose R123-phases do not form the barium ← REE substitution solid solutions. It was also established [281] that the reason for growth of the needle-shaped crystals is closely related to the features of the phase diagram of the Nd – Ba – Cu – O system, in particular, to the increased deviation of the composition of the equilibrium phase of the $Nd_{1+x}Ba_{2-x}Cu_3O_z$ solid solution towards $x > 0$ which occurs on raising the temperature. In this case, the phase with $x = 0$ decomposes on heating with the formation of a solid solution with $x \simeq 0.1$, a non-superconducting $Nd_4Ba_2Cu_2O_{10}$ phase and a melt L. At the initial moment, the composition of the liquid phase L can differ from the equilibrium composition, thus providing the driving force for the growth of $Nd_{1+x}Ba_{2-x}Cu_3O_z$ and $Nd_4Ba_2Cu_2O_{10}$ crystals not only under isothermal conditions, but (probably) also even with increasing temperature (mention may be made here that single crystals of HTSC are usually obtained by cooling of melts).

S.9. Single-phase specimens of mercury-containing HTSC and especially mercury-containing crystals can hardly be obtained because of extremely high volatility of mercury and its compounds. Therefore, the preparation of the crystals of the most promising Hg1223-homologue with unique physical characteristics [283] by the ampoule synthesis is of considerable interest. Single crystals of $HgBa_2Ca_{n-1}Cu_nO_z$ ($n < 4$) with $T_c \simeq 130$ K were synthesised by spontaneous crystallisation from PbO or $BaCuO_2$ – CuO flux in a crucible made of stabilised zirconium dioxide (crystallisation temperature $930 < T < 1070$ °C) in an autoclave at an Ar pressure of $(10-15) \times 10^3$ atm.[284, 285] Introduction of rhenium in order to stabilise the structure makes it also possible to grow single crystals of $Hg_{0.75}Re_{0.22}Ba_2Ca_5Cu_6O_{15}$ ($T_c = 100$ K) and $Hg_{1-x}Re_xBa_2Ca_6Cu_7O_{16+4x+z}$ ($T_c = 84$ K) homologues.[68]

S.10. The uniqueness of the HTSC – manganite hetero-structure [286] shown in Fig. 21 is that it comprises two promising and intensively studied phases with nonlinear electrophysical properties, *viz*., the superconducting cuprate phase and the manganite phase exhibiting a giant magnetoresistance effect. Such heterostructures are promising for the use in microelectronics.

A microstrip resonator can be considered as an example of devices manufactured using conventional elements (HTSC-films and a dielectric substrate). In this case, the double-sided deposition of a superconducting film on the single-crystal substrate was carried out by CVD methods.[287]

S.11. Phases of the $RBa_2Cu_3O_z$ type can be synthesised over a period of about 10 to 30 min at 500 – 550 °C using a mechanoactivated decomposite mixture, *i.e*., a mixture of copper-free and copper-rich reagents ($Y_4Ba_3O_9$ and CuO) compacted at 250 °C.[288]

S.12. Recently, the formation of antisite defects in the barium and neodymium sublattices in the fully oxidised $NdBa_2Cu_3O_{6.9}$ phase with a low transition temperature to the superconducting state was found by X-ray spectral and X-ray structural analysis and by Raman spectroscopy.[279]

S.13. A cuprate melt considered as a high-temperature solvent is characterised by a density from 4.8 to 5.4 g cm^{-3}. The minimum density is observed for an eutectic composition 28 mol. % BaO : 72 mol. % CuO.[289] Such melts have similar temperature dependences of the surface tension and viscosities which increase as the BaO concentration increases.[289] Above 955 °C, the surface tension coefficient of the melt lies in the range $\sim 0.3-0.6$ N m^{-1}. The calculated radii of the viscous flow units suggest that the melts have a 'slightly ionic' nature and a low aggregation degree of the ions in the melt. The melts exhibit a mixed (mostly electron-type) conductivity.

Two factors should be considered when discussing the limiting stages of single-crystal growth from a liquid (in particular, by the modified Czochralski method). First, this is the steady-state growth of the single crystal. This requires meeting the condition for the balance of the amount of R_2O_3 in the flux and that necessary for the deposition of the R123-phase on a crystal face, written over the liquid – solid interface. Second, crystallisation can be characterised by relatively high near-boundary supersaturation with respect to R_2O_3 (in the so-called boundary layer) due to kinetically hindered crystal face growth. The following approximate formula for the crystal face growth rate (υ), which includes the diffusion of Y^{3+} ions in the melt, was proposed [8] under some assumptions as a first approximation.

$$\upsilon = \frac{D_L^{2/3}\omega^{1/2}\left[(T_b - T_p)/m_L^{211} + (T_p - T_i)/m_L^{123}\right]}{1.6\nu^{1/6}(c_s^{123} - c_i)}.$$

Here, D_L is the coefficient of bulk diffusion from the Y_2O_3 source phase (Y_2BaCuO_5) contacting the melt at the temperature T_b to the face of the $YBa_2Cu_3O_z$ crystal (the peritectic decomposition temperature T_p) that grows from the melt at the temperature T_i; ω is the angular velocity of crystal rotation; m_L^{211} and m_L^{123} are the slopes of the tangent to the liquidus above and below T_p; ν is the kinematic viscosity of the melt; and c_s^{123} and c_i are the concentrations of Y^{3+} ions in the solid phase (crystal) and in the melt near the growing crystal, respectively. The maximum crystal face growth rate that can be achieved in the absence of kinetic complications is $\upsilon_{max} \simeq 0.36$ mm h^{-1}. However, it is 3 times higher than that observed experimentally (0.108 mm h^{-1}). This indicates that the growth of single crystals of the Y123-phase using the modified Czochralski method is likely to be controlled not only by diffusion of the components through the melt, but also by the interphase kinetics of deposition of the Y123-phase.

The hydrodynamic conditions of the experiments on the growth of large HTSC-crystals and their effects on the morphological features of $RBa_2Cu_3O_z$ crystals have been analysed in detail using the generalised 'dimensionless analysis' approach.[290] Growth of a crystal by the modified Czochralski method is characterised by an increase in the diameter of the crystal with time, which continuously changes the conditions for crystal growth. Generally, the relative contribution of convection due to (i) the density difference between the melts with different temperatures (natural convection) and (ii) rotation of the crystal (forced convection) can be assessed as the ratio of the Reynolds and Grasshof numbers. The dimensionless temperature

$$\Theta = \frac{T_i - T_{top}}{T_b - T_{top}}$$

of the 'crystal – melt' contact surface (T_i) and the top region of the crucible (T_{top}), normalised to the overall temperature gradient between the bottom (T_b) and top regions of the crucible can be estimated (from experimental data) as $\Theta = 0.47Re^{0.028}Pr^{0.041}Gr^{0.019}Dsc^{0.064} + 0.10$ (Dsc is the geometrical factor). According to this expression, the steady-state crystal growth requires a precise control over the rotation velocity taking into account the increase in the crystal diameter during the growth. Otherwise, a crucible of a large diameter should be used.

S.14. The results of recent studies confirm the existence of a superconducting $PrBa_2Cu_3O_7$ phase; however, this issue remains a moot question as yet.[291, 292]

This review has been written with the financial support by the Russian Foundation for Basic Research (Projects Nos 98-03-32575a and 98-03-32585a), the Federal Complex Programme 'Actual Trends in Physics of Condensed Matter' (Project No. 9607, the 'Superconductivity' investigation line) and the International Scientific-Technical Programme of the Ministry of Science and Technologies of the Russian Federation (the 'Composite' Project).

References

1. D L Nelson, M S Whittingham, T F George (Eds) *Chemistry of High-Temperature Superconductors* (Washington, DC: American Chemical Society, 1987)
2. *Zh. Vses. Khim. O-va im. D I Mendeleeva* **34** 436 (1989) [a]
3. A R Kaul', I E Graboi, Yu D Tretyakov *Sverkhprovodimost'* **1** 8 (1987)
4. Yu D Tretyakov, Yu G Metlin *Zh. Vses. Khim. O-va im. D I Mendeleeva* **36** 265 (1991) [a]
5. Yu D Tretyakov, Yu G Metlin *Zh. Vses. Khim. O-va im. D I Mendeleeva* **36** 644 (1991) [a]
6. M Murakami (Ed.) *Melt Processed High-Temperature Superconductors* (Singapore: World Scientific Publishing, 1992)
7. M Murakami, N Sakai, T Higuchi, S I Yoo *Supercond. Sci. Technol.* **9** 1015 (1996)
8. Y Shiohara, A Endo *Mater. Sci. Eng.* **R19** 1 (1997)
9. E A Goodilin, N N Oleinikov *Sverkhprovodimost'. Issled. Razrab.* **5–6** 81 (1995)
10. S R Li, N N Oleinikov, E A Goodilin *Neorg. Mater.* **29** 3 (1993) [b]
11. E A Goodilin, N N Oleinikov, S R Li, Yu D Tretyakov *Zh. Neorg. Khim.* **39** 1043 (1994) [c]
12. S K Agarwal, A V Narlikar *Progr. Crystal Growth Charact. Mater.* **28** 219 (1994)
13. J L MacManus-Driscoll *Adv. Mater.* **9** 457 (1997)
14. Yu D Tretyakov, Yu G Metlin *Materialovedenie* **8** 2 (1998)
15. *ISTEC J.* **11** (1998)
16. B J Batlogg, R Buhrman, J R Clem, D Gubser, D Larbalestier, D Liebenberg, J Rowell, R Schwall, D T Shaw, A W Sleight *J. Supercond.* **10** 583 (1997)
17. F Izumi, E Takayama-Muromachi, in *High-Temperature Superconducting Materials Science and Engineering. New Concepts and Technology* (Ed. D Shi) (Oxford: Pergamon Press, 1995) p. 81
18. J M S Skakle *Mater. Sci. Eng.* **R23** 1 (1998)
19. D M Ginsberg (Ed.) *Physical Properties of High Temperature Superconductors I* (Singapore: World Scientific, 1989)
20. Yu G Metlin, Yu D Tretyakov *J. Mater. Chem.* **4** 1659 (1994)
21. L N Dem'yanets *Usp. Fiz. Nauk* **161** 71 (1991) [d]
22. A A Kiselev (Ed.) *Vysokotemperaturnaya Sverkhprovodimost'. Fundamental'nye i Prikladnye Issledovaniya* (High-Temperature Superconductivity. Fundamental and Applied Investigations) No. 1 (Leningrad: Mashinostroenie, 1990)
23. E E Hellstrom *J. Met.* **10** 48 (1992)
24. O Yu Gorbenko, V N Fuflygin, A R Kaul' *Sverkhprovodimost'. Issled. Razrab.* **5–6** 38 (1995)
25. H Kamerlingh-Onnes *Leiden Commun.* 124 (1911)
26. J S Blakemore *Solid State Physics* (Cambridge: Cambridge University Press, 1985)
27. H J Scheel, in *Handbook of Crystal Growth* Vol. 1a (Ed. D T J Hurle) (Amsterdam: North-Holland, 1993) p.18
28. M B Maple, O Fischer *Superconductivity in Ternary Compounds II. Superconductivity and Magnetism (Top. Curr. Phys. 34)* (Berlin: Springer, 1982)
29. J G Bednorz, K A Müller *Z. Phys. B, Condens. Matter* **64** 189 (1986)
30. I S Shaplygin, B G Kakhan, V B Lazarev *Zh. Neorg. Khim.* **24** 1478 (1979) [c]
31. N Nguyen, J Choisnet, M Hervieu, B Raveau *J. Solid State Chem.* **39** 120 (1981)
32. M K Wu, J R Ashburn, C J Torng, P H Hor, R L Meng, L Gao, Z J Huang, Y Q Wang, C W Chu *Phys. Rev. Lett.* **58** 908 (1987)
33. H Maeda, Y Tanaka, M Fukutomi, T Asano *Jpn. J. Appl. Phys., Pt. 2* **27** L209 (1988)
34. Z Z Sheng, A M Hermann *Nature (London)* **332** 55 (1988)
35. S N Putilin, E V Antipov, O Chmaissem, M Marezio *Nature (London)* **362** 226 (1993)
36. A M Abakumov, E V Antipov, L M Kovba, E M Kopnin, S N Putilin, R V Shpanchenko *Usp. Khim.* **64** 769 (1995) [*Russ. Chem. Rev.* **64** 719 (1995)]
37. R F Kerl *Usp. Fiz. Nauk* **168** 331 (1998) [d]
38. S Maekawa *Science* **273** 1515 (1996)
39. N N Oleinikov, E A Goodilin, Yu D Tretyakov, in *Rossiiskaya Nauka. Vystoyat' i Vozrodit'sya* (Russian Science. Survive and Revive) (Moscow: Nauka, 1997) p. 167
40. Yu D Tretyakov *Z. Phys. Chem.* **207** 93 (1998)
41. Z Zou, K Oka, Y Nishihara, J Ye *Phys. Rev. Lett.* **80** 1074 (1998)
42. S V Samoylenkov, O Yu Gorbenko, A R Kaul *Physica C* **278** 49 (1997)
43. J G Lin, C Y Huang, Y Y Xue, C W Chu, X W Cao, J C Ho *Phys. Rev. B, Condens. Matter.* **51** 12900 (1995)
44. V Petrykin, M Kakihana, Yu D Tretyakov, in *High-Temperature Superconductors and Novel Inorganic Materials* (Eds G Van Tendeloo, E V Antipov, S N Putilin) (Dordrecht; Boston; London: Kluwer Academic, 1998) p. 173
45. J-H Choy, S-J Kwon, G-S Park *Science* **280** 1589 (1998)
46. S R Lee, M S Kuznetzov, N P Kiryakov, D A Emelyanov, Yu D Tretyakov *Physica C* **291** 275 (1997)
47. S R Lee, N P Kiryakov, D A Emelyanov, M S Kuznetzov, Yu D Tretyakov, V V Petrykin, M Kakihana, H Yamauchi, Y Zhuo, M-S Kim, S-I Lee *Physica C* **305** 57 (1998)
48. R V Shpanchenko, M G Rozova, A M Abakumov, E I Ardashnikova, M L Kovba, S N Putilin, E V Antipov, O I Lebedev, G Van Tendeloo *Physica C* **280** 272 (1997)
49. L A Reznitskii *Sverkhprovodimost'. Fiz. Khim. Tekhn.* **6** 183 (1993)
50. A P Mozhaev, S V Chernyaev *J. Mater. Chem.* **4** 1107 (1994)
51. E B Rudnyi, V V Kuzmenko, G F Voronin *J. Phys. Chem. Ref. Data* **27** 855 (1998)
52. H Zhang, H Sato *Physica C* **214** 265 (1993)
53. P Majewsky *Adv. Mater.* **6** 460 (1994)
54. W Zhang, E A Goodilin, E E Hellstrom, A Pashitski, D C Larbalestier *Supercond. Sci. Technol.* **9** 211 (1996)
55. E A Goodilin, Candidate Thesis in Chemical Sciences, Moscow State University, Moscow, 1995
56. M P Kuznetsov, A P Mozhaev, M A Dikusar, Yu D Tretyakov, N Ya Filatov, E V Skobtsev, V A Nikonorov, F V Loskutov *Sverkhprovodimost'. Fiz. Khim. Tekhn.* **8** 123; 709; 729 (1995)
57. M Nunez-Regueiro, J L Tholence, E V Antipov, J J Capponi, M Marezio *Science* **262** 97 (1993)
58. A Daridon, H Siegenthaler, F Arrouy, E J Williams, E Machler, J P Locquet *J. Alloy Compd.* **251** 118 (1997)
59. W Wong-Ng, L P Cook, B Paretzkin, M D Hill, J K Stalick *J. Am. Ceram. Soc.* **77** 2354 (1994)
60. S F Pashin, E V Antipov, L M Kovba *Sverkhprovodimost'. Fiz. Khim. Tekhn.* **2** 102 (1989)
61. R G Grebenshchikov (Ed.) *Diagrammy Sostoyaniya Sistem Tugoplavkikh Oksidov (Spravochnik) Sistemy Keramicheskikh Vysokotemperaturnykh Sverkhprovodnikov* [State Diagrams of High-Melting Oxide Systems (Handbook) The Systems of High-Temperature Ceramic Superconductors] (St. Petersburg: Nauka, 1997) No. 6
62. M Park, M J Kramer, K W Dennis, R W McCallum *Physica C* **259** 43 (1996)
63. K Osamura, W Zhang *Z. Met.* **84** 522 (1993)
64. W Wong-Ng, L P Cook, A Kearsley, G Lawrence, W Greenwood, in *High-Temperature Superconductors and Novel Inorganic Materials* (Eds G Van Tendeloo, E V Antipov, S N Putilin) (Dordrecht; Boston; London: Kluwer Academic, 1998) p. 63
65. S R Li, N P Kiryakov, O A Plesenkova, D A Emel'yanov, V V Petrykin, Yu D Tretyakov *Zh. Neorg. Khim.* **42** 1765 (1997) [c]
66. S Reich, D Veretnik *Physica C* **231** 1 (1994)
67. V A Alyoshin, D A Mikhailova, E V Antipov *Physica C* **271** 197 (1996)
68. H Schwer, R Molinski, E Kopnin, G I Meijer, J Karpinski *J. Solid State Chem.* **143** 277 (1999)
69. I E Arshakyan, N N Oleinikov, Yu D Tretyakov *Neorg. Mater.* **30** 824 (1994) [b]
70. L Dimesso, M Marchetta, G Calestani, A Migliori, M Masini *Supercond. Sci. Technol.* **10** 347 (1997)
71. W Bieger, G Krabbes, P Schatzle, L Zelenina, U Wiesner, P Verges, J Klosowski *Physica C* **257** 46 (1996)
72. V V Petrykin, E A Goodilin, M Kakihana, Yu D Tretyakov *Key Eng. Mat.* **132–136** 1285 (1997)
73. M Kambara, Y Watanabe, K Miyake, A Endo, K Murata *J. Mater. Res.* **12** 2873 (1997)
74. G Krabbes, W Bieger, P Schatzle, U Wiesner *Supercond. Sci. Technol.* **11** 144 (1998)
75. H Wu, M J Kramer, K W Dennis, R W McCallum *Physica C* **290** 252 (1997)

76. E A Goodilin, N N Oleynikov, G Yu Popov, V A Shpanchenko, E V Antipov, G V Balakirev, Yu D Tretyakov *Physica C* **272** 65 (1996)
77. E A Trofimenko, D I Grigorashev, N N Oleinikov, V A Ketsko, Yu D Tretyakov *Dokl. Akad. Nauk* **356** 208 (1997) [e]
78. E A Goodilin, N Khasanova, X J Wu, T Kamiyama, F Izumi, S Tajima, S Shiohara, in *High-Temperature Superconductors and Novel Inorganic Materials* (Eds G Van Tendeloo, E V Antipov, S N Putilin) (Dordrecht; Boston; London: Kluwer Academic, 1998) p. 145
79. M Kambara, M Tagami, X Yao, E Goodilin, Y Shiohara, T Umeda *J. Am. Ceram. Soc.* **81** 2116 (1998)
80. E A Goodilin, M Kambara, T Umeda, Y Shiohara *Physica C* **289** 251 (1997)
81. E A Goodilin, A Oka, J G Wen, Y Shiohara, M Kambara, T Umeda *Physica C* **299** 279 (1998)
82. V S Urusov *Teoriya Izomorfnoi Smesimosti* (The Theory of Isomorphous Miscibility) (Moscow: Nauka, 1977)
83. S I Yoo, R W McCallum *Physica C* **210** 147 (1993)
84. M J Kramer, S I Yoo, R W McCallum, W B Yelon, H Xie, P Allenspach *Physica C* **219** 145 (1994)
85. C U Segre, B Dabrowski, D G Hinks, K Zhang, J D Jorgensen, M A Beno, I K Schuller *Nature (London)* **329** 227 (1987)
86. T Wada, N Suzuki, A Maeda, T Yabe, K Uchinokura, S Uchida, S Tanaka *Phys. Rev. B, Condens. Matter* **39** 9126 (1989)
87. D V Fomichev, O G D'yachenko, A V Mironov, E V Antipov *Physica C* **225** 25 (1994)
88. M J Kramer, A Karion, K W Dennis, M Park, R W McCallum *J. Electron. Mater.* **23** 1117 (1994)
89. E A Goodilin, M F Limonov, A Panfilov, N Khasanova, A Oka, S Tajima, Y Shiohara *Physica C* **300** 250 (1998)
90. M F Limonov, E A Goodilin, X Yao, S Tajima, Y Shiohara, Y Kitaev *Phys. Rev. B, Condens. Matter* **58** 12368 (1998)
91. T Egi, J G Wen, K Kuroda, H Mori, H Unoki, N Koshizuka *Physica C* **270** 223 (1996)
92. N Chikumoto, J Yoshioka, M Otsuka, N Hayashi, M Murakami *Physica C* **281** 253 (1997)
93. M Sarikaya, E A Stern *Phys. Rev. B, Condens. Matter* **37** 9373 (1988)
94. Z Hiroi, I Chong, M Takano *J. Solid State Chem.* **138** 98 (1998)
95. T A Vanderah, R S Roth, H F McMurdie (Eds) *Phase Diagrams of High-T_c Superconductors II* (American Ceramic Society, 1997)
96. T Aselage, K Keefer *J. Mater. Res.* **3** 1279 (1988)
97. R W McCallum *J. Met.* **41** 50 (1989)
98. M Maeda, M Kadoi, T Ikeda *Jpn. J. Appl. Phys.* **28** 1417 (1989)
99. G Krabbes, W Bieger, U Wiesner, K Fischer, P Schatzle *J. Electron. Mater.* **23** 1135 (1994)
100. P Karen, O Braaten, A Kjekshus *Acta Chem. Scand.* **52** 805 (1992)
101. W Assmus, W Schmidbauer *Supercond. Sci. Technol.* **6** 555 (1993)
102. H J Scheel *MRS Bull.* (9) 26 (1994)
103. B J Lee, D N Lee *J. Am. Ceram. Soc.* **72** 78 (1991)
104. J Sestak, G K Moiseev, D S Tzagareishvili *Jpn. J. Appl. Phys.* **33** 97 (1994)
105. V E Lamberti, M A Rodriguez, J D Trybulski, A Navrotsky *Chem. Mater.* **9** 932 (1997)
106. G F Voronin *Zh. Vses. Khim. O-va im. D I Mendeleeva* **34** 466 (1989) [a]
107. R Beyers, B T Ahn *Ann. Rev. Mater. Sci.* **21** 335 (1991)
108. J Karpinski, E Kaldis, S Rusiecki *J. Less-Comm. Met.* **150** 207 (1989)
109. E A Goodilin, M Kambara, T Umeda, Y Shiohara *Physica C* **289** 37 (1997)
110. K Kuroda, K Itoi, J Okano, S Segawa, K Abe, I Choi *Jpn. J. Appl. Phys.* **36** 6730 (1997)
111. M Kambara, M Nakamura, Y Shiohara, T Umeda *Physica C* **275** 127 (1997)
112. C Klemenz, H J Scheel *J. Cryst. Growth* **129** 421 (1993)
113. Ch Krauns, M Sumida, M Tagami, Y Yamada, Y Shiohara *Z. Phys. B, Condens. Matter* **96** 207 (1994)
114. X Yao, Y Shiohara *Supercond. Sci. Technol.* **10** 249 (1997)
115. A N Maljuk, A B Kulakov, G A Emel'chenko *J. Cryst. Growth* **151** 102 (1995)
116. D K Aswal, M Shinmura, Y Hayakawa, M Kumagawa *J. Cryst. Growth* **193** 61 (1998)
117. C T Lin, A M Niraimathi, Y Yan, K Peters, H Bender *Physica C* **272** 285 (1996)
118. G A Emelchenko, A A Zhokhov, I G Naumenko, G K Baranova, S A Zver'kov, M Ya Kartsovnik, A E Kovalev, G Yu Logvenov, L N Pronina, S S Khasanov *Supercond. Sci. Technol.* **7** 541 (1994)
119. Ch Changkang, A J S Chowdhury, H Yongle *Supercond. Sci. Technol.* **7** 795 (1994)
120. Y Yamada, Y Niiori, I Hirabayashi, S Tanaka *Physica C* **278** 180 (1997)
121. U Wiesner, G Krabbes, M Ueltzen, C Magerkurth, J Plewa, H Altenburg *Physica C* **294** 17 (1998)
122. B N Sun, H Schmid *J. Cryst. Growth* **100** 297 (1990)
123. Y Yamada, M Nakamura, Y Shiohara, S Tanaka *J. Cryst. Growth* **148** 241 (1995)
124. C Klemenz, H J Scheel *Physica C* **265** 126 (1996)
125. Y Kanamori, Y Shiohara *J. Mater. Res.* **11** 2693 (1996)
126. Th Wolf *J. Cryst. Growth* **166** 810 (1996)
127. E A Goodilin, N N Oleinikov, A N Baranov, Yu D Tretyakov *Neorg. Mater.* **29** 1443 (1993) [b]
128. E A Goodilin, N N Oleinikov, G Yu Popov, Yu D Tretyakov *Neorg. Mater.* **31** 1 (1995) [b]
129. E A Goodilin, N N Oleinikov, Yu D Tretyakov *Zh. Neorg. Khim.* **41** 887 (1996) [c]
130. V M Kuznetsov, N N Oleinikov, A N Baranov, Yu D Tretyakov *Neorg. Mater.* **32** 1021 (1996) [b]
131. W Lo, D A Cardwell, S-L Dung, R G Barter *J. Mater. Res.* **116** 39 (1996)
132. H S Chauhan, A Endo, M Kambara, T Umeda, Y Shiohara *Adv. Superconduct. IX* 161 (1997)
133. M Kambara, T Umeda, H S Chauhan, A Endo, Y Shiohara *Physica C* **282**–**287** 447 (1997)
134. E A Goodilin, D B Kvartalov, N N Oleynikov, Yu D Tretyakov *Physica C* **235**–**240** 449 (1994)
135. E A Goodilin, N N Oleinikov, D B Kvartalov, V A Ketsko, G P Murav'eva *Zh. Neorg. Khim.* **41** 357 (1996) [c]
136. E A Eremina, Ya A Rebane, Yu D Tretyakov *Neorg. Mater.* **30** 867 (1994) [b]
137. Y A Rebane, I E Korsakov, A V Kandidov, E A Eremina, Yu D Tretyakov *Physica C* **235**–**240** 605 (1994)
138. J A Rebane, A R Kaul, Yu D Tretyakov *Fresenius J. Anal. Chem.* **356** 484 (1996)
139. J A Rebane, N V Yakovlev, D S Chicherin, Yu D Tretyakov, L I Leonyuk, V G Yakunin *J. Mater. Chem.* **7** 2085 (1997)
140. T D Dzhafarov *Phys. Status Solidi A* **158** 335 (1996)
141. T B Lindemer, E D Specht *Physica C* **268** 271 (1996)
142. J Hauck, K Bickmann, K Mika *Supercond. Sci. Technol.* **11** 63 (1998)
143. A P Mozhaev, G N Mazo, A A Galkin, N V Khramova *Zh. Neorg. Khim.* **41** 916 (1996) [c]
144. T E Os'kina, Yu D Tretyakov, E A Soldatov *Sverkhprovodimost'. Fiz. Khim. Tekhn.* **2** 24 (1989)
145. T E Os'kina, Yu D Tretyakov, Yu V Badun *Sverkhprovodimost'. Fiz. Khim. Tekhn.* **3** 2249 (1990)
146. I E Graboi, A R Kaul, Yu D Tretyakov, I V Zubov, I G Muttik *Physica C* **185**–**189** 527 (1991)
147. D Fontaine, G Ceder, M Asta *Nature (London)* **343** 544 (1990)
148. J L Tallon, N E Flower *Physica C* **204** 237 (1993)
149. T M Shaw, S L Shinde, D Dimos, R F Cook, P R Duncombe, C Kroll *J. Mater. Res.* **4** 248 (1989)
150. V I Voronkova, Th Wolf *Physica C* **218** 175 (1993)
151. M Nakamura, Y Yamada, Y Shiohara *J. Mater. Res.* **9** 1946 (1994)
152. V V Petrykin, N N Oleinikov, V A Ketsko *Neorg. Mater.* **32** 188 (1996) [b]
153. T B Tang, W Lo *Physica C* **174** 462 (1991)
154. S I Bredikhin, G A Emel'chenko, V Sh Shekhtman, A A Zhokhov, S Carter, R J Chater, J A Kilher, B C H Steele *Physica C* **179** 286 (1991)
155. X M Xie, T G Chen, Z L Wu *Phys. Rev. B, Condens. Matter* **40** 4549 (1989)
156. S J Rothman, J L Routbort, U Welp, J E Baker *Phys. Rev. B, Condens. Matter.* **44** 2326 (1991)
157. A Erb, B Greb, G Muller-Vogt *Physica C* **259** 83 (1996)
158. D Shi, J Krucpzak, M Tang, N Chen, R Bradra *J. Appl. Phys.* **66** 4325 (1989)

159. Y Yamada, Y Shiohara *Physica C* **217** 182 (1993)
160. E Kemnitz, A A Galkin, T Olesch, S Scheurell, A P Mozhaev, G N Mazo *J. Therm. Anal.* **48** 997 (1997)
161. A A Galkin, G N Mazo, V V Lunin, S Sheurel, E Kemnitts *Zh. Fiz. Khim.* **72** 1618 (1998) [f]
162. Yu D Tretyakov, N N Oleinikov, A A Vertegel *Zh. Neorg. Khim.* **41** 932 (1996) [c]
163. M Kakihana *J. Sol-Gel Sci. Technol.* **6** 7 (1996)
164. S V Kalinin, Yu G Metlin, N N Oleynikov, Yu D Tretyakov, A A Vertegel *J. Mater. Res.* **13** 901 (1998)
165. Yu D Tretyakov, A P Mozhaev, N N Oleinikov *Osnovy Kriokhimicheskoi Tekhnologii* (Foundations of Cryochemical Technology) (Moscow: Vysshaya Shkola, 1987)
166. O A Shlyakhtin, Yu D Tretyakov *Mater. Technol.* **12** 158 (1997)
167. Yu D Tretyakov, O A Shlyaktin, in *High-Temperature Superconductors and Novel Inorganic Materials* (Eds G Van Tendeloo, E V Antipov, S N Putilin) (Dordrecht; Boston; London: Kluwer Academic, 1998) p. 57
168. Yu D Tretyakov, N N Oleynikov, O A Shlyakhtin *Cryochemical Technology of Advanced Materials* (London: Chapman and Hall, 1997)
169. A A Burukhin, N N Oleinikov, B R Churagulov, Yu D Tretyakov *Dokl. Akad. Nauk* **358** 778 (1998) [e]
170. B R Churagulov, N N Oleinikov, S L Lyubimov, O V Galas, S B Abramov *Zh. Neorg. Khim.* **40** 202 (1995) [c]
171. C T Chu, B Dunn *J. Am. Ceram. Soc.* **70** C375 (1987)
172. S Chadda, T L Ward, A Carim, T T Kodas, R Ott, D Kroeger *J. Aerosol Sci.* **22** 601 (1991)
173. N N Oleynikov, S R Lee, E A Goodilin, P E Kazin *J. Alloys Compd.* **195** 27 (1993)
174. O A Shlyakhtin, A L Vinokurov, A N Baranov, Yu D Tretyakov *J. Supercond.* **11** 507 (1998)
175. S R Lee, O A Shlyakhtin, M-K Bae, M-O Mun, S-I Lee *Supercond. Sci. Technol.* **8** 60 (1995)
176. A Goyal, D P Norton, D K Christen, E D Specht, M Paranthaman, D M Kroeger, J D Budai, Q He, F A List, R Feenstra, H R Kerchner, D F Lee, E Hatfield, P M Martin, J Mathis, C Park *Appl. Supercond.* **4** 403 (1996)
177. V N Fuflygin, M A Novozhilov, A R Kaul', Yu D Tretyakov *Zh. Neorg. Khim.* **41** 903 (1996) [c]
178. O Yu Gorbenko, A R Kaul, S V Pozigun, V A Alekseev, Yu D Tretyakov, V I Scritnii *Physica C* **190** 1929 (1991)
179. O Yu Gorbenko, A R Kaul, S A Pozigun, E V Kolosova, S N Polyakov, V I Scritny *Mater. Sci. Eng.* **B17** 157 (1993)
180. T Usagawa, Y Ishimaru, J Wen, S Koyama, Y Enomoto *Jpn. J. Appl. Phys.* **36** L100 (1997)
181. E Goodilin, F Saba, Y Enomoto, Y Shiohara *Adv. Supercond. X* 717 (1998)
182. O Yu Gorbenko, V N Fuflyigin, Yu Yu Erokhin, I E Graboy, A R Kaul, Yu D Tretyakov, G Wahl, L Klippe *J. Mater. Chem.* **4** 1585 (1994)
183. S V Samoylenkov, O Yu Gorbenko, A R Kaul, Yu D Tretyakov *J. Mater. Chem.* **6** 623 (1996)
184. I E Graboy, A R Kaul, N V Markov, V A Maleev, S N Polyakov, V L Svechnikov, H W Zandbergen, K-H Dahmen *J. Alloys Compd.* **251** 318 (1997)
185. V A Legasov, N N Oleinikov, Yu D Tretyakov *Zh. Neorg. Khim.* **31** 1637 (1986) [c]
186. N N Oleinikov, S R Li, P E Kazin, G P Murav'eva, A A Petryanik *Sverkhprovodimost'. Fiz. Khim. Tekhn.* **5** 105 (1992)
187. M Kimura, H Tanaka, H Horiuchi, M Morita, M Matsuo, H Morikawa, K Sawano *Physica C* **174** 263 (1991)
188. J P Zhou, S X Dou, A J Bourdillon, H K Liu, C C Sorrell *J. Mater. Sci. Lett.* **8** 1147 (1989)
189. R L Meng, Y Y Sun, P H Hor, C W Chu *Physica C* **179** 149 (1991)
190. S E Babcock, T F Kelly, P J Lee, J M Seuntjens, D C Larbalesfier, L A Lavanier *Physica C* **152** 25 (1988)
191. K B Alexander, D M Kroeger, J Bentley *Physica C* **180** 337 (1991)
192. M Wacenovsky, R Miletich, H W Weber, M Murakami *Cryogenics* **33** 70 (1993)
193. V Hardy, J Provost, P Groult *J. Alloys Compd.* **195** 395 (1993)
194. M Murakami, T Oyama, H Fujimoto, T Tagychi, S Gotoh, Y Shiohara, N Koshizuka, S Tanaka *Jpn. J. Appl. Phys.* **29** L1991 (1990)
195. M Mironova, D F Lee, K Salama *Physica C* **211** 188 (1993)
196. Z L Wang, A Goyal, D M Kroeger *Phys. Rev. B, Condens. Matter* **47** 5373 (1993)
197. D Shi, S Sengupta, J S Luo, C Varanasi, P J McGinn *Physica C* **213** 179 (1993)
198. S Jin, G W Kammlott, T H Tiefel, T T Kodas, T L Ward, D M Kroeger *Physica C* **181** 57 (1991)
199. D F Lee, V Selvamanickam, K Salama *Physica C* **202** 83 (1992)
200. D W A Willer, K Salama *Physica C* **201** 311 (1992)
201. L T Romano, O F Schilling, C R M Grovenor *Physica C* **178** 41 (1991)
202. I Monot, T Higuchi, N Sakai, M Murakami *Supercond. Sci. Technol.* **7** 783 (1994)
203. R Weinstein, R P Sawh, Y Ren, D Parks *Mater. Sci. Eng.* **B53** 38 (1998)
204. C B Eom, A F Marshall, Y Suzuki, P Boyer, R F W Pease, T H Geballe *Nature (London)* **353** 544 (1991)
205. J W Ekin, K Salama, V Selvamanickam *Appl. Phys. Lett.* **59** 360 (1991)
206. R A Camps, J E Evetts, B A Glowacki, S B Newcomb, R E Somekh, W M Stobbs *Nature (London)* **329** 229 (1987)
207. S Jin, G W Kammlot, T H Tiefel *Physica C* **198** 333 (1992)
208. B Hensel, J-C Grivel, A Jeremie, A Perin, A Pollini, R Flukiger *Physica C* **205** 329 (1993)
209. D Shi *Appl. Supercond.* **1** 61 (1993)
210. D Delagnes, N Pellerin, A R Fert, X Bozec, J P Redoules, P Odier, A Mari *Physica C* **211** 355 (1993)
211. V R Todt, G J Schmitz *J. Mater. Res.* **8** 411 (1993)
212. N Ogawa, I Hirabayashi, S Tanaka *Physica C* **177** 101 (1991)
213. J-H Park, H-W Kim, J-T Song *J. Mater. Sci.* **4** 77 (1993)
214. Z Lian, Z Pingxiang, J Ping *IEEE Trans. Magn.* **27** 912 (1991)
215. V Selvamanickam, A Goyal, D M Kroeger *J. Electron. Mater.* **23** 1160 (1994)
216. C-J Kim, K-B Kim, G-W Hong *Mater. Lett.* **21** 9 (1994)
217. C-J Kim, K-B Kim, G-W Hong *Physica C* **232** 163 (1994)
218. M Arnott, B A Glowasky, B Soylu *IEEE Trans. Appl. Supercond.* **3** 1037 (1993)
219. Y Idemoto, K Fueki *Jpn. J. Appl. Phys.* **29** 2729 (1990)
220. K Fisher, N M Chebotarev, S Naumov *J. Cryst. Growth* **132** 444 (1993)
221. M A Black, P J McGinn *J. Electron. Mater.* **23** 1121 (1994)
222. Z Lian, T Ping, D Shejun *Adv. Cryog. Eng.* **38** 943 (1992)
223. K Sawano, M Morita, M Tanaka, T Sasaki, K Kimura, S Takebayashi, M Kimura, K Miyamoto *Jpn. J. Appl. Phys.* **30** L1159 (1991)
224. P Gautier-Picard, X Chaud, E Beaugnon, A Erraud, R Tournier *Mater. Sci. Eng.* **B53** 66 (1998)
225. T Meighan, P J McGinn, C Varanasi *Supercond. Sci. Technol.* **10** 109 (1997)
226. A Endo, H S Chauhan, Y Nakamura, Y Shiohara *J. Mater. Res.* **11** 1114 (1996)
227. B Soylu, J Christiansen, D M Astill, R P Baranowski, J Engel, J E Evetts *Inst. Phys. Conf. Ser.* **148** 135 (1995)
228. G J Schmitz, O Kugeler *Physica C* **275** 205 (1997)
229. A Holloway *J. Appl. Phys.* **70** 5716 (1991)
230. M R Lees, D Bourgault, P de Rango, P Lejay, A Sulpice, P Tournier *Philos. Mag. B* **65** 1395 (1992)
231. M Morita, S Takebayashi, M Tanaka, K Kimura, K Miyamoto, K Sawano *Adv. Supercond. III* 733 (1990)
232. M Murakami, S I Yoo, T Higuchi, N Sakai, N Koshizuka, S Tanaka *Jpn. J. Appl. Phys.* **33** L715 (1994)
233. A Erb, E Walker, J-Y Genoud, R Flukiger *Physica C* **282 – 287** 89 (1997)
234. A A Zhukov, I V Gladyshev, S I Gordeev, V A Murashov *Sverkhprovodimost'. Fiz. Khim. Tekhn.* **4** 1268 (1991)
235. R J Cava, A W Hewat, E A Hewat, B Batlogg, J J Krajewski, W F Peck, L W Rupp, K M Rabe, M Marezio *Physica C* **165** 419 (1990)
236. J D Jorgensen, B W Veal, A P Paulikas, L J Nowicki, J W Crabtree, H Claus, W K Kwok *Phys. Rev. B, Condens. Matter* **41** 1863 (1990)
237. Y Zhu, in *High-Temperature Superconducting Materials Science and Engineering. New Concepts and Technology* (Ed. D Shi) (Oxford: Pergamon Press, 1995) p. 199

238. C Thomsen, in *Light Scattering in Solids VI* (Ed. M Cardona) (Berlin: Springer, 1991) p. 285
239. M Kambara, X Yao, M Nakamura, Y Shiohara, T Umeda *J. Mater. Res.* **12** 2866 (1997)
240. L E C van de Leemput, P J M Bentum, F A J M Driessen, J W Gerritsen, H van Kempen, L W M Schreurs, P Bennema *J. Cryst. Growth* **98** 551 (1989)
241. H Asaoka, H Takei, Y Iye, M Tamura, M Kinoshita, H Takeya *Jpn. J. Appl. Phys.* **32** 1091 (1993)
242. Y Namikawa, Y Shiohara *Physica C* **268** 1 (1996)
243. M Egami, Y Shiohara *Adv. Supercond. IX* 809 (1997)
244. H Zhang, G Wang, H Wu *J. Cryst. Growth* **154** 293 (1995)
245. D K Aswal, S K Gupta, S C Gadkari, S C Sabharwal, M K Gupta, K D S Mudher, L C Gupta *Supercond. Sci. Technol.* **8** 710 (1995)
246. R Liang, P Dosanjh, D A Bonn, D J Baar, J F Carolan, W N Hardy *Physica C* **195** 51 (1992)
247. T E Os'kina, D Wehler, H Piel, R Roth, Yu D Tretyakov *Physica C* **242** 85 (1995)
248. A Erb, E Walker, R Flukiger *Physica C* **245** 245 (1995)
249. L F Schneemeyer, J V Waszczak, T Siegrist, R B Van Dover, L W Rupp, B Batlogg, R J Cava, D W Murphy *Nature (London)* **328** 601 (1987)
250. Y Namikawa, M Egami, S Koyama, Y Shiohara *J. Mater. Res.* **11** 804 (1996)
251. C T Lin, A M Niraimathi, Y Yan, K Peters, H Bender, E Schonherr, E Gmelin *Physica C* **272** 285 (1996)
252. Z Zou, J Ye, K Oka, Y Nishihara *Phys. Rev. Lett.* **80** 1074 (1998)
253. Yu D Tretyakov, N N Oleinikov, E A Goodilin, A A Vertegel, A N Baranov *Neorg. Mater.* **30** 291 (1994) [b]
254. T E Os'kina, Yu D Tretyakov *Zh. Neorg. Khimii* **39** 707 (1994) [c]
255. T E Os'kina, Yu D Tretyakov, Ya G Ponomarev, H Piel *J. Mater. Chem.* **5** 611 (1995)
256. T E Os'kina, Ya G Ponomarev, H Piel, Yu D Tretyakov, B Lehndorff *Physica C* **266** 115 (1996)
257. E F Talantsev *Supercond. Sci. Technol.* **7** 491 (1994)
258. T E Os'kina, Yu D Tretyakov *Dokl. Akad. Nauk* **330** 594 (1993) [e]
259. Yu D Tretyakov, T E Os'kina, V I Putlyaev *Zh. Neorg. Khimii* **35** 1635 (1990) [c]
260. T E Os'kina, P E Kazin, Yu D Tretyakov, V F Kozlovskii, I E Lapshina *Sverkhprovodimost'. Fiz. Khim. Tekhn.* **5** 1298 (1992)
261. D I Grigorashev, V V Lennikov, G P Murav'eva, N N Oleinikov, Yu D Tretyakov *Neorg. Mater.* **31** 1078 (1995) [b]
262. V I Pytlyaev, S V Sokolov, P E Kazin, A G Veresov, Yu D Tretyakov *Solid State Ionics* **101–103** 1075 (1997)
263. Yu D Tretyakov, P E Kazin *Neorg. Mater.* **29** 1571 (1993) [b]
264. P E Kazin, M Jansen, A Larrea, G F Fuente, Yu D Tretyakov *Physica C* **253** 391 (1995)
265. P E Kazin, V V Poltavets, Yu D Tretyakov, M Jansen, B Freitag, W Mader *Physica C* **280** 253 (1997)
266. P E Kazin, M V Makarova, M Jansen, Th Adelsberger, Yu D Tretyakov *Supercond. Sci. Technol.* **10** 616 (1997)
267. P E Kazin, V V Poltavets, M S Kuznetsov, D D Zaytsev, Yu D Tretyakov, M Jansen, M Schreyer *Supercond. Sci. Technol.* **11** 880 (1998)
268. P E Kazin, M A Uskova, Yu D Tretyakov, M Jansen, S Scheurell, E Kemnitz *Physica C* **301** 185 (1998)
269. V V Lennikov, P E Kazin, V I Putlyaev, Yu D Tretyakov, M Yansen *Zh. Neorg. Khimii* **41** 911 (1996) [c]
270. P E Kazin, V V Poltavets, V V Lennikov, R A Shuba, E A Eremina, Yu D Tretyakov, M Jansen, B Freitag, G F Fuente, A Larrea, in *High-Temperature Superconductors and Novel Inorganic Materials* (Eds G Van Tendeloo, E V Antipov, S N Putilin) (Dordrecht; Boston; London: Kluwer Academic, 1998) p. 69
271. S V Samoylenkov, O Yu Gorbenko, I E Graboy, A R Kaul, H W Zandbergen, E Connoly *Chem. Mater.* **11** 2417 (1999)
272. M A G Aranda, J P Attfield *Angew. Chem., Int. Ed. Engl.* **32** 1454 (1993)
273. G F Voronin, S A Degterov *J. Solid State Chem.,* **110** 50 (1994)
274. A F Maiorova, S N Mudretsova, Yu Ya Skolis, M L Kovba, M V Gorbacheva *Thermoch. Acta* **269**/**270** 567 (1995)
275. A F Maiorova, S N Mudretsova, M L Kovba, Yu Ya Skolis, M V Gorbacheva, G N Mazo, L A Khramtsova *Thermoch. Acta* **269**/**270** 101 (1995)
276. A F Maiorova, S N Mudretsova, M L Kovba, A S Monaenkova, A A Popova *Physica C* **218** 137 (1993)
277. E A Goodilin, A P Soloshenko, V V Lennikov, A V Knot'ko, N N Oleynikov, Yu D Tretyakov, in *Proceedings of MSM-99, Sharif University of Technology, Tehran, 2000*
278. V V Petrykin, P Berastegui, M Kakihana *Chem. Mater.* **11** 3445 (1999)
279. E A Goodilin, I S Bezverhiy, Y D Tretyakov, V V Petrykin, M Kakihana, J Hester, in *MRS'99 Fall Meeting, Boston, MA, 1999* II3.17, p. 603
280. V Petrykin, M Kakihana, Y Tretyakov, in *High-Temperature Superconductors and Novel Inorganic Materials* (Eds G.Van Tendeloo, E V Antipov, S N Putilin) (Dordrecht; Boston; London: Kluwer Academic, 1999) p. 173
281. E A Goodilin, A P Soloshenko, V V Lennikov, A V Knot'ko, D A Vetoshkin, N N Oleinikov, Yu D Tretyakov *Zh. Neorg. Khim.* **45** 917 (2000) [c]
282. I Steinbach, F Pezzolla, B Nestler, M Seebelberg, G J Schmitz *Physica D* **94** 135 (1996)
283. S R Lee, T Akao, H Suematsu, H Yamauchi, N P Kiryakov *Appl. Phys. Lett.* **73** 3586 (1998)
284. J Karpinski, H Schwer, E Kopnin, R Molinski, G I Meijer *Physica C* **282–287** 77 (1997)
285. A Morawski, T Lada, A Paszewin, K Przybylski *Supercond. Sci. Technol.* **11** 193 (1998)
286. S V Samoylenkov, O Yu Gorbenko, I E Graboy, A R Kaul, O Stadel, G Wahl, V L Svetchnikov, H W Zandbergen, in *Trilateral German-Russian-Ukrainian Seminar on HTSC, Göttingen, 1998* p. 17
287. S V Samoylenkov, O Yu Gorbenko, A R Kaul, A R Kuzhakhmetov, S A Zhgoon, G Wahl In *Studies Appl. Electromagn. Mechan.* **13** 87 (1998)
288. E A Goodilin, G Yu Popov, N N Oleinikov, G P Murav'eva, P E Kazin, Yu D Tretyakov *Dokl. Akad. Nauk* **344** 773 (1995) [e]
289. N G Makarova, A N Nikolaevskii, A V Belyi, T M Dmitruk, O P Kniga *Fiziko-Khimicheskie Aspekty Rosta Monokristallov $YBa_2Cu_3O_z$ iz Rastvora v Rasplave (Preprint DonGU-96-1)* [Physicochemical Aspects of the Growth of $YBa_2Cu_3O_z$ Single Crystals from Solution in Melt (Preprint DonGU-96-1)] (Donetsk: Donetsk State University, 1996)
290. Y Namikawa, M Egami, Y Shiohara *J. Jpn. Inst. Met.* **10** 1047 (1995)
291. A Shukla, B Barbiellini, A Erb, A Manuel, T Buslaps, V Honkimaki, P Suortti *Phys. Rev. B, Condens. Matter* **59** 12127 (1999)
292. M Muroi, R Street *Physica C* **314** 172 (1999)

[a] — *Mendeleev Chem. J. (Engl. Transl.)*
[b] — *Inorg. Mater. (Engl. Transl.)*
[c] — *Russ. J. Inorg. Chem. (Engl. Transl.)*
[d] — *Physcs-Uspekhi (Engl. Transl.)*
[e] — *Dokl. Chem. Technol., Dokl. Chem. (Engl. Transl.)*
[f] — *Russ. J. Phys. Chem. (Engl. Transl.)*